

NASA Contractor Report 3438

NASA-CR-3438 19810016602

Conceptual Design Studies for Large Free-Flying Solar-Reflector Spacecraft

John M. Hedgepeth, Richard K. Miller,
and Karl Knapp

CONTRACT NAS1-15347
JUNE 1981

LIBRARY COPY

JUL 8 1981

LANGLEY RESEARCH CENTER
LIBRARY, NASA
HAMPTON, VIRGINIA

FOR REFERENCE

NOT TO BE TAKEN FROM THIS ROOM

NASA



NASA Contractor Report 3438

Conceptual Design Studies for Large Free-Flying Solar-Reflector Spacecraft

John M. Hedgepeth, Richard K. Miller,
and Karl Knapp
Astro Research Corporation
Carpinteria, California

Prepared for
Langley Research Center
under Contract NAS1-15347



National Aeronautics
and Space Administration

**Scientific and Technical
Information Branch**

1981

PREFACE

The successful performance of any structure depends largely on the identification of the critical or primary loads and design criteria on which the design is based. The future promises large structures which must be deployed, erected, assembled, or fabricated in space. For such structures, which are in a collapsed, packaged condition during the launch environment, the primary design requirements will be derived from the space-flight environment and will deal with phenomena as primary criteria which have been considered as only secondary in the past. The design of such genuine "space" structures will require a solid foundation of critical criteria.

Astro Research Corporation (Astro) has a contract from NASA Langley Research Center to study critical design criteria for large space structures. The objective is to identify and establish critical baseline design requirements for a family of structures by a series of rational parametric analyses. The results, presented clearly and in detail, should improve the basis for future space structures system and technology efforts. They will also form the beginning of the needed solid foundation of design criteria.

This report is one of a series dealing with critical design requirements for large space structures. In particular, this paper reports the results of design studies for Earth-orbiting, solar-reflecting spacecraft intended to enhance solar-energy collection at several Earth sites. Motivation for the study of such spacecraft was provided, in this case, by the SOLARES concept, which involves the use of a swarm of free-flying, solar-reflecting satellites which act intelligently and cooperatively to concentrate solar energy at several energy conversion stations on Earth. Each satellite must rotate as it passes over a ground site where power is being generated so that the reflected sunlight falls within the site.

Previous preliminary structural designs of free-flying, solar-reflecting satellites were studied in 1978 and are reported in ref. 1. These describe a triangular design suitable for small sizes (100-meter) and a nearly circular configuration suitable for larger satellites (1000-meter). In the current studies, we have reexamined these concepts and also considered multifaceted designs before selecting a circular configuration as the baseline. Special emphasis has been placed on the incorporation of control actuator in the design and on the use of realistic techniques for automatic deployment.

Part I of this report deals with the specific requirements and design variations for attitude control actuators. The baseline design for a 1-kilometer-diameter satellite is described in Part II.

TABLE OF CONTENTS

PREFACE	iii
SUMMARY	1
LIST OF SYMBOLS	2
<u>PART I: CONCEPTUAL DESIGN</u>	
<u>OF AN ATTITUDE CONTROL ACTUATOR</u>	5
SECTION 1: INTRODUCTION	7
SECTION 2: TRACKING AND REORIENTATION REQUIREMENTS	9
2.1 Over-Site Tracking Maneuvers	9
2.2 Between-Site Reorientation Maneuvers	14
2.3 Optimal Flight Plan Studies	16
SECTION 3: CONTROL ACTUATOR SIZING AND DESIGN	19
3.1 Potential Control Actuator Configuration	19
3.2 Comparisons Between Most Attractive Configurations	29
3.3 Features of a Baseline Design Control Actuator Configuration	38
3.4 Effect of CMG Flexibility on Pointing Accuracy	39
SECTION 4: INTERORBIT MANEUVERING WITH SOLAR PRESSURE	41
<u>PART II: POINT DESIGN OF A DEPLOYABLE-REFLECTOR</u>	
<u>SATELLITE WITH ONE-KILOMETER DIAMETER</u>	45
SECTION 1: INTRODUCTION	47
SECTION 2: REFLECTOR SPACECRAFT DESIGN	48
2.1 Discussion	48
2.2 Design Approach	49
2.3 Spacecraft Loads	50
2.4 Mirror Flatness Requirements	53
2.5 Membrane Tension Requirements	53
2.6 Membrane Support Requirements	54
2.7 Thermal Design Requirements	55
2.8 Baseline Design of a Reflector Spacecraft	57

2.9	On-Orbit Deployment	66
2.10	Parametric Mass Equations	70
2.11	Vibration Frequencies	71
SECTION 3:	CONCLUSIONS	74
REFERENCES	109

LIST OF TABLES

TABLE I.	REQUIRED TORQUES AND ANGULAR IMPULSES DURING OVER-SITE TRACKING MANEUVERS FOR THE BASELINE SATELLITE	75
TABLE II.	REQUIRED TORQUES AND ANGULAR IMPULSES DURING REORIENTATION MANEUVERS FOR THE BASELINE SATELLITE	76
TABLE III.	MASS, POWER, AND ENERGY REQUIREMENT FOR BASELINE CONTROL ACTUATORS FOR TRACKING TWO EQUIDISTANT EARTH SITES	77
TABLE IV.	DETAILS OF BASELINE BIAXIAL TWIN-ROTOR CONTROL-MOMENT GYROSCOPE DESIGN	78
TABLE V.	DETAILS OF BASELINE MAGNETIC-LOOP CONTROL ACTUATOR DESIGN	79
TABLE VI.	MASS SUMMARY FOR BASELINE 1-km-DIAMETER REFLECTOR SPACECRAFT	80
TABLE VII.	PROPERTIES OF COMPOSITE MATERIALS	81

LIST OF ILLUSTRATIONS

Figure 1.	Geometry of geocentric satellite orbit coplanar with Earth and Sun	82
Figure 2.	Kinematics of satellite tracking maneuver for an orbital altitude of 2400 km	83
Figure 3.	Kinematics of satellite tracking maneuver for an orbital altitude of 4146 km	84
Figure 4.	Increase in total reflected energy as a function of control torque ratio for two Sun angles	85
Figure 5.	Increase in total reflected energy as a function of control torque ratio for two Sun angles	86
Figure 6.	Increase in total reflected energy as a function of control torque ratio for two Sun angles	87
Figure 7.	Normalized total reflected energy \hat{E}_1 as a function of local Sun angle ϵ for two orbital altitudes	88
Figure 8.	Deployable filamentary flywheel for control-moment gyro	89
Figure 9.	Closeup of center body showing twin- rotor control-moment gyro	90
Figure 10.	Cutaway view of center body showing details of twin-rotor control-moment gyro	91
Figure 11.	Typical MLC circuit loop	92
Figure 12.	Angle-of-attack program for maximum net thrust .	93
Figure 13.	Variation of average net thrust with dynamic pressure	94
Figure 14.	Trip time to 2400 km	95
Figure 15.	Maximum lateral loads on reflecting films at different orbital altitudes	96
Figure 16.	Effect of local gradients on mirror beam spreading	97
Figure 17.	Film tension required to limit membrane reflector curvature	98
Figure 18.	Circular solar-reflector spacecraft design . . .	99

Figure 19.	Baseline design of the film-expansion compensator	100
Figure 20.	Schematic of film-expansion compensator	101
Figure 21.	Baseline configuration of a solar-reflector spacecraft	102
Figure 22.	1-km-diameter reflector spacecraft packaged for Shuttle cargo bay	103
Figure 23.	First phase of deployment showing truss-rim canisters after 90-degree rotation . . .	104
Figure 24.	Solar-reflector spacecraft during early part of second deployment phase	105
Figure 25.	Progressive deployment of masts and film in second deployment phase	106
Figure 26.	Third phase of the deployment sequence	107
Figure 27.	Structural mass fraction for circular reflector satellite	108

SUMMARY

The orientation requirements for a large free-flying, solar-reflector spacecraft and the selection of a suitable control actuator to meet these requirements for a 1-km-diameter spacecraft are discussed in Part I of this report. The spacecraft angular acceleration required to maintain the necessary orientation of the reflected beam, as well as that necessary to reorient the spacecraft between Earth sites, are studied as examples of mission-dependent attitude-control requirements. Also studied are a variety of potential control-system actuator configurations capable of providing the required attitude control torque for a large space structure; and criteria are established for the evaluation of the power and mass requirements of each system.

A twin-rotor, control-moment gyroscope has been selected as the best type of actuator for this application, based on its moderate mass and low power requirements. A conceptual design of this system, employing deployable mesh rotors, is described, along with a supplementary magnetic load control.

A conceptual design of a 1-km-diameter free-flying, solar-reflector spacecraft, which can be launched by a single flight of the Space Shuttle and deployed automatically on orbit, is described in Part II of this report. The average specific mass of this structure, which includes a deployable twin-rotor, control-moment gyroscope as the control actuator, is less than 12 g/m^2 . This weight is based on the use of an aluminized Kapton film with a specific mass of 4 g/m^2 .

LIST OF SYMBOLS

A	area
α	angle of attack
\underline{B}	magnetic field vector
b	nondimensional satellite altitude
β	satellite angular position relative to site vertical
D	satellite diameter
d	distance from ground site to satellite
δ	satellite angular orientation relative to site vertical, or axial deflection
E	energy per unit area received at ground site after reflection by satellite, or modulus of elasticity
ϵ	local Sun angle measured from site vertical, or unit error in length
E_s	energy storage
η	ratio of solar radius to satellite radius
F	force
f	frequency
g	acceleration due to gravity
γ	Sun angle of incidence on satellite surface
H	central mast height, or orbital energy
h	satellite orbital altitude
H_w	angular momentum of wheel
i	current
I_{sp}	specific impulse
I_{tot}	total angular impulse
I_y	mass moment of satellite inertia measured about a diameter
I_z	polar mass moment of satellite inertia
k	spring constant
L	stay length

ℓ	length
λ	fraction of plasma particles
M	mass
m_a	mass per unit area
N	number of equally spaced ground sites, or number of electrical loops, or membrane tension
\underline{n}	magnetic moment vector
Ω	dimensionless parameter of momentum wheel
P	power, or load
p	ground site, or pressure
p_0	solar pressure
ϕ	satellite angular position relative to Earth, or angle between the Sun vector and the normal to the flight path
q	dynamic pressure
R	satellite orbital radius
r	radius
R_e	Earth radius
ρ	mass density
S	Sun
s	satellite
σ	electrical resistivity
σ_w	working stress
T	torque
t	time, or thickness
T_{GG}	gravity-gradient torque
T_R	control torque during reorientation
T_T	control torque during tracking
T_0	tension
θ	gimbal angle of momentum wheel
$\dot{\theta}$	gimbal rate of momentum wheel
U	flight speed
w	surface deflection

Subscripts

1	first site
2	second site

PART I

CONCEPTUAL DESIGN
OF AN ATTITUDE CONTROL ACTUATOR

This Page Intentionally Left Blank

SECTION 1

INTRODUCTION

The spacecraft angular acceleration required to maintain the necessary orientation of the reflected beam, as well as that necessary to reorient the spacecraft between Earth sites, are studied in this part as examples of mission-dependent attitude-control requirements which govern the selection of a suitable spacecraft control system. Also studied are a variety of potential control-actuator configurations capable of providing the required attitude control torque for a large space structure; and criteria are established for the evaluation of the power and weight requirements of each system.

Two substantial limitations apply to the results presented in this study. These limitations result from simplifying assumptions which are necessary for preliminary design studies. The first such assumption is that the required spacecraft kinematics during tracking and reorientation maneuvers may be estimated from a simplified analysis of circular geocentric orbits for which the Earth, spacecraft, and Sun are coplanar. It has been reported that the angular accelerations required for certain demanding noncoplanar tracking maneuvers may be as much as an order of magnitude larger than the results obtained for the simpler coplanar case (ref. 1). However, these large accelerations are typically required only when the spacecraft, Sun, and ground site are nearly colinear; in which case it happens that the energy reflected from the satellite is so small as to eliminate such maneuvers from practical consideration. In this report, a factor of two increase in tracking control requirements is included to account for noncoplanar effects.

The other major simplifying assumption employed in this study is that the large spacecraft behaves essentially as a rigid body during maneuvers so that unfavorable dynamic interactions between

the control system and the flexible structure may be ignored. The designs must, on this basis, be considered incomplete. For some past systems (for example, the square solar sailer), the dynamic and helioelastic effects made gross changes in the design necessary. The criteria presented herein would not yield useful results in that case. For the present study, it is hoped that substantial requirements for the stability of structural shape under static loads will be sufficiently demanding to result in a valid foundation for preliminary design. Even if dynamic effects are found to be important, the criteria presented herein may still be useful as a first step in the synthesis of a satisfactory control system.

In addition to parametric investigations of several different types of control actuators, the details of a baseline design for a control actuator are presented. The design of this control actuator is based on the rigid-body mass properties of a 1-km-diameter baseline spacecraft design, which is discussed in detail in Part II. For control-system design purposes, this spacecraft is modeled as a uniform flat circular disk with radius 500 m and mass density of approximately 10 g/m^2 . In order to estimate power requirements and component masses for the baseline design control actuator, it was necessary to make certain arbitrary assumptions regarding the relative size of such secondary components as motors, bearings, linkages, fittings, and the like. It is believed that all such assumptions are conservative, and that they may be eliminated only after more detailed hardware-definition studies have been completed.

Use of trade names or names of manufacturers in this report does not constitute an official endorsement of such products or manufacturers, either expressed or implied, by the National Aeronautics and Space Administration.

SECTION 2

TRACKING AND REORIENTATION REQUIREMENTS

Reported in this section are the results of kinematic and insolation studies for a solar-reflecting satellite in a geocentric circular orbit coplanar with the Earth and Sun. Three separate aspects of the study are reported: (1) satellite accelerations, velocities, and displacements during over-site tracking maneuvers; (2) satellite accelerations, velocities, and displacements during between-site reorientation maneuvers; (3) satellite accelerations from solar sailing; and (4) optimal flight plan studies that investigated the maximum-total-insolation maneuver between closely spaced sites.

2.1 OVER-SITE TRACKING MANEUVERS

Consider a satellite in circular Earth orbit, coplanar with the Earth and Sun. Let the Earth and Sun represent stationary points in space, and assume that the Earth-to-Sun distance is arbitrarily large in comparison with the Earth-to-satellite distance. This situation is depicted in Figure 1, where the Earth is labeled E, the Sun S, and the satellite s. Furthermore, the point on the Earth's surface located at the center of the reflected light beam is labeled p.

Assuming that the orbital period of the satellite is much smaller than the Earth's rotational period of 24 hours, we neglect the rotation of the Earth about its spin axis. Thus, the fixed reference direction E_p may be chosen as a basis for angle measurement. Note that E_p coincides with the local zenith at the insolation-receiving site on Earth. Now the "local Sun angle" (or time of day) at p may be specified by the angle ϵ between E_p and ES. Furthermore, the position of the satellite relative to the Earth is specified by the geocentric angle ϕ between E_p and Es. Let the radius of the Earth be $R_e = 6,372$ km, which is also

the length of E_p . Let the geocentric altitude of the satellite be R , the length of E_s . Then the satellite altitude above the Earth's surface is $h = R - R_e$.

Relative to the Earth site p , the satellite is located by the colatitude β , the angle between E_p and ps . The elevation angle θ of the satellite relative to the horizon at p is $\pi/2 - \beta$. The "range" of the satellite d relative to p is the length of ps .

Let θ denote the angular orientation of the satellite relative to E_p . Furthermore, let γ denote the angle of incidence of sunlight on the reflecting film of the satellite, as shown.

A nondimensional measure of the satellite altitude is given by b where

$$b = \frac{R}{R_e} = 1 + \frac{h}{R_e} \quad (1)$$

It has been shown in ref. 1 that in terms of the satellite geocentric angle ϕ , the range of the satellite is given by

$$d = cR_e \quad (2)$$

where

$$c^2 \equiv 1 + b^2 - 2b \cos \phi \quad (3)$$

Furthermore,

$$\beta = \phi + \sin^{-1} \left(\frac{\sin \phi}{c} \right) \quad (4)$$

$$\delta = \frac{1}{2} (\epsilon + \beta) \quad (5)$$

$$\gamma = \frac{1}{2} (\pi - \epsilon + \beta) \quad (6)$$

For sufficiently large ϕ , the satellite is not visible at the Earth site p. Thus, the satellite is considered to be "over the site" at p whenever $-\pi/3 < \beta < \pi/3$. This condition defines a 60-degree "useful viewing cone" whose axis is E_p , the zenith at the Earth site p. The range of values of ϕ corresponding to the satellite being over the site is then given by

$$-\left[\frac{\pi}{3} - \sin^{-1} \left(\frac{\sqrt{3}}{2b}\right)\right] \leq \phi \leq \left[\frac{\pi}{3} - \sin^{-1} \left(\frac{\sqrt{3}}{2b}\right)\right] \quad (7)$$

Under these conditions, the angular position, velocity, and acceleration of the satellite regarded as a function of ϕ may be expressed as

$$\delta = \frac{1}{2} \left[\epsilon + \phi + \sin^{-1} \left(\frac{\sin \phi}{c} \right) \right] \quad (8)$$

$$\dot{\delta} = \frac{\dot{\phi}}{2} \left\{ 1 + \frac{1}{c} \frac{\left[\cos \phi - b \left(\frac{\sin \phi}{c} \right)^2 \right]}{\sqrt{1 - \left(\frac{\sin \phi}{c} \right)^2}} \right\} \quad (9)$$

$$\ddot{\delta} = - \frac{\dot{\phi}^2 b(b^2 - 1) \sin \phi}{2c^4} \quad (10)$$

where

$$\dot{\phi} = b^{-3/2} (g/R_e)^{1/2} \quad (11)$$

is the constant orbital angular velocity of the satellite in circular Earth orbit, and $g = 9.81 \text{ m/s}^2$ is the acceleration of gravity on Earth.

Presented in Figures 2 and 3 are plots of δ , $\dot{\delta}$, and $\ddot{\delta}$ for the tracking maneuver described above as functions of ϕ , θ , and time on parallel scales. Several features of these plots are noteworthy. First, the angular acceleration time history is anti-symmetric about the midpoint in the maneuver, and the angular velocity time history is therefore symmetric, with equal velocities at entry and exit. This feature has a major bearing on the selection of a suitable control actuator configuration since it results in a requirement for zero net angular impulse during the maneuver. This fact may be demonstrated as follows: Let I_Y represent the mass moment of inertia of the satellite about a diameter ($I_Y \approx 4.91 \times 10^8 \text{ kg-m}^2$ for the baseline design). Then the required control torque T on the satellite during the tracking maneuver is

$$T = I_Y \ddot{\delta} \quad (12)$$

Thus, the angular impulse accumulated between times t_0 and t_1 is

$$\int_{t_0}^{t_1} T dt = \int_{t_0}^{t_1} I_Y \ddot{\delta} dt = I_Y [\dot{\delta}(t_1) - \dot{\delta}(t_0)] = I_Y \Delta \dot{\delta} \quad (13)$$

where $\Delta \dot{\delta}$ represents the net change in satellite angular velocity $\dot{\delta}$. Since there is no net change in $\dot{\delta}$ during the complete maneuver, the required control actuator need not expend any net angular impulse during the maneuver. This result provides a significant advantage for momentum storage control systems, as later shown.

A second important feature shown in Figures 2 and 3 is the near linearity of the time history of δ (or $\delta - \epsilon/2$). This shows that the required angular orientation of the satellite during maneuvers deviates very little (only a few degrees) from the orientation which would naturally result if the satellite were allowed to freely tumble at a constant average angular velocity.

Given in Table I are the maximum angular acceleration and maximum angular velocity change dictated by the kinematics of Eqs. (8) through (10) for an orbital altitude of $h = 2400$ km and $h = 4146$ km. Also presented in this table are the corresponding maximum control torques and maximum angular impulses which result for the baseline satellite with $I_y = 4.91 \times 10^8$ kg-m².

Because of the large size of the baseline satellite design, the control actuator will have to perform tracking maneuvers in the presence of substantial and unfavorable gravity-gradient loading. Let I_z denote the polar mass moment of inertia of the satellite, and let I_y denote the mass moment of inertia about a diameter. It may then be shown (ref. 2) that the component of the satellite gravity-gradient torque T_{GG} in the direction of δ has a maximum magnitude of

$$T_{GG} = \frac{3}{2} \dot{\phi}^2 I_y \left(\frac{I_z - I_y}{I_y} \right) \quad (14)$$

when $\delta = \phi + \pi/4$. For the baseline satellite, $I_y = 4.91 \times 10^8$ kg-m². Furthermore, modeling the satellite as a uniform flat disk results in $I_z = 2 I_y$.

Presented in Table I are the values for the worst-case gravity-gradient torques T_{GG} resulting from Eq. (14) when the values for I_y and I_z indicated above are used, and when Eq. (11) is used to obtain ϕ at orbital altitudes of 2400 km and 4146 km. Also presented in Table I are values for the equivalent maximum angular

acceleration, determined by dividing T_{GG} and I_y . Conservative estimates of the maximum angular impulse and angular velocity change due to gravity-gradient loading were determined by multiplying the torque and the angular acceleration values, respectively, presented in the table by the total time duration of the tracking maneuver, or "time over the site."

2.2 BETWEEN-SITE REORIENTATION MANEUVERS

The flight plan calls for the satellite to track more than one Earth site during each orbit. This requires the satellite to reorient its angular position and velocity while it is between the useful viewing cones of adjacent Earth sites. A minimum-time strategy for achieving the reorientation results in the application of a "bang-bang" control torque time history while the satellite is between sites. The amplitude and duration of the control torques during the acceleration and deceleration phases of the reorientation maneuver depend on the time available for the maneuver and the net change in angular position and velocity which the maneuver must accomplish. However, since the required angular velocity of the satellite upon exit from a typical tracking maneuver is identical to that required upon entry, the reorientation maneuver must accomplish no net change in angular velocity, and hence, no net angular impulse is required of the control actuator during reorientation. This fact again favors momentum storage control actuators as previously discussed. The resulting bang-bang position control strategy requires the application of equal and opposite control torque pulses of equal duration. The magnitude of the satellite angular acceleration $\ddot{\delta}_0$ during such a maneuver is then given by

$$\ddot{\delta}_0 = \frac{4 \Delta \delta}{(\Delta t)^2} \quad (15)$$

where $\Delta\delta$ is the net change in angular position which the reorientation maneuver must accomplish, and Δt is the "between-site time," or the total time available for reorientation while the satellite is between the useful viewing cones of adjacent Earth sites.

For the case in which the flight plan calls for tracking N equally spaced Earth sites on each orbit, it can be shown that

$$\Delta t = 2 b^{3/2} (g/R_e)^{-1/2} \left[\frac{\pi}{N} - \frac{\pi}{3} + \sin^{-1} \left(\frac{\sqrt{3}}{2b} \right) \right] \quad (16)$$

where b is given by Eq. (1). Since both sides of the film surface of the satellite may be used to reflect sunlight during tracking, the maximum net change $\Delta\delta$ in satellite angular position which could ever be required during reorientation is

$$\Delta\delta_{\max} = \frac{\pi}{2} \quad (17)$$

Thus, a worst-case estimate of required angular acceleration levels during reorientation may be obtained by substituting from Eqs. (16) and (17) into Eq. (15). The results for the cases of $N = 1$ and 2 for altitudes of $h = 2400$ km and $h = 4146$ km are presented in Table II. Also presented are corresponding values for control torque $T = I_y \ddot{\delta}_0$, maximum angular velocity change $\Delta\dot{\delta}_{\max} = \dot{\delta}_0(\Delta t)/2$, and maximum angular impulse $= I_y \Delta\dot{\delta}_{\max}$. It is later shown that for cases when $N = 1$ and 2 , the largest control torque and angular impulse requirements are the result of over-site tracking and not between-site reorientation maneuvers.

When $N = 6$, it is found that reorientation maneuvers place larger demands on the control actuator than tracking maneuvers. In fact, the demands are so large that none of the candidate control actuators is capable of providing the worst-case control capability without excessive control-system weight. For this reason, a refinement in the analysis was made for $N = 6$. A detailed examination of the required angles in this case reveals that

$$\Delta\delta = \begin{cases} -0.818 \text{ radian at } h = 2400 \text{ km} \\ -0.563 \text{ radian at } h = 4146 \text{ km} \end{cases} \quad (18)$$

Substituting the values presented in Eq. (18) into Eq. (15) results in angular acceleration, maximum angular velocity change, control torque, and maximum angular impulse presented in Table II for $N = 6$. However, it is later shown that even for the detailed (as opposed to worst-case) results presented in Table II for $N = 6$, none of the candidate control actuators is capable of meeting the demands without becoming excessively large or heavy.

An analysis for serving four equally spaced sites along the equator by reflector spacecraft in a 2720-km equatorial orbit resulted in an angular acceleration of $1.86 \times 10^{-6} \text{ rad/s}^2$ which is nearly equal to the coplanar tracking value ($1.87 \times 10^{-6} \text{ rad/s}^2$) shown in Table I. Therefore, it appears feasible to serve four sites during a single orbit pass from 2720 km without exceeding the structural load limits established in this study.

2.3 OPTIMAL FLIGHT PLAN STUDIES

In order to maximize the total amount of solar energy received by the Earth during each orbit of a satellite, it is desirable to track more than one Earth site. However, tracking many Earth sites results in very little time for between-site reorientation, and correspondingly high levels of control torque required for reorientation maneuvers. Furthermore, this effect is exaggerated at high altitudes because the distance between useful viewing cones of adjacent sites decreases rapidly with increasing altitude. Eventually the cones intersect and overlap at sufficiently high altitudes leaving no time at all for reorientation. While the tracking of multiple sites at high altitudes may result in excessive control requirements for reorientation, it is found that high altitude orbits have the compensating advantage of delivering more reflected solar energy to an Earth site during each tracking

maneuver than possible at lower altitudes. It is also found that the Sun angle ϵ (or local Sun time) plays an important role in this characterization of satellite performance.

The tradeoff between excessive reorientation control requirements and increased energy delivery for multiple-site flight plans was studied, and a brief summary of the results is presented in this section. The study centered on determining the total reflected solar energy per unit area E_{1+2} received on the Earth at two adjacent sites p_1 and p_2 during a typical tracking-reorientation-tracking maneuver. In particular, the percentage of increase in E gained by tracking the second site p_2 in addition to site p_1 was examined as a function of several variables. Included among these variables are the available level of control torque T_R during bang-bang reorientation maneuvers, and the time of initiation of reorientation maneuvers for cases in which the required reorientation time must displace a portion of the tracking time at either site. Let E_1 be the total reflected solar energy per unit area received at site p_1 during a complete over-site tracking maneuver, and let T_T be the required level of control torque for the tracking maneuver. Then for the case when p_1 and p_2 are separated by 20 degrees longitude, and for an orbital altitude of 2400 km, the results for E_{1+2}/E_1 versus T_R/T_T are presented in Figure 4 for a local Sun angle at site 1 of $\epsilon_1 = 10$ degrees (near noon) with a solid line and $\epsilon_1 = 100$ degrees (near dusk) with a broken line. The curves represent values which have been optimized over the time of initiation of the reorientation maneuver, in order to maximize the results for E_{1+2}/E_1 for a given T_R/T_T . When the orbital altitude is increased to 4146 km, the analogous results are presented in Figure 5. The figures show that even for a reorientation torque T_R which is 100 times larger than the tracking torque T_T , the total reflected solar energy is increased by less than 60 percent in all cases and less than 28 percent in one case. These results apply to the case of 20 degrees longitudinal spacing between sites p_1 and p_2 , or equivalently, to 18 equidistant Earth sites.

For the case of 60 degrees longitudinal spacing between sites (six equidistant Earth sites) at an orbital altitude of 2400 km, similar results are presented in Figure 6. (The effects of satellite eclipsing have been included in the analysis.) This time it is found that a maximum percentage increase in E of less than 50 percent is possible in either case while the increased separation between sites has lowered the required reorientation torque T_R to about 10 times T_T .

From these studies it was concluded that the costs in terms of excessive control actuator weight and power requirements necessary to track more than two or three Earth sites were not justified by the relatively small gain in total reflected solar energy E which is obtained. Furthermore, it was decided that a flight plan calling for the tracking of two equidistant Earth sites each orbit, the sites having a local Sun time near dawn and dusk, respectively, was a near optimal baseline flight plan for the satellite. The particular choice of local Sun times for the Earth sites is justified by the results shown in Figure 7. This figure presents plots of \hat{E}_1 , a normalized version of E_1 , versus local Sun time ϵ_1 , for orbital altitudes of $h = 2400$ km and $h = 4146$ km. In particular, \hat{E}_1 is equal to E_1 divided by the local solar radiant power flux at the site p_1 at high noon, and has units of seconds (or "Sun seconds"). As shown in the figure, each curve has a large peak near dawn or dusk, then drops to zero for larger sun angles due to eclipsing. It is also clear from this figure that \hat{E}_1 increases markedly with increasing orbital altitude.

SECTION 3

CONTROL ACTUATOR SIZING AND DESIGN

Reported in this section are a comparison of several potential control actuator configurations capable of meeting the mission requirements, the reasons for the selection of a primary Control-Moment Gyro (CMG) system and a secondary Magnetic Loop Control (MLC) system, and the main features of the baseline design of each.

3.1 POTENTIAL CONTROL ACTUATOR CONFIGURATIONS

A total of seven different control system concepts were considered including CMGs, MLCs, reaction wheels, solar-pressure panels, multifaceted reflector panels, retractable weight controllers, and reaction control jets. In contrasting these systems, attention was focused on three main aspects: (1) available torque and angular impulse; (2) required mass, power, and energy storage; and (3) stowage and deployment requirements.

3.1.1 Control Moment Gyroscopes (CMG)

CMGs have been used extensively for spacecraft attitude control and constitute a familiar technology. Basically, a CMG consists of a constant speed flywheel mounted through gimbals to the spacecraft. Control torques are produced by tilting the flywheel spin axis with respect to the spacecraft, using torque motors, which results in gyroscopic moments being transmitted through the gimbal bearings.

The particular CMG considered is a counter-rotating, twin-rotor configuration with a coning suspension to minimize cross-coupling between control axes and to take advantage of mechanical torque amplification. The rotor spin axes are nominally aligned along the Astromast column hub which provides attitude control in

essentially every direction except spin about the column hub. The control torque vector available from such a 2-degree-of-freedom CMG lies in the plane of the reflecting film and has a magnitude approximately proportional to the product of the angular momentum of the wheels and the gimbal angular velocities (rates) relative to the spacecraft. Thus, large control torques may be developed by simply producing large gimbal rates with the torque motors. However, maneuvers requiring large angular impulses may result in large gimbal angles, and eventually "gimbal lock," wherein the CMG is said to be saturated. A primary consideration in selecting and sizing a CMG for a given maneuver is, therefore, the total angular impulse it may deliver before saturation occurs.

An analysis of the dynamics of a rigid satellite with a twin-rotor CMG is presented in Jacot and Liska in ref. 3. For the case when gimbal angles are small (to avoid saturation) and gimbal rates are much larger than vehicle rates (for large control torques), they present in their Eq. (16) the following vehicle equation of motion:

$$2H_w \dot{\theta} \cong I_y \ddot{\delta} \quad (19)$$

where H_w is the magnitude of the angular momentum of each wheel, $\dot{\theta}$ is the gimbal rate, I_y is the satellite mass moment of inertia about a diameter, and $\ddot{\delta}$ is the satellite angular acceleration about a diameter. Now, integrating Eq. (19) with respect to time for a given satellite maneuver, such as tracking or reorientation, one obtains

$$2H_w \theta_{\max} = I_y \dot{\delta}_{\max} \quad (20)$$

where the quantity on the right-hand side is the maximum angular impulse required for the satellite maneuver, and θ_{\max} is the maximum gimbal angle which accumulates during the maneuver.

Equation (20) may be used for preliminary CMG design by, for example, selecting θ_{\max} to be conveniently small to avoid saturation (say 10 degrees), and then solving for the required angular momentum H_w of each wheel. The selection of an acceptable flywheel may then be made using this estimate of the required H_w and current flywheel and material technology (ref. 4).

As reported later, the required H_w for the baseline satellite and maneuvers was so large as to make very unattractive the notion of using a rigid flywheel capable of fitting within the Shuttle bay. Instead, a large deployable filamentary flywheel design was selected.

The peak power required to drive the gimbals of a CMG during maneuvers is nearly equal to the peak power transmitted to the satellite during maneuvers by the control torque. For the baseline configuration, this power is very small, as is the required energy storage for maneuvers during an entire Earth orbit.

3.1.2 Magnetic Loop Controllers (MLC)

The interaction of the Earth's magnetic field with the magnetic field produced by conductor loops carrying electric current onboard the spacecraft may be used to provide torques for spacecraft attitude control (refs. 5 and 6). If a current i is passed through a coil of N turns lying in a plane with unit normal vector \underline{n} and enclosing an area A_c , the resultant torque \underline{T} on the satellite will be

$$\underline{T} = (NA_c i) \underline{n} \times \underline{B} \quad (21)$$

where \underline{B} is the Earth's magnetic induction vector in the vicinity of the satellite. Because of the large area A_c enclosed within the perimeter of large space structures, substantial control torques may be produced without requiring large currents. This advantage has been recognized in previous design studies for large spacecraft in Earth orbit (refs. 7 and 8). However, as a result of the cross product in Eq. (21), the direction of the control torque available from an MLC is restricted to the plane orthogonal to the local magnetic induction vector \underline{B} . In order to produce a control torque oriented arbitrarily within the plane orthogonal to \underline{B} , an ensemble of many separate coils with end points staggered around the rim, and with independently controlled reversible currents may be employed (ref. 9). Note that a MLC could produce only small pitching moments for maneuvers in an equatorial orbit.

As seen in Eq. (21), the magnitude of the torque is proportional to the current in the conductor loops. Furthermore, it may be shown that the electric power required to provide the torque is given by

$$P = (\pi D)^2 (iN)^2 \sigma \rho / M_c \quad (22)$$

where D is the diameter of the coil, σ is the resistivity of the conductor material, ρ is the mass density of the conductor material, and m_c is the total mass of the coiled conductor. Eqs. (21) and (22) may be used to determine the size of the required conductor coil as follows. First, Eq. (21) may be used to determine the current multiple iN required for a given torque magnitude T , magnetic induction B , and enclosed area A_c . To account for unfavorable orientation of \underline{B} , and angle θ (say 45 degrees) between \underline{n} and \underline{B} may be used to determine the required total mass M_c of coiled conductor of a known material, for a specified power level P . If the power is selected to be sufficiently small (on the)

order of 100 watts), solar photovoltaic cells may be used for continuous power so that a minimum of energy storage is required, and the system is not limited in ability to produce large angular impulses. Furthermore, the system has the advantage of stowage and deployment within the reflector rim structure, and an anticipated high reliability due to a minimum of moving mechanical parts.

As reported later, an MLC was selected for the baseline design to provide continuous control of such secondary disturbances as CMG desaturation and small continuous environmental torques due, for example, to misalignment between the solar pressure resultant and the satellite center of gravity.

3.1.3 Reaction Wheels

Reaction wheels are perhaps the simplest momentum storage devices for the spacecraft attitude control and have long been used for this purpose. A reaction wheel consists of a flywheel with a spin axis fixed to the spacecraft. Control torques are produced by accelerating or decelerating the flywheel relative to the spacecraft with a torque motor. The magnitude of the available control torque is determined by the rate of acceleration or deceleration of the flywheel so that large torques may be obtained by rapid flywheel acceleration or deceleration. However, maneuvers requiring sustained control torques and correspondingly large angular impulses tend to deplete the angular momentum stored in the wheel. Thus, the maximum angular impulse required for maneuvers is a primary design consideration for reaction wheels as it was for CMGs. For a single-rotor, single-axis reaction wheel, it can be shown that the minimum angular momentum H_w which must be stored in the flywheel is determined by

$$H_w = I_y \dot{\Delta\delta}_{\max} \quad (23)$$

where the quantity on the right-hand side is just the maximum angular impulse required for satellite maneuvers. The selection of an acceptable flywheel may be made using this estimate of the required momentum, together with current flywheel and material technology (ref. 4).

Reaction wheels were not chosen for this large space structure application because of their inherent disadvantages of large power and energy storage requirements, large mass, and large torque motors which are required for their operation. It can be shown that the power required for the torque motor to accelerate and decelerate the flywheel is proportional to the ratio of the mass moment of inertia of the satellite about a diameter to the spin axis moment of inertia of the flywheel. For large space structures, the satellite moment of inertia is several orders of magnitude larger than the flywheel moment of inertia, even for deployable flywheels which are quite large by current technological standards. For the particular flat-disk shaped satellite application, reaction wheels of the required size are difficult to integrate with the membrane and structural configuration to form a multiaxis control system. Also, the required torque motors must be capable of delivering directly all of the required torque for satellite maneuvers while operating over a large speed range at high power.

3.1.4 Solar-Pressure Panels

Because the proposed orbital altitude for the satellite is well above 800 km, the solar pressure is larger than atmospheric drag, opening the possibility of solar-pressure control. This possibility is further enhanced by the large area of reflecting film which forms a major part of the satellite. However, in order to obtain controllable forces and torques during maneuvers, one method is to append solar-pressure panels to the satellite in such a manner that they may be individually "feathered" or oriented with respect to the Sun.

To investigate the practicality of solar-pressure panels for the application at hand, a particular configuration consisting of two circular panels of radius r attached to the satellite rim are considered. The panels are assumed to be attached at points which lie on a diameter of the satellite, and it is assumed that they may be rotated relative to the satellite about this diameter. For such a configuration, it is clear that the maximum moment is produced about the satellite center of mass when the Sun direction is orthogonal to one of the panels with the other panel fully feathered. When the contribution of the two panels to the satellite moment of inertia is accounted for, the greatest satellite angular acceleration $\ddot{\delta}$ which is produced in such a configuration can be shown to be

$$\ddot{\delta} = \frac{8p_0}{m_a D} \frac{\eta^2 (1 + \eta)}{1 + 2\eta^4 + 8\eta^2 (1 + \eta)^2} \quad (24)$$

where $p_0 = 0.905 \times 10^{-5} \text{ N/m}^2$ is the solar pressure near the Earth, m_a is the average mass per unit surface area of satellite and solar panel system, D is the satellite diameter, and $\eta = 2r/D$ is the ratio of the solar panel to satellite radius. Maximizing the function of η , it can be shown that the maximum possible angular acceleration may be obtained by requiring the panel radius r to take on the value

$$r_{\text{opt}} = 0.274 D \quad (25)$$

This results in the areas of each panel being 30.1 percent of the area of the satellite reflector surface; the resulting upper bound on available angular acceleration is

$$\ddot{\delta}_{\max} = 0.134 \frac{4p_0}{m_a D} \quad (26)$$

When the values for m_a and D , appropriate to the satellite baseline design configuration, are substituted into Eq. (26), it is found that the resulting upper bound $\ddot{\delta}_{\max}$ is too small to provide the required vehicle accelerations either for oversite tracking or between-site reorientation, with the possible exception of reorientation for one site only within each orbital period at an altitude of 4146 km. While other panel shapes and configurations may result in improved system performance, it is not likely that any other configuration will produce an improvement sufficient to make this concept more attractive than the deployable CMG previously mentioned. Furthermore, the anticipated benefits of unlimited angular impulse and low power and energy storage requirements inherent with a solar-pressure controller must be weighed against the substantial increase in vehicle mass for panels of the size required for a large space structure, and significantly increased stowage, deployment, and structural attachment problems.

3.1.5 Multifaceted Reflector Panels

Consideration was given to a control concept based on a completely different structural configuration for the large reflector surface. Instead of forming the reflector surface out of one very large membrane stretched within one very large circular rim, the surface may be formed from an assemblage of many smaller panels or facets, each with its own structural support which is attached to an overall rigid frame. By essentially gimbaling each facet to the frame, and coordinating the relative motion of each facet, it becomes possible to control or change the direction of the reflected light beam without having to change the orientation of the overall satellite frame. Thus, the satellite frame may continue to tumble in a free fall during tracking maneuvers while minor

corrections in facet orientation relative to the frame are accomplished. Such a "venetian blind" arrangement would require less control power and energy than would be required to reorient the entire satellite frame. Furthermore, the need for between-site satellite frame reorientation is greatly reduced, which makes it possible to track more Earth sites on a single orbit. An analysis of a rectangular frame with many movable narrow horizontal facets confirmed that for practical mass distributions the facet motion is largely uncoupled from frame motion under the requirement of conservation of satellite angular momentum. Control of facet orientation could be accomplished by small solar-cell-powered torque motors.

Although the concept appears to be quite feasible and promising from the point of view of reducing the requirements for satellite attitude control, it has several inherent disadvantages which prevented further consideration. Chief among these disadvantages is the complexity of the required structural gimbals connections at the facet-frame interface and the difficulty in conceiving a compactly stowed, self-deploying configuration for such a satellite. The multifaceted reflector panel concept would be considerably more attractive if it were practical to assemble the satellite in space.

3.1.6 Retractable Weight Controllers

As previously noted, the basic over-site tracking maneuver in the coplanar case reveals that satellite angular velocity at entry and exit of the maneuver are exactly equal. This fact suggests the possibility of accomplishing the maneuver by simply moving weights along the satellite column hub to vary the overall satellite mass moment of inertia. Such a concept would provide the capability to increase or decrease the satellite angular velocity by simply moving a pair of weights in toward or away from the satellite center of mass, in a manner analogous to a

spinning figure skater extending and retracting her arms. A simple analysis for a typical tracking maneuver reveals that while the required control power and energy storage requirements are small, the required movable control masses must weigh at least as much as the entire satellite. Such a large relative mass for a control system would be impractical. Another major disadvantage of such a control system is that it is not capable of changing the instantaneous axis of rotation of the satellite and would only be useful for coplanar tracking maneuvers.

3.1.7 Reaction Control Jets

Reaction control jets are probably the oldest and most familiar of all modern spacecraft attitude and position control systems. The thrust produced by unidirectional expulsion of mass from a control jet located on the rim of the satellite could be used to provide control forces and torques for maneuvers. The high specific impulse available from the contemporary generation of control jets makes them quite efficient as thrust sources for many applications. However, control jets have several disadvantages which make them much less attractive than momentum storage devices for the particular baseline satellite maneuvers considered herein. Chief among these disadvantages is the fact that control jets must expel mass with every usage and cannot be recharged by solar cells or other continuous-power sources. As noted earlier, the angular impulses required from the control actuator during the first and second half of the coplanar oversite tracking maneuver are exactly equal and opposite. This fact provides considerable advantage for momentum storage devices which may recover, during the second half, the angular impulse expended during the first half of the maneuver. On the other hand, reaction control jets do not benefit in any particular way from this characteristic of the required maneuver and must be launched with sufficient expellent mass to provide the capability for all maneuvers during the unattended lifetime of the satellite.

For a reaction-jet control actuator with four jets equally spaced around the satellite rim, the total required expellent mass m_e is given by

$$m_e = \frac{I_{tot}}{D I_{sp}} \quad (27)$$

where I_{tot} is the total satellite angular impulse required for attitude control and all maneuvers during the entire lifetime of the satellite, D is the satellite diameter, $g = 9.81 \text{ m/s}^2$ is the acceleration of gravity on Earth, and I_{sp} is the specific impulse of the particular control jet under consideration. Using a value of $I_{sp} = 200$ seconds typical for the current generation of chemical propulsion systems, and estimating I_{tot} for the baseline satellite maneuver for a 5-year lifetime to be 1.16×10^{11} N-m-s for an altitude of 2400 km, and 1.22×10^{10} N-m-s for 4146 km, Eq. (27) reveals for a 1-kilometer-diameter satellite that the required expellent mass is approximately seven times the total satellite mass for the lower altitude and 70 percent for the higher altitude. It is possible that future developments in solar-electric (ion propulsion) devices may provide specific impulses on the order of $I_{sp} = 10,000$ seconds. In that case, the required expellent mass drops to 14 percent of the vehicle mass for the lower altitude, and only 1.4 percent for the higher altitude. But such devices are not currently available and require significant technological advances.

3.2 COMPARISONS BETWEEN MOST ATTRACTIVE CONFIGURATIONS

As previously discussed, the use of solar pressure panels as a control system configuration must be eliminated for the application at hand since it is not capable of producing enough control torque to accomplish the baseline maneuvers. Multifaceted reflector panels must also be eliminated because of difficulties

in deployment, stowage, and structural design. Furthermore, the mass of a properly sized reaction control jet or retractable weight control system would equal or exceed the total vehicle mass, so they must also be discarded. In what follows, the remaining three potential control systems are evaluated and compared quantitatively on the basis of the required mass, power, and energy storage for the baseline satellite and baseline maneuvers for an altitude of 2400 km and an altitude of 4146 km.

3.2.1 Deployable Filamentary Control-Moment Gyroscopes (CMG)

Consider a CMG to be capable of producing the required angular impulse for both oversite tracking in the presence of unfavorable gravity-gradient torques, and between-site reorientation. Furthermore, to account for noncoplanar maneuvers and the maintenance of attitude stability, let the CMG be designed for twice the required angular impulse determined by the criteria just described. Finally, let the total mass of the CMG wheels determine according to these criteria be doubled to account for gimbals, linkages, motors, fittings, etc. A summary of the results obtained by this procedure and explained below is presented in Table III.

From Table I, the required satellite angular impulse for the over-site tracking phase is 7.46×10^5 N-m-s for an orbital altitude of 2400 km, and 5.67×10^5 N-m-s at 4146-km altitude. From Table II for two Earth sites, the required angular impulse for the between-site reorientation phase is 4.92×10^5 N-m-s for an altitude of 2400 km, and 4.19×10^5 N-m-s at 4146-km altitude. Hence, the tracking requirements govern the design in the case of two Earth sites.

Using the maximum angular impulses determined above, and an arbitrarily selected maximum gimbal angle of $\theta_{\max} = 0.175$ rad (10 degrees), Eq. (20) may be used to show that the minimum flywheel

momentum storage requirement is 2.13×10^6 N-m-s at 2400-km altitude, and 1.62×10^6 N-m-s at 4146-km altitude. Doubling these values to account for noncoplanar maneuvers, etc., results in the design momentum storage requirements of $H_w = 4.26 \times 10^6$ N-m-s at 2400-km altitude, and $H_w = 3.24 \times 10^6$ N-m-s at 4146-km altitude.

The selection of a flywheel capable of storing a given angular momentum H_w is governed by both the geometrical shape of the wheel and the specific working stress of the material (ref. 4). The optimal flywheel shape for momentum storage is that of a radially thin annular ring of average radius r . For such a wheel made of a material with working stress σ_w and mass density ρ , it may be shown that

$$H_w = Mr \sqrt{\frac{\sigma_w}{\rho}} \quad (28)$$

where M is the mass of the wheel. For a wheel made of glass fiber with $\sigma_w = 7.58 \times 10^8$ N/m² (110,000 psi) and $\rho = 2.08 \times 10^3$ kg/m³ (0.075 lb/in³), and for a radius of $r = 2$ m small enough to fit within the Shuttle bay, Eq. (28) can be used to show that the required wheel mass is $M = 3,530$ kg for an altitude of 2400 km, and $M = 2,680$ kg at a 4146-km altitude. The twin-rotor CMG requires two such wheels. Doubling the total wheel mass to account for gimbals, motors, and linkages results in a total CMG mass of $M_{CMG} = 14,120$ kg for an altitude of 2400 km, and $M_{CMG} = 10,720$ kg at 4146-km altitude. Since these CMG masses (which are overly) optimistic in terms of the wheel geometry) are larger than the mass of the entire satellite, the notion of using rigid flywheels with radius sufficiently small to fit within the Shuttle bay must be discarded.

From Eq. (28) it is clear that the CMG mass may be reduced only by increasing the wheel radius r , which means that a deployable flywheel is required. The feasibility of using deployable

wheels for momentum and energy storage was first discussed 10 years ago (refs. 10 and 11). Such wheels could be made of fine mesh or cloth of small filaments with fiber paths chosen to result in constant fiber tension at all locations. Such "isotensoid" wheels utilize the fiber material in an optimal manner. For the particular isotensoid case of helical fiber paths with circular projections on the equatorial plane as shown in Figure 8, the replacement for Eq. (128) is

$$H_w = \frac{1}{2} Mr \sqrt{\frac{\Omega \sigma_w}{\rho}} \quad (29)$$

where Ω is a dimensionless parameter which depends on the thickness-to-radius ratio of the wheel (ref. 11). (For a flat disk, $\Omega = 2$.) Since a spinning flexible flat disk is known to undergo significant warping of the equatorial plane during forced precession of the spin axis, a design configuration with thickness-to-radius ratio of 0.1 was selected, which resulted in a significantly three-dimensional wheel with cross section shown in Figure 8. It is anticipated that such a shape will substantially restrict this warping during CMG gimbal motions. For this particular shape, it may be shown that $\Omega = 1.998$. Substituting $\Omega = 2$ in Eq. (29), arbitrarily selecting a wheel radius of $r = 20$ m, and using the same glass fiber properties, gives the required wheel mass to be $m = 499$ kg at 2400-km altitude, and $M = 380$ kg at 4146-km altitude. The resulting total CMG mass obtained as previously described is then $M_{CMG} = 2000$ kg at 2400-km altitude and $M_{CMG} = 1520$ kg at 4146-km altitude. These parameters were chosen for the baseline design of the primary satellite control actuator and appear in Table III. For comparison purposes, a satellite flight plan requiring the tracking of six equidistant Earth sites would result in a CMG design governed by between-site reorientation maneuvers, and a total CMG mass of $M_{CMG} = 5260$ kg for 2400-km altitude (9460 kg using NASA-supplied accelerations of 3.5×10^{-5} rad/s²), and $M_{CMG} = 15,200$ kg at 4146-km altitude.

An overall view of the baseline twin-rotor CMG with coupling suspension mounted on the satellite center body is shown in Figure 9. The broken lines in the figure indicate the positions of the wheels at the maximum gimbal angle of 10 degrees. A cutaway view through a wheel hub in Figure 10 indicates one simple method of providing the necessary coning suspension for the wheels. Basically, the arrangement consists of a biaxially gimballed inner (nonrotating) bearing race whose gimbal angles are controlled by push rods driven by torque motors equidistant between the wheels. Coning action is achieved by driving the push rods for both wheels through a common bell crank with the same torque motor, as shown. The resulting suspension produces the same kinematic relation between wheel orientations as that indicated schematically in Figure 9 of ref. 3. Also located within the inner bearing is a "pancake" electric motor for controlling the flywheel spin velocity.

The power required by the torque motors to drive the gimbals during maneuvers may be obtained by multiplying the instantaneous torque on the gimbals by the corresponding instantaneous angular velocity of the gimbals relative to the satellite. By linearizing the equations of motion presented in ref. 3 as previously described, an estimate of the average power required by the CMG is obtained

$$P_{avg} = \frac{2 (I_y \dot{\Delta\delta}_{max}) \dot{\Delta\delta}_{max}}{t} \quad (30)$$

where $(I_y \dot{\Delta\delta}_{max})$ is the maximum angular impulse which must be applied to the satellite during a maneuver, $\dot{\Delta\delta}_{max}$ is the maximum angular velocity change of the satellite during the maneuver, and t is the total time duration of the maneuver. For the particular tracking maneuver used in the baseline design, one obtains $P_{avg} = 1.20$ watts for an altitude of 2400 km, and $P_{avg} = 0.485$ watts for 4146-km altitude. Assuming that the peak power is twice as large as the average power, and including an additional factor of

two for power required by the spin motors to maintain constant wheel velocity results in $P_{\max} = 4.80$ watts at 2400-km altitude and $P_{\max} = 1.94$ watts at 4146-km altitude. These values appear in Table III as requirements of the baseline design. For comparison, the peak power required by the satellite in absence of all environmental disturbances is just the maximum value of the product of the required control torque and the corresponding satellite angular velocity during the maneuver. For the tracking maneuver used in the baseline design, the results are $P_{\max} = 1.06$ watts at 2400-km altitude, and $P_{\max} = 0.134$ watts at 4146-km altitude. Hence, the required CMG power is larger than the required satellite tracking power, but still remains quite small.

Such small power requirements can easily be supplied by the satellite's solar cell array while operating in direct sunlight. However, for low orbits the satellite must spend a significant percentage of each orbit in the shadow of Earth. During such eclipsed periods, the satellite must accomplish between-site re-orientation maneuvers on power supplied by batteries. An estimate of the total energy storage required for such eclipsed maneuvers may be obtained by multiplying the required average power by half an orbital period. For the baseline control system, this procedure yields $E_s = 2.73$ watt-hr at 2400-km altitude and $E_s = 1.45$ watt-hr at 4146-km altitude. These values are also presented in Table III.

3.2.2 Magnetic Loop Control (MLC) Actuator

Consider a MLC system to be capable of providing such secondary control services as counteracting solar-pressure-misalignment torque and desaturating the CMG. In the absence of detailed studies necessary to size such a system, and in order to establish a conservative method of sizing, assume that the MLC is to be capable of producing ten times the steady torque required to counteract a solar-pressure

torque due to a misalignment between the center of solar pressure and the satellite center of mass of 0.1 percent of the satellite diameter. For design purposes, an angle of 45 degrees between the direction of the Earth's magnetic field vector \underline{B} and the satellite magnetic moment of direction \underline{n} is to be used. A summary of the results obtained by this procedure and explained below is presented in Table III.

For a satellite with a diameter $D = 1000$ m, the magnitude of maximum solar pressure resultant force is $p_0 \pi D^2 / 4 = 7.11$ N. A misalignment of $(0.001)(D) = 1$ m between the center of solar pressure and the satellite center of mass results in a solar pressure misalignment torque of 7.11 N-m, as indicated in Table I. Thus, the design torque is 71.1 N-m.

The required ampere-turns (Ni) necessary to provide the design torque can be determined from Eq. (23). Assuming that the magnitude of the Earth's magnetic induction vector \underline{B} is 2×10^{-5} Weber/ m^2 at an altitude of 2400 km and 1.5×10^{-5} Weber/ m^2 at 4146-km altitude (ref. 5), using $\pi D^2 / 4$ as the area enclosed by the current loop, and using 45 degrees as the angle between \underline{n} and \underline{B} , one obtains $(Ni) = 6.40$ ampere-turns at 2400-km altitude and $(Ni) = 8.53$ ampere-turns at 4.46-km altitude.

The total required conductor mass M_C may be determined from Eq. (22) for given material and power level. In particular, for an arbitrary power level of 100 watts, and a conductor material of aluminum with a resistivity of $\sigma = 2.83 \times 10^{-8}$ Ωm and a density of $\rho = 2.7 \times 10^3$ kg/ m^3 , Eq. (22) yields a conductor mass of $M_C = 309$ kg at 2400-km altitude and $M_C = 549$ kg at 4.46-km altitude. Including an additional 9 percent allowance for radial spoke conductors which complete the circuit between the rim and power supply at the hub, yields a total conductor mass of $M_C = 337$ kg at 2400-km altitude and $M_C = 598$ kg at 4146-km altitude. These values are presented in Table III for the baseline control actuator.

The power required for continuous MLC operation may be supplied by the satellite's solar-cell array while operating in direct sunlight, but all power must be supplied by batteries during periods of eclipse. However, solar-pressure misalignment torques vanish during such periods of eclipse, so that the demand of control torques by the MLC during such periods is greatly reduced. Estimating total energy-storage requirements for the MLC to be the product of the average power and a time duration arbitrarily selected as one-tenth an orbital period, one obtains $E_s = 2.27$ watt-hr at 2400-km altitude and $E_s = 29.8$ watt-hr at 4.46-km altitude. These values are presented in Table III for control actuators for the baseline design.

3.2.3 Deployable Isotensoid Reaction Wheels (RW)

Consider an RW control actuator capable of providing the primary control services described previously for the CMG control system and designed with the same degree of conservatism. A summary of the results obtained by this procedure and explained below is presented in Table III.

For a flight plan requiring the tracking of two Earth sites on each Earth orbit, the required satellite angular impulse for maneuvers is 7.46×10^5 N-m-s at an altitude of 2400 km and 5.67×10^5 N-m-s at 4146-km altitude, as previously shown. Using these angular impulses in Eq. (23) and doubling the resulting wheel momentum to account for noncoplanar maneuvers, one obtains $H_w = 1.49 \times 10^6$ N-m-s at 2400-km altitude and $H_w = 1.13 \times 10^6$ N-m-s at 4146-km altitude. Even though this momentum requirement is only about one-third that for a comparison CMG system, it is still sufficiently high that the notion of using rigid flywheels with sufficiently small radius to fit within the Shuttle bay is not attractive. For example, an RW system using rigid glass fiber wheels of 2-m radius results in a total mass of $M_{RW} = 4940$ kg at 2400-km altitude and $M_{RW} = 3740$ kg at 4146-km altitude

(from Eq. (28)). These RW control actuator masses exceed 50 percent of the total mass of the satellite. An even greater disadvantage of such small wheels is their excessive power requirements which approach one-quarter of a megawatt for this application. Thus, deployable flywheels are again made attractive.

Using the design momentum requirements presented above and Eq. (29) for deployable filamentary glass fiber wheels with radius $r = 20$ m and shape specified in Figure 8, results in a required wheel mass for a single-axis RW of $M = 175$ kg at 2400-km altitude and $M = 132$ kg at 4146-km altitude. These wheel masses must be doubled to obtain a dual-axis RW control system so the total wheel mass is $M = 350$ kg at 2400-km altitude and $M = 264$ kg at 4146-km altitude. Finally, doubling the total wheel mass to account for motors, bearings, and fittings, the total RW control system mass is $M_{RW} = 700$ kg at 2400-km altitude and $M_{RW} = 528$ kg at 4146-km altitude. These values are presented in Table III for the baseline design.

The average power required by torque motors to accelerate and decelerate an RW flywheel during maneuvers may be estimated as

$$P_{avg} = \frac{I_y}{I_w} (I_y \ddot{\delta}_{avg}) (\dot{\delta}_{avg}) \quad (31)$$

where I_y is the satellite mass moment of inertia about a diameter, I_w is the flywheel mass moment of inertia about its spin axis, $(I_y \ddot{\delta}_{avg})$ is the average torque applied by the control actuator on the satellite during maneuvers, and $\dot{\delta}_{avg}$ is an average satellite angular velocity during maneuvers. Using $I_y = 4.91 \times 10^8 \text{ kg-m}^2$ for the baseline satellite design, values for $(I_y \ddot{\delta}_{avg})$ and $\dot{\delta}_{avg}$ estimated from Table I for the over-site tracking mission in presence of unfavorable gravity-gradient torques and assuming $I_w = Mr^2/2$ where M is the mass of a single-axis RW wheel presented above and $r = 20$ m, one finds the average power required

is $P_{avg} = 7200$ watts at 2400-km altitude and $P_{avg} = 2530$ watts at 4146-km altitude. Estimating the peak power requirements by doubling these average powers results in $P_{max} = 14,400$ watts at 2400-km altitude and $P_{max} = 5,060$ watts at 4146-km altitude. These values are presented in Table III.

An estimate of the required energy storage for battery operation of such a control actuator during periods of eclipse may be obtained by multiplying the average power requirement by the duration of half an orbit. This results in an energy storage requirement of $E_s = 1.54 \times 10^4$ watt-hr at 2400-km altitude, and $E_s = 7.55 \times 10^3$ watt-hr at 4.46-km altitude. These values are presented in Table III for the baseline design.

3.3 FEATURES OF A BASELINE DESIGN CONTROL ACTUATOR CONFIGURATION

After comparing the mass, power, and energy requirements of the CMG and RW control actuators in Table III, a baseline control actuator consisting of a deployable twin-rotor CMG for primary control functions and a MLC system for secondary control functions was selected. The mass, power, and energy storage requirements of this baseline configuration are those given the first two rows of Table III.

The basic design features of the CMG have already been discussed. The shape of the deployable filamentary flywheels is shown in Figure 8. A view of the overall twin-rotor CMG with coning suspension is shown in Figure 9. The maximum required slewing angle was chosen in the design phase to be 0.175 radian (10 degrees). Shown in Figure 10 is a cutaway of the satellite center tube showing the gimbaled inner bearing race and coning suspension pushrod-and-bellcrank linkage. Additional detailed features of this CMG design are presented in Table IV.

The baseline MLC consists of 45 independent circuit loops each with 3.74 turns, so that the spoke conductors completing the circuit to the power supply on the column hub of the satellite are not colinear, as shown in Figure 11. It can be shown that by independently controlling the current in each circuit that it is possible to obtain an arbitrary orientation of the magnetic moment on the satellite in the plane orthogonal to \underline{B} (ref. 9). Presented in Table V are detailed features of a 45-circuit MLC design, including circuit current and voltage levels necessary to produce the design level of precessional torque.

3.4 EFFECT OF CMG FLEXIBILITY ON POINTING ACCURACY

The deployable CMG control actuator is composed of many small glass fibers in order to provide adequate structural flexibility for compact stowage. However, when fully deployed, each CMG wheel should behave essentially as a rigid body during maneuvers. The effect of structural flexibility of the fully deployed CMG wheels on the pointing accuracy of the control system are considered in this section. For this analysis, the spacecraft structure will be considered a rigid body, and it will be assumed that an accurate positional reference system is employed.

According to the approaches of refs. 12 and 13, it can be shown that the flexibility of the CMG wheels will not cause either undesirable interaction with the control system or significant pointing errors so long as

$$f_c/f_n < 0.1 \quad (32)$$

where f_n is the lowest natural frequency of a spinning CMG wheel and f_c is the control frequency. Since the CMG wheels are spin-stiffened structures, f_n may be estimated conservatively as

$$f_n \geq 0.1 \Omega/2 \quad (33)$$

where Ω is the CMG wheel spin velocity in radians per second (ref. 14). Furthermore, f_c may be defined as (refs. 12 and 13)

$$f_c = \frac{1}{2\pi} \sqrt{\ddot{\delta}_{\max} / \Delta\delta_e} \quad (34)$$

where $\Delta\delta_e = 0.25$ mrad is the maximum allowable pointing error and $\ddot{\delta}_{\max}$ is the maximum angular acceleration provided by the CMG during maneuvers. For the baseline design CMG wheels, $\Omega = 42.8$ rad/s (Table IV) and $\ddot{\delta}_{\max}$ may be estimated to be 2.75×10^{-6} rad/s² for an orbital altitude of 2400 km and 9.77×10^{-7} rad/s² for an orbital altitude of 4146 km (Tables I and II). Using these values results in a frequency ratio f_c/f_n of 0.0245 for a 2400-km altitude, and 0.0146 for a 4146-km altitude. Consequently, it does not appear that the flexibility of the CMG wheels will cause significant deterioration in pointing accuracy for the baseline design.

SECTION 4

INTERORBIT MANEUVERING WITH SOLAR PRESSURE

The extremely small unit mass of the kilometer-sized reflector satellite (see Part II) suggests the possibility of using solar sailing to change orbits. In fact, it would be very attractive to be able to construct (by assembly or deployment) the satellite in LEO and then "fly" it to the operational altitude. The problem is to overcome the deleterious effects of air drag on this maneuver.

If one assumes that the reflecting surface is perfectly specular, then the component of force/unit mass in the direction of flight is

$$\frac{F}{M} = \frac{p_0}{m} \cos^2 (\phi - \alpha) \sin \alpha - \frac{2q}{m} (1 - \lambda + 2\lambda \sin^2 \alpha) \sin \alpha \quad (35)$$

where p_0 is the solar pressure ($0.9 \times 10^{-5} \text{ N/m}^2$), m is the spacecraft mass per unit area, q is the dynamic pressure of the exospheric plasma, ϕ is the angle between the Sun vector and the normal to the flight path, and α is the angle of attack. Note that a form of modified Newtonian flow is used wherein a fraction λ of the plasma particles is assumed to bounce specularly from the surface and the remaining fraction $(1 - \lambda)$ is assumed to be absorbed. A value of $\lambda = 0.25$ yields a maximum drag coefficient of 2.5 for $\alpha = 90$ degrees.

The spacecraft is in sunlight for slightly more than one-half of each orbit. The assumption is made that the half orbit for which $|\phi| < 90$ degrees is used for adding energy to the orbit at a maximum rate and the other half be used to circularize the orbit with no energy change. In this way, the orbit can be considered to be essentially circular. Note that a much more detailed analysis would be required to show that circularization is indeed

possible over the quasi-shaded half of the orbit, but the results obtained here would not be changed markedly if it were necessary to devote an occasional orbit to the circularization task.

During the sunlit half-orbit, the angle of attack α should be controlled so as to maximize the thrust as ϕ changes. This optimal programming is shown in Figure 12 for various values of q/p_0 and for $\lambda = 0.25$.

The average thrust per unit mass for an entire orbit achieved with this angle of attack on the sunlit side is

$$\left(\frac{F}{M}\right)_{\text{ave}} = 0.219 \frac{p_0}{m} f(q/p_0) \quad (36)$$

where the influence of air drag is contained in the function f as shown in Figure 13 for $\lambda = 0.25$.

The rate of orbital energy increase per unit mass is

$$\frac{dH}{dt} = \left(\frac{F}{M}\right)_{\text{ave}} \dot{\phi} R$$

But the orbital energy per unit mass is

$$H = -\frac{1}{2} \dot{\phi}^2 R^2 \quad (37)$$

where the orbital rate is

$$\dot{\phi} = \sqrt{\frac{g R_e^2}{R^3}} \quad (38)$$

Combining the foregoing equations gives

$$\dot{R} = 0.438 \frac{p_0}{m} f(q/p_0) \sqrt{\frac{R^3}{gR_e^2}} \quad (39)$$

For no air drag, this can be integrated to yield

$$\Delta t = 4.57 \frac{\sqrt{gR_e}}{p_0/m} \left(\frac{1}{\sqrt{R_1}} - \frac{1}{\sqrt{R_2}} \right) \quad (40)$$

as the time required to raise the orbit from R_1 to R_2 . For example, to raise the orbit from an altitude of 2400 km to 4000 km, for a spacecraft with a mass per unit area of 12 g/m^2 , would take $3.3 \times 10^6 \text{ s}$ or about 38 days.

The effects of air drag become significant at altitudes below about 1000 km. The influence on trip time can be obtained from Eq. (39) by numerical integration. The results depend on the density of the exosphere which is highly variable. If the density variation is taken from Table B-5 of ref. 15 for a temperature of 1250 K, the trip time to an altitude of 2400 km for a 12 g/m^2 spacecraft is as shown in Figure 14. It can be seen that the trip time is reasonable as long as the initial altitude is high enough to avoid the very fast drag rise that occurs when the dynamic pressure approaches one-half the solar pressure. Incidentally, the value of q/p_0 , at an altitude of 700 km, is 0.435. A value of 0.4 would appear to be a safe cutoff to keep the air-drag effect within bounds.

The foregoing analysis assumes that the desired angle-of-attack maneuvers are possible. Examination of the variation of angle of attack with orbital angle (Figure 12) shows moderate angular accelerations. In fact, the accelerations are less than those required by operational oversite tracking at 2400 km. However, the requirement to return the spacecraft to near-zero angle of attack on the dark from the 90-degree condition at the end of

the sunlit portion would present a problem. Probably an auxiliary gas-jet torqueing system would be required to provide adequate control for the lower altitudes. Once the air drag becomes negligible, then the operational torquers would be adequate.

PART II

POINT DESIGN OF A DEPLOYABLE-REFLECTOR SATELLITE
WITH ONE-KILOMETER DIAMETER

This Page Intentionally Left Blank

SECTION 1

INTRODUCTION

The conceptual design of a 1-km-diameter circular configuration capable of being transported in the Shuttle and deployed automatically in space is described in this Part. The spacecraft incorporates a twin-rotor control-moment gyro as the primary control system with a supplementary magnetic loop control. The effects of loads characteristic of the environment and a typical mission have been considered in developing this design.

The design approach used in these studies is an expansion of that described in ref. 1. For convenience, some of the explanation has been repeated in this Part.

SECTION 2

REFLECTOR SPACECRAFT DESIGN

2.1 DISCUSSION

In previous reflector spacecraft studies at Astro, point designs were examined for a triangular configuration and a nearly circular configuration. The circular design proved to be much lighter than the triangular design for sizes in the 1-km-diameter range. The triangular design was mass efficient for diameters in the 100-m-diameter range. As part of the current studies, these concepts were reexamined along with multifaceted configurations consisting of many small reflecting segments mounted in a large supporting structure.

The selection of an appropriate control system from among various candidates is described in Part I, which also describes the acceleration and torque loads resulting from site tracking and reorientation during a typical mission. These studies indicate that the number of ground sites must be limited to two or three for a 1-km-diameter spacecraft operating at an altitude as low as 2400-km. A large number of ground sites would require an excessively heavy control system and an increase in structural mass, as well, which eliminates the possibility of placing the spacecraft in orbit with a single Shuttle launch.

Serious consideration was given to a faceted configuration where the overall spacecraft would provide rough pointing and the individual facets would be moved at their edges to provide precision pointing. This design was not selected for the final baseline because of the difficulty envisioned in achieving automatic deployment. A circular spacecraft configuration which uses a twin-rotor control-moment gyro as the primary control system

was selected as the baseline design on the basis of low weight and relative ease of deployment. The 1-km-diameter conceptual design, described in this report, can be packaged for launch in the Shuttle cargo bay and deployed automatically after it has been placed at the desired orbital altitude. Although the baseline design is basically suitable for a wide range of orbits, the control systems, which are approximately 25 percent of the total mass, have been sized for 2400- and 4146-km orbital altitudes.

2.2 DESIGN APPROACH

A thin metallized polymer film suspended as a membrane is the payload of a reflector spacecraft. The supporting structure, control system, power supply, and other subsystems are required to keep the membrane acceptably flat and to orient it and reorient it as the mission requires. The approach that Astro has taken in establishing a structural design is as follows:

1. Determine the external loads, due to environment and mission requirements, on the membrane mirror.
2. Determine the required flatness of the mirror.
3. Determine how much tension must be placed in the membrane to maintain the required flatness in the presence of the external loads.
4. Design a structure which is capable of being automatically deployed on-orbit to apply that required tension.
5. Design a control system capable of meeting the site tracking and reorientation requirements of the mission.
6. Verify that the structure is capable of supporting the internal loads applied by the control system, and modify the design (if required).

This approach does not consider dynamic effects such as possible unfavorable interaction between the structure and the control system. It is expected that the structural design resulting from

the stringent accuracy requirements and this "static" approach will be stiff enough to avoid the undesirable dynamic behavior without unduly complicating the control logic.

2.3 SPACECRAFT LOADS

The various loads that are applied to an operational space vehicle have been quantitatively described in ref. 1. In order that comparisons can be made between the magnitudes of the types of loading, the loadings have been expressed as equivalent pressures or forces per unit area and plotted in Figure 15. Each load is a worst-case estimate. The nature of each of these various loads is briefly summarized below.

2.3.1 Solar Pressure

The force-per-unit area on an Earth-orbiting perfectly reflecting surface is normal to the surface and has a magnitude of

$$\frac{F}{A} = 0.905 \times 10^{-5} \cos^2 \gamma \text{ N/m}^2$$

where γ is the angle between the Sun's rays and the surface's normal.

2.3.2 Aerodynamic Drag

An estimate of the dynamic pressure on a surface due to the plasma in space can be obtained by setting

$$\frac{F}{A} = 1.25 \rho U^2$$

where ρ is the density of the plasma and U is the flight speed on the surface normal to the plasma. This load increases rapidly with decreasing altitude and is large below 650 km.

2.3.3 Gravity Gradient

This force, which is the combined result of the change in gravitational force and centrifugal force at points distant from the spacecraft center of gravity, can be approximated for the worst-case orientation as

$$\frac{F}{A} = 3\Omega^2 m_a r$$

where r is the distance from the center of gravity, Ω is the orbital angular velocity, and m_a is the local mass per unit area. This load is significant at low altitudes where the angular velocity is high.

2.3.4 Control Loads

The angular acceleration loads occurring during ground-site tracking and reorientation between sites have recently been reinvestigated as part of Astro's study of the control system design for reflector spacecraft (see Part I). These loads occur during the two different maneuvers that the spacecraft must make, site tracking and reorientation. During reorientation between sites, the flatness of the membrane surface is not relevant; however, the entire structure must safely withstand the reorientation loads without failure.

The consideration of orientation dynamics for the reflector spacecraft can be simplified to two issues; the maximum angular acceleration which establishes the maximum load on the structure, and the maximum angular impulse for the operation which sizes the control system. In considering the mission dynamics for altitudes of 2400 and 4146 km, respectively, in the simplified case of a coplanar Sun-satellite-site system, it was observed that the maximum angular impulse for site tracking and reorientation

were approximately equal if two equidistant sites were illuminated each orbit. If a larger number (six) of the sites were illuminated, the reorientation required a very robust control system and the torques applied to the rest of the spacecraft became large (10^4 to 10^5 N-m). Since the illumination of two different sites each orbit can take advantage of optimum Sun locations, the control system was sized for this case with a factor of two to account for noncoplanar dynamics. Under the restriction, the maximum angular accelerations occur during the site tracking operation as described in Part I.

It has been observed that the dynamics of a typical noncoplanar case require much larger maximum accelerations than the coplanar case. However, these maximums occur when the satellite is closest to the Sun line as it passes over the site. This is a situation where sunlight is not being reflected efficiently. In the scheme of illuminating only two sites per orbit, the site tracking occurs when the Sun is on or over the horizon and the satellite is overhead or off towards the opposite horizon. Therefore, for structural sizing we have assumed the coplanar dynamics give a representative value for the maximum acceleration loads. The line drawn on Figure 15 for $m_a r = 1$ kg/m is characteristic of the average maximum loading on the reflector film material in the baseline design. The maximum loading would occur near the rim where $m_a r = 2$ kg/m.

2.3.5 Other Loads

The following loads have been examined and found to be at least an order of magnitude smaller than those described above:

- Effect of orbital perturbations due to the nonsphericity of the gravity field
- Solar wind
- Averaged micrometeoroid flux
- Electrostatic and electromagnetic forces due to spacecraft charging

2.4 MIRROR FLATNESS REQUIREMENTS

The optimum reflector for a typical mission where sunlight is reflected to specific sites on the Earth by a passing spacecraft would be a perfectly flat, specularly reflective mirror. Deviations from this ideal condition caused by lateral-load-induced curvatures, local surface irregularities, and diffuse reflectivity will cause dispersion of the reflected light. As previously reported in ref. 2, Astro has conducted studies to determine the amount of light that would be dispersed by a non-flat reflector outside of the ground image reflected by a perfectly flat mirror. Calculations were conducted for the case of spherical curvature and for a case with a random gradient distribution. The results, which are shown in Figure 16, indicate that there is little difference between the beam widening energy losses of these two different cases if they are compared on the basis of root-mean-square gradient.

The baseline design calculations were conducted on the basis of a maximum rms gradient of 0.00082 rad, corresponding to an edge gradient of 0.001 rad for a spherically curved circular membrane. This corresponds to an energy loss of 18 percent of the illumination, which seems reasonable when compared to other losses due to imperfect reflection and pointing errors.

2.5 MEMBRANE TENSION REQUIREMENTS

The deflection of smooth tensioned membranes of constant thickness under uniform lateral loads has been studied by Astro and reported in ref. 16. The film membrane for the reflector spacecraft must be held so that it is very flat as indicated above. If a circular membrane is under tension N and a uniform lateral pressure p , then the surface will form a spherical shape where the maximum gradient at the rim is

$$(\text{grad } w)_{\text{max}} = \frac{pD}{4N}$$

where D is the membrane diameter. It is interesting that the thickness of the film influences this deflection only if a significant portion of the lateral load p results from angular accelerations or gravity-gradient loads of which depend on the mass per unit area m_a .

The film membrane tension required to limit the edge gradient to 0.001 rad under a lateral loading of $1 \times 10^{-5} \text{ N/m}^2$ is shown in Figure 17 where it is plotted, along with film stress, showing the effects of reflector size. The tension required for the baseline design is only 2 N/m. The corresponding stress is low, but at the lower end of a range which may cause some creep under prolonged loading.

The thin reflecting film must be handled and packaged before it is used in space. The tensions required to flatten creases or eliminate embossing are generally higher than those required to hold the smooth film (ref. 17). The development of a thin-film material (along with the handling and packaging techniques) that can be flattened with low stresses is an important and required technology advance for the reflector spacecraft. These considerations again indicate the need for reflector films of minimum thickness so that there is sufficient stress available for flattening without high tensions and consequent large loads on the structure.

2.6 MEMBRANE SUPPORT REQUIREMENTS

Polymer films, such as Kapton, have high temperature coefficients of expansion compared to materials which might be used for the supporting structure. Furthermore, these coefficients often vary with direction as a result of the film manufacturing process. As a result, even if long-term inelastic effects such

as shrinkage under radiation exposure or creep under load can be eliminated, there will be substantial dimensional changes between the film and the support structure. The film will be near its highest operational temperatures when it is reflecting sunlight on an Earth site and it must be unwrinkled and under a low tension to perform that mission efficiently. The lowest temperatures will occur when the spacecraft enters the Earth's shadow with the film cooling more rapidly than the structural members. Since the in-plane stiffness of the film is high, a rigid attachment to the supporting structure would cause unreasonable loads as the film cooled. A calculation based on an average thermal-expansion coefficient of $20 \times 10^{-6}/^{\circ}\text{C}$ for Kapton and 250°C change in film temperature predicted by a preliminary thermal analysis indicates that the film will vary as much as 0.5 percent in dimension due to temperature effects. In the baseline design, it is assumed that a total dimensional change of 1 percent (± 0.5 percent) between the film and the structure must be compensated for.

A solution to the support of a material that exhibits the properties described above is to allow the film to expand and contract, and to devise a mechanism that maintains an appropriate low tension on the film at the same time. Astro has devised one such solution in the form of soft-spring attachments to the rim truss and sliding edge tendons which are enclosed in a bias-mesh hem bonded to the film edges. The attachments, which are described as film-expansion compensators, are illustrated in Figures 18, 19, and 20 and their design is discussed in Section 2.8.3. The edge tendons are shown on these same figures and are discussed in Section 2.8.2. Each film-expansion compensator is attached to a ring on the rim truss along with an upper and lower stay tape.

2.7 THERMAL DESIGN REQUIREMENTS

Large orbiting spacecraft experience substantial temperature changes as their orbit passes from the Sun side of Earth into the

Earth's shadow and out again. The design of the reflector spacecraft must take into account the thermal influence on structural shape and loads resulting from thermal strain. In addition, the materials used in the design must be suitable for use through their entire expected temperature range in orbit and angle to withstand prolonged exposure to the vacuum and radiation environment. An example of these considerations has already been discussed in the case of the reflecting film material in the preceding section of this report.

The thermal characteristics of thin aluminized Kapton films have recently been thoroughly investigated as a part of solar sailing studies. A solar absorptivity α of approximately 0.15 and a total thermal emittance ϵ of 0.25 are realistic values for 2- μ m Kapton based on the data in ref. 18. Since the reflector spacecraft mission is optimized by using both sides of the film as a reflector, the use of coatings developed to increase the emittance of the unaluminized side is not appropriate to this application. The above properties will result in a maximum film temperature of approximately 350 K (77°C) when the film is normal to the Sun's illumination. The minimum film temperature will be approximately 100 K (-173°C) when the film is in the Earth's shadow but warmed slightly by the Earth's infrared emission in an orbit with a few-thousand-kilometer altitude.

Low thermal-expansion materials, such as graphite/epoxy composites, are preferred for structural members because this property tends to minimize differential thermal expansions which create dimensional imperfections. The combination of low expansion materials and the open nature of the trusses used in the baseline results in acceptable small distortions in the trusses themselves.

Certain situations will result in substantial differential changes in length between the truss structures and the stay tapes, even though both are made of graphite/epoxy. For example, when the spacecraft first enters the Earth's shadow, the tapes will cool much faster than the rods in the masts. For this reason, the stay tape reels at the tip of each central mast are locked together after deployment to act as a single reel with a constant torque device to provide pretension. In this manner, the tapes can adjust in length at the same time, but not individually, and avoid any unreasonable loads due to thermal strain. The tapes will each have at least one twist along their length so that their view factor with respect to the Sun is less position-dependent. It is interesting that the reflector surface tends to ensure an almost even illumination of all tapes on the Sun side of the spacecraft even as the relative Sun angle changes. In a nonreflector spacecraft, there are certain Sun angles where some tapes see nearly full illumination and others see almost none of the same side of the spacecraft.

2.8 BASELINE DESIGN OF A REFLECTOR SPACECRAFT

The design of the structure to support the film membrane, the design of the control actuator, and the smaller subsystems are discussed in the following text. The overall configuration selected as the baseline design is a 1-km-diameter circular spacecraft which is illustrated in Figures 18 and 21. In its final deployed condition, the spacecraft consists of a 1-km-diameter metallized film supported by a circular truss rim around its perimeter. The truss rim is stabilized by stay tapes attached to each end of a slender central hub. The central hub consists of two 250-m deployable masts extending from each end of a center body. The twin-rotor control-moment gyro, solar power system, batteries, and communications and control electronics are attached to the center body. The center of the reflecting film is also attached

to the midpoint of the center body. The design is similar to the one described in ref. 1 and Part I, except that the rim truss structure and method of deployment have been changed and both a twin-rotor control-moment gyro and a magnetic-loop controller have been included in the design along with other subsystems necessary for independent satellite operation.

The reasons for selecting this particular design, and size, for the baseline can be summarized as follows:

- The 1-km-diameter size can be packaged within the volume and mass restraints of the Space Shuttle.
- The circular configuration is structurally efficient with a total support structure mass which is about equal to the payload mass.
- The design can be deployed in a controlled reliable sequence.
- The combined control systems can be packaged for the Shuttle and have a reasonable total mass and power requirement.
- Versions of all the required components have either been used successfully in space or demonstrated in ground tests.

The dimensions of the deployed spacecraft are included in Figure 21 and the mass breakdown is presented in Table VI. Details of the control-moment gyro and center body are shown in Figures 8, 9, and 10.

2.8.1 Membrane Reflector

An aluminized Kapton polymer film with a thickness of 2- μm (0.08 mil) and a mass density of 4 g/m² has been selected for the membrane reflector material. The design tension is 2.5 N/m with a stress of 125 N/cm². The 1-km-diameter reflector membrane has an area of $7.85 \times 10^5 \text{ m}^2$ and a total mass of 3142 kg. The mass is proportional to the square of the reflector diameter.

Kapton is not currently manufactured for commercial use in the desired thickness, but pilot production tests have shown that it is possible to do so. A larger thickness can be used but it will result in an increase in control system mass as well as membrane mass, and the overall size of the spacecraft would have to be reduced for a Shuttle launch.

2.8.2 Edge Tendons

The edge tendons apply an even tension to the film along edge-scallop arcs between the film-expansion compensators which are attached to the rim truss. The tendons are sized by the amount of tension they must carry, which in turn is proportional to the square of the reflector diameter and the scallop radius. This radius has been arbitrarily selected as one half of the reflector diameter, so that the tendon mass is proportional to the cube of the reflector diameter. For the baseline design, the total mass of the 90 edge tendons is 12 kg, where the material is unidirectional graphite/epoxy and the safety factor is three.

2.8.3 Film-Expansion Compensators

The film-expansion compensators adjust for changes in the required length of the edge tendons and in the overall dimension of the reflecting film, while maintaining a nearly constant tension in the film. This is accomplished by using two sets of buckling columns in compression as illustrated in Figures 19 and 20. The operation of this device is analyzed in ref. 19. The film-expansion compensators for the baseline design can accommodate a total change in film dimensions of 5 m which is 1 percent of the reflector radius. The total mass, which varies in proportion to the cube of the reflector diameter, is 330 kg for the 90 units required in the baseline design.

2.8.4 Circular Rim Truss

Astro's earlier reflector spacecraft design incorporated an "expandable truss column" as the rim truss around the perimeter of the reflector membrane. In the current study, it was observed that the desired method of deployment would allow the use of the same design, which stores in a small diameter, or the use of a coilable longeron lattice Astromast column, which stores in shortened length with full-column diameter. Since the Astromast column and methods of deploying it are well understood and have already been used in space, it was selected for the rim truss for the current baseline design. The "expandable truss column," which would weigh less than an Astromast, is still an excellent candidate for this application; however, reliable methods of canister deployment of this mast need to be developed and demonstrated.

The proposed Astromast, shown in Figure 18, would be manufactured with the outside longeron longer than the two inner longerons and with appropriate changes in diagonal lengths so that the mast would be precurved along its length with a radius of 500 m. The rim truss is subject to a nominal compression load of 1875 N, two-thirds of which is due to the film tension, and one-third of which is due to edge tendon tensions. The properties of the Astromast, sized to accommodate combined compression and bending due to precurvature (see ref. 20), with a safety factor of 1.25 ($P_{ult} = 2344$ N) are:

Column length between attachments = 34.9 m

Column radius = 0.58 m

Bay length = 0.73 m

Longerons = 6.4 mm x 7.7 mm graphite/epoxy rods

Battens and diagonals are graphite/epoxy rods

The overall Euler buckling of the column would be 12,560 N for a straight 34.9-m length. Incidentally, the safety factor and ultimate strength are actually higher than indicated above because the analysis of the curved mast assumes a worst case where one

longeron buckles, whereas in this application, two longerons would be located on the inside of the curved column. The bending-moment capability of the rim truss is approximately 1900 N-m, which is more than 30 times the maximum gravity-gradient torque during deployment. The total mass of the baseline design is 1760 kg which is 2.5 times the mass of the longerons. Previous detailed design studies of similar graphite/epoxy masts indicate that the total mass, including hardware, will be 2.0 to 2.5 times that mass of the longerons.

The mass of the truss rim could be reduced by using straight truss sections between the film-expansion compensator attachment points. This was not done in the baseline design because it involves an unproven modification to the mast design and deployment. If straight rim segments are used and the design is geometrically similar with 90 segments, the rim truss mass will vary as the cube of the reflector diameter.

The mass of the six deployment canisters and their mechanisms has been estimated on the basis of an area density equivalent to 2 mm of graphite/epoxy over their surfaces. The total mass for the six units is 552 kg for the baseline design. An allowance of 30 kg has been made for the six rim hinges and motors. It is assumed that these masses vary with the square of the reflector diameter.

2.8.5 Front and Back Stays

The purpose of these stays is to prevent general instability of the rim. Each pair of stays acts as a truss which provides a spring restraint to the rim attachment points. The spring stiffness in the softer (axial) direction is

$$k = \frac{EA H^2}{2L^3}$$

where EA is the extensional stiffness of the stay tape, H is the height of the central mast, and L is the stay length. The condition for stability of a segmented, spring-restrained column with a load P and a segment length ℓ is

$$k > \frac{2P}{\ell}$$

which does not take into account assistance from the bending stiffness of the continuous column.

In order to be conservative and to forestall load-induced growth of imperfections, the design stiffness is taken to be three times the minimum required. The force P is that part of the rim compression which counteracts the membrane tension and the small stay pretension forces are neglected. The design stay is then

$$A = 6 \frac{DL^3}{\ell H^2} \frac{N}{E}$$

For the baseline design and graphite/epoxy material, this area is 2.4 mm^2 , and the total mass of the 180 stay tapes is 367 kg. The total mass of the stay tapes is proportional to the cube of the diameter for a geometrically similar spacecraft. Each stay in the baseline design is assumed to be the equivalent of a $0.4 \times 6.0 \text{ mm}$ tape, although the flight design would use a multifilar design for micrometeoroid survivability.

2.8.6 Center Hub

The center hub consists of two slender masts extending from the ends of a center body. Its function is to support the tension in the front and back stays.

The amount of pretension can be determined in terms of the out-of-flatness of the rim as follows. Let the axial deflection be δ at one rim corner and $-\delta$ at the next. The rim compression produces an axial kick load at each joint of

$$2 \frac{ND}{\ell} \delta$$

This reduces the pretension in the compressed stay by

$$2 \frac{NDL}{\ell H} \delta$$

A primary cause of the imperfection δ is errors in the lengths of the stays. Let ϵ be the unit error in stay length and let front and back stays have opposite errors. Then

$$\delta = \frac{2L^2}{H} \epsilon$$

Let the design pretension be equal to this worst-case compression. Then, for each stay

$$T_0 = \frac{4NL^3 D}{\ell H^2} \epsilon$$

For the baseline design and value of ϵ of 10^{-5} , this pretension is 2.0 N per stay. The ultimate axial compression load on the central masts is then 100.9 N.

In order to account for local and overall imperfections in the construction of the central masts, set the design load to be three times the ultimate load. Then the minimum mass coilable longeron Astromast column, using graphite/epoxy rods for longerons, has

a diameter of 2.5 m and a total mass of 152 kg. However, when the control torque requirements for a 2400-km altitude orbit are examined, the above mass has insufficient bending moment capability. Redesigning masts that will support a control system torque of 500 N-m each and will store in a height less than 1 m, results in a column with the following properties:

Total length of two masts	500 m
Column radius	1.47 m
Bay length	1.84 m
Longerons	6.6 mm x 8.0 mm graphite/epoxy rods
Total mass	301 kg
P_{ult}	338 N
P_E	845 N ($2.5 P_{ult}$)

The total mass of the two masts is 2.5 times the total mass of the longerons and is proportional to the cube of the reflector diameter of geometrically similar spacecraft. The mass of two canisters with mechanisms which are each 1.0-m long, is 63 kg for the baseline design, assuming an area density equivalent to 2 mm of graphite/epoxy over their cylindrical surfaces. At the tip of each mast, stay-tape reels are mounted. An allowance of 42 kg has been made for the stay-tape reels and their associated mechanisms. These last two mass quantities are assumed to be proportional to the square of the reflector diameter.

The maximum control-system torque required for the 4146-km altitude orbit and two equidistant sites is lower than that of the 2400-km altitude case and the smaller mast designed for pre-tension loads can be used. The resulting mass reduction would be 149 kg.

2.8.7 Center Body

The center body of the baseline design consists of a 1-m-diameter graphite/epoxy cylinder with the central mast canisters mounted at each end and the twin-rotor control-moment gyro surrounding the tube, as shown in Figure 10. The batteries, power conditioning equipment, computer, and communications and data handling electronics are mounted in an annular bay which surrounds one of the mast canisters. The solar cells are mounted on a cylindrical surface surrounding this equipment and on the surface of the second mast canister. The only mass not accounted for separately is the graphite/epoxy tube which has a wall thickness of approximately 1.25 mm in the baseline design. Its total mass is 48 kg which is assumed to be proportional to the cube of the reflector diameter.

2.8.8 Control Actuator

The design and selection of the control actuator is thoroughly discussed in Part I. It consists of a twin-rotor control-moment gyro which is illustrated in Figures 9 and 10 as a primary control actuator, and a magnetic loop control actuator which is used to compensate for those long-term unbalances which tend to saturate the control-moment gyro. The rotors of the control-moment gyro are a mesh-deployable type with overall dimensions shown in Figure 8. The control-moment gyro suspension system includes bearings for the two rotors, torque motors, and mechanisms for tilting the two rotors as required. The mass of the two 40-m-diameter rotors is 1000 kg in the baseline design and it can be shown that this mass is proportional to the cube of the reflector diameter. The suspension system mass is another 1000 kg and is assumed to be proportional to the cube of the reflector diameter.

The magnetic loop control consists of a bundle of wires included within the rim truss. These wires make up 45 independent circuits which are connected to the center body via conductors

along the stay tapes. Control moments are developed when currents are put through these circuits as the spacecraft moves through the Earth's varying magnetic field. The mass of the baseline system is 335 kg which is proportional to the spacecraft diameter.

There is surprisingly small change in the control actuator masses at the higher 4146-km altitude. The total control-moment gyro mass drops to 1520 kg, but the magnetic loop control increases to 598 kg. The total for the two systems is 2118 kg, compared with 2335 kg for the 2400-km altitude case. The magnetic loop control mass increases under an assumption of constant power available because of the decrease in the Earth's magnetic field with increased altitude. The mass of the total system might be dropped by increasing the available power, which was not considered in the baseline design because any substantial power increase would require double deployable solar panels. The gains which might be achieved do not seem worth the added complexity.

2.8.9 Other Subsystems

The electrical subsystems and their baseline design masses consist of the following which are considered to be independent of reflector diameter:

Solar power supply (200 W avg.)	60 kg
Hemispherical antennas (2)	20 kg
Rate gyros and sensors	50 kg
Communications and data handling	100 kg
Computer	46 kg

2.9 ON-ORBIT DEPLOYMENT

Three requirements were placed on the deployment techniques for this large space structure. First, the deployment must be capable of being stopped and subsequently restarted at any point.

Second, most of the structure must be either fully deployed or fully stowed during deployment with a minimum amount of structure in a partially deployed state. Finally, the kinematics must be entirely predictable with every item having a unique predictable position during each state of the deployment. The baseline design meets all of these requirements.

2.9.1 Shuttle Package

The completely packaged baseline design occupies a nearly cylindrical volume with a 4.3-m-maximum diameter and a 15-m-maximum length suitable for launch in the Space Shuttle cargo bay. The remaining length of the cargo bay might be occupied by a propulsion system capable of boosting the spacecraft to the desired orbit between 1000 and 5000 km in altitude. The packaged spacecraft is illustrated in Figure 22. Six slender canisters contain the rim truss and attachment rings, which are preconnected to the stay ends and the film-expansion compensators. The reflector film is stored in multiple folds in a bin mounted between paired mast canisters. The film corner compensators fold within the film as do most of the stay tapes. At each end of the central hub, a hemispherical omnidirectional antenna and thin stay reels are mounted at the tip of a central mast stored within its canister. The electronics and batteries are mounted in an annular space around one of the two canisters and can be serviced or replaced without removing masts or film. Solar cells are mounted on the exterior of one canister and on a cylindrical shell surrounding the electronics. Thermal control radiators with vanes are mounted at the end of the annular bay. At the center of the package, the two deployable mesh rotors of the control-moment gyro are stored around their hubs in a manner similar to that described by Figure 14 of ref. 10. A soft cylindrical thermal blanket covers the control-moment gyro mechanisms and the center tube. This cover also prevents snags with the rotor mesh or the film during deployment.

2.9.2 Deployment Sequence

The deployment of this large reflector spacecraft can be divided into four phases following insertion into operational orbit.

Phase 1: Restraints required for interorbit transfer, including those securing the rim truss canisters and the film bins, are first released. The tips of the undeployed rim truss masts remain attached to a support on one end of the center body, and the six canisters are rotated by motors at these attachments until they are in a plane perpendicular to the center body as shown in Figure 23.

Phase 2: The six mast segments are deployed simultaneously with the undeployed portion of each mast remaining inside its canister as the assemblies of bin and paired canisters move away from the center body as shown in Figure 24. The lower central mast is extended at the same time, but at a slower rate. The three pairs of stay tapes attached to the hinged intersections between the deploying canisters are deployed by motorized reels at the tip of each central mast, and in this manner, the location of the deploying rim masts are controlled so that the inside end of these masts are always perpendicular to the central column.

As each 34.9-m segment of the rim masts is deployed, an indexed attachment ring, stored in a stack at the end of each canister, is engaged. The ring engagement completes a mechanical attachment for the stays and corner compensators and provides an electrical connection for one of the rim circuits. Each ring has been preattached to an upper and lower stay tape and corner compensator attached to the film. The film is sequentially unfolded as the six masts are deployed as shown in Figure 25. The entire film, except for a few irregular folds near the edge, is folded in a regular pattern and deploys under very small forces. The

film is confined to three regions during deployment: fully deployed, but still slack film in the center; partially deployed folded film along the edges; and undeployed film stowed in the bins moving out with the rim-mast canisters.

Figures 25 and 26 are intended to show the film deployment with stay tapes holding the film close to the center hub. If this is not done, the shape of the deployed film between two sets of extending masts is more complicated to illustrate but equally acceptable for deployment.

At the end of this phase, the entire film area and the lengths of rim truss are deployed but not established in the final circular planar configuration. The lower central mast is completely extended and the three stay tapes running from the tip of this mast to the inboard hinged joints of the rim truss control the position of the deployed but still slack film.

Phase 3: The upper central mast is first deployed to approximately 40 percent of its length, as limited by the length of the stay tapes running from its tip to the outboard hinged joints of the rim truss. The attachments between the inboard rim truss hinges and the center body are released. Motors on the six rim truss hinges are operated in synchronism to rotate the truss sections and attached film outwards as shown in Figure 26. The position of the center body with respect to the deploying truss rim is established by computer control of the four motorized reels for the 12 stay tapes fastened to the rim hinges. Near the end of this operation, the upper central mast is completely extended. At the end of this operation, the rim trusses latch together at the six hinge points to form a continuous circular rim. The intermediate stay tapes, which were originally folded within the film, are all deployed to their predetermined equal lengths, and the stay reels at each end are latched together to act as single reels.

At the end of this deployment phase, the rim truss is fully established and the film has been pretensioned during final motion of the rim into one plane. The final portion of this phase will be completed with some warming illumination on the film so that it is not contracted to its minimum size, and the amount of work required to pretension the film is minimized.

Phase 4: The two deployable mesh rotors of the control-moment gyro are deployed by spinning them up, and after they are fully deployed increasing their rotation rate to the operational value. The spacecraft is now fully deployed and operational. The solar power supply is sized to operate with illumination on either side of the reflector and is functional from the time the packaged spacecraft is removed from the Shuttle cargo bay.

The entire deployment sequence would be programmed in the spacecraft computer with information about the state of deployment transmitted back to the Shuttle or a ground station. The entire sequence would be conducted in a slow, controlled manner requiring several orbits for completion. The sequence could be stopped by remote control at any point if time is required to investigate an abnormality.

2.10 PARAMETRIC MASS EQUATIONS

2.10.1 Mass Variation with Size

If all of the masses are combined, the following equation for the mass as a function of diameter is obtained.

$$M = 9358 \left[0.0402 + 0.0358 \left(\frac{D}{1000} \right) + 0.4092 \left(\frac{D}{1000} \right)^2 + 0.5148 \left(\frac{D}{1000} \right)^3 \right]$$

which is valid for reasonable changes in diameter. The equation should be restricted to spacecraft performing the mission of the baseline design at an altitude of 2400 km or more and with a film mass of 4 g/m². The baseline design has a total mass per unit area of 11.9 g/m².

2.10.2 Structural Mass Fraction

If the reflector membrane is considered to be the payload, then the ratio of structural and mechanism mass to payload mass is

$$\frac{M_{\text{str}}}{M_{\text{pay}}} = 1.116 \left[0.196 + 0.804 \frac{D}{1000} \right]$$

which is shown in Figure 27 plotted against reflector area. Designs smaller than the baseline offer the lowest mass per unit area. Larger sizes, which would exceed the volume capacity of the Shuttle anyway, become very inefficient since the structural mass becomes much larger than the payload mass as the area increases.

2.11 VIBRATION FREQUENCIES

Accurate determination of the various vibration modes and frequencies of the spacecraft will require more definition and investigation. Approximate frequencies, however, can be obtained as follows.

2.11.1 Membrane Vibration

The shape of the lowest-frequency membrane mode that couples with spacecraft rotation is $J_1(\lambda r) \cos \theta$ where J_1 is a Bessel function. The frequency is

$$f_{\text{membrane}} = 1.216 \sqrt{\frac{N}{\rho t D^2}} \quad \text{Hz}$$

where ρt is the membrane density. For the baseline design,

$$f_{\text{membrane}} = 0.03 \text{ Hz}$$

2.11.2 Stay Vibration

The "violin-string" mode of each stay has a frequency fundamental of

$$f_{\text{stay}} = \frac{1}{2} \sqrt{\frac{T}{\rho A L^2}} \text{ Hz}$$

where T is the stay tension, ρA its mass density, and L its length. For the baseline design

$$f_{\text{stay}} = 0.021 \text{ Hz}$$

2.11.3 Center-body Vibration

The moment of inertia of the center body in the pitch direction is about $2 \times 10^5 \text{ kg-m}^2$ and is composed mainly of the static moment of inertia of the flywheels. The frequency of vibration due to the flexibility of the central column is about 0.25 Hz.

2.11.4 Implications

The center-body vibration frequency is probably the lowest of the modes involving structural straining. It appears to be high enough to avoid interactive difficulties with the control system. The vibration frequency of the stays is quite low, but the amount of mass involved is small enough to avoid major difficulties, particularly since the stay-to-stay variations of properties would tend to keep all of them from acting in concert.

Membrane vibration apparently presents the most severe challenge to the control-logic designer. The frequency is low (0.03 Hz),

the mass is fairly large and the damping can be expected to be low. Artificial damping may be required to cope with these vibrations.

SECTION 3

CONCLUSIONS

This study has shown that a 1-km-diameter spacecraft should have a total specific mass of less than 12 g/m^2 . A major finding of the study is that there is at least one technique for packaging this large structure for a Shuttle launch with a subsequent automatic deployment on-orbit. The mass of the circular rim truss and canisters, which are currently 25 percent of the spacecraft mass, might be reduced by the use of expandable truss columns. However, reliable sequential deployment mechanisms need to be developed and tested for this type of mast.

The major technical development required before this reflector spacecraft can be designed for flight is the manufacture, handling, and packaging of a thin aluminized Kapton film that can be deployed as a smooth flat surface in space without the need to apply flattening tensions which exceed those required to balance the environmental and dynamic loads. The analysis of this spacecraft structure as a flexible structure is also left for the future.

The design of the reflector-spacecraft structure is very dependent on the mission, particularly the number of ground sites that are to be illuminated each orbit. The results of the current studies should prove useful in the consideration of a system involving many satellites and ground sites. The effect of non-coplanar dynamics in an efficiently designed mission requires a careful and thorough study because of the significant influence on control system mass and structural loadings.

TABLE I. REQUIRED TORQUES AND ANGULAR IMPULSES DURING OVER-SITE
TRACKING MANEUVERS FOR THE BASELINE SATELLITE

$$(I_y = 4.91 \times 10^8 \text{ kg-m}^2)$$

SOURCE	ALTITUDE = 2400 km (ORBITAL PERIOD = 8179 s) (TIME OVER THE SITE = 955 s)				ALTITUDE = 4146 km (ORBITAL PERIOD = 10,739 s) (TIME OVER THE SITE = 1691 s)			
	MAX. ANG. ACCEL. (rad/s ²)	MAX. ANG. VEL. CHANGE (rad/s)	MAX. TORQUE (N-m)	MAX. ANG. IMPULSE (N-m-s)	MAX. ANG. ACCEL. (rad/s ²)	MAX. ANG. VEL. CHANGE (rad/s)	MAX. TORQUE (N-m)	MAX. ANG. IMPULSE (N-m-s)
Coplanar tracking kinematics	1.87×10^{-6}	6.79×10^{-4}	918	3.33×10^5	4.42×10^{-7}	2.88×10^{-4}	217	1.41×10^5
Worst-case* gravity gradient ($\delta = \phi + 45^\circ$)	8.85×10^{-7}	8.45×10^{-4}	432	4.13×10^5	5.13×10^{-7}	8.67×10^{-4}	252	4.26×10^5
Solar pressure* misalignment (0.1%)	1.45×10^{-8}	1.38×10^{-5}	7.11	6.79×10^3	1.45×10^{-8}	2.45×10^{-5}	7.11	1.20×10^4

*Note: Maximum angular impulse and angular velocity change were determined by assuming constant torque and angular acceleration for the total time oversite.

TABLE II. REQUIRED TORQUES AND ANGULAR IMPULSES DURING BANG-BANG REORIENTATION MANEUVERS FOR THE BASELINE SATELLITE

$$(I_y = 4.91 \times 10^8 \text{ kg-m}^2)$$

SOURCE	ALTITUDE = 2400 km (ORBITAL PERIOD = 8179 s)				ALTITUDE = 4146 km (ORBITAL PERIOD = 10,739 s)			
	MAX. ANG. ACCEL. (rad/s ²)	MAX. ANG. VEL. CHANGE (rad/s)	MAX. TORQUE (N-m)	MAX. ANG. IMPULSE (N-m-s)	MAX. ANG. ACCEL. (rad/s ²)	MAX. ANG. VEL. CHANGE (rad/s)	MAX. TORQUE (N-m)	MAX. ANG. IMPULSE (N-m-s)
Six equidistant Earth sites (detailed anal.)	1.96×10^{-5} (3.5×10^{-5})	3.99×10^{-3} (7.14×10^{-3})	9.62×10^6 (1.72×10^4)	1.96×10^6 (3.51×10^6)	2.34×10^{-4}	1.15×10^{-2}	1.15×10^5	5.64×10^6
Two equidistant Earth sites (worst-case)	6.39×10^{-7}	1.00×10^{-3}	313	4.92×10^5	4.64×10^{-7}	8.53×10^{-4}	228	4.19×10^5
One Earth site (worst-case)	1.20×10^{-7}	4.32×10^{-4}	59.1	2.13×10^5	7.68×10^{-8}	3.48×10^{-4}	37.7	1.71×10^5

*Note: Numbers in parentheses were determined from an angular acceleration of 3.5×10^{-5} rad/s² provided by J. Canady of NASA LaRC. Other numbers determined as explained in text.

TABLE III. MASS, POWER, AND ENERGY REQUIREMENT FOR
BASELINE CONTROL ACTUATORS FOR TRACKING
TWO EQUIDISTANT EARTH SITES

CONTROL ACTUATOR TYPE	ALTITUDE = 2400 km			ALTITUDE = 4146 km		
	TOTAL MASS (kg)	PEAK POWER (W)	ENERGY STORAGE (W-hr)	TOTAL MASS (kg)	PEAK POWER (W)	ENERGY STORAGE (W-hr)
Control moment gyroscope (r = 20 m)	2,000	4.80	2.73	1,520	1.94	1.45
Magnetic loop controller	335	100	22.7	598	100	29.8
Reaction wheels (r = 20 m)	700	14,400	16,400	528	5,060	7,550

Note: For tracking six equidistant Earth sites, the required mass of a control moment gyroscope system is 5,260 kg at 2400 km (9,460 kg using NASA-supplied acceleration levels of 3.5×10^{-5} rad/sec²) and 15,200 kg at 4146-km altitude.

TABLE IV. DETAILS OF BASELINE BIAxIAL TWIN-ROTOR
CONTROL MOMENT GYROSCOPE DESIGN

ITEM	ALTITUDE = 2400 km	ALTITUDE = 4146 km
Control torque capacity	1,350 N-m	469 N-m
Angular impulse capacity	7.46×10^5 N-m-s	5.67×10^5 N-m-s
Angular momentum capacity	4.26×10^6 N-m-s	3.24×10^6 N-m-s
Mass of flywheels (2)	1000 kg	760 kg
Flywheel design		
Radius	20 m	20 m
Material	Glass fiber	Glass fiber
Working stress	7.58×10^8 N/m ²	7.58×10^8 N/m ²
Mass density	2.03×10^3 kg/m ³	2.03×10^3 kg/m ³
Surface density of fibers	0.199 kg/m ²	0.151 kg/m ²
Number of fibers	475,000	370,000
Fiber diameter	0.01 mm	0.01 mm
Spin velocity	42.8 rad/sec	42.8 rad/sec
Fiber velocity at tip	856 m/sec	856 m/sec
Mass of bearings, motors, and linkages	1000 kg	760 kg
Flywheel spin motor type	Electric (pancake)	Electric (pancake)
Pushrod compressive load	794 N	276 N
Pushrod length	4 m	4 m
Bellcrank radius	0.148 m	0.148 m

(Baseline flight plan: Tracking of two Earth sites each orbit

TABLE V. DETAILS OF BASELINE MAGNETIC-LOOP CONTROL ACTUATOR DESIGN

ITEM	ALTITUDE = 2400 km	ALTITUDE = 4146 km
Control precessional torque capacity	71.1 N-m	71.1 N-m
Magnitude of Earth's magnetic induction, \underline{B}	2×10^{-5} Weber/m ²	1.5×10^{-5} Weber/m ²
Current in each circuit	38.0 milliamp	50.7 milliamp
Voltage on each circuit	58.5 volts	43.8 volts
Power in each circuit	2.22 watts	2.22 watts
Total power, all circuits	100 watts	100 watts
Resistance of each circuit	1540 Ω	864 Ω
Resistivity of conductor (aluminum)	2.83×10^{-8} Ω m	2.83×10^{-8} Ω m
Mass density of conductor (aluminum)	2.7×10^3 kg/m ³	2.7×10^3 kg/m ³
Total loop mass, all circuits	309 kg	551 kg
Total conductor mass, including spokes, all circuits	335 kg	598 kg
Loop mass, each circuit	6.87 kg	12.2 kg
Wire volume, each circuit loop	2.54×10^{-3} m ³	4.52×10^{-3} m ³
Wire cross-sectional area, all circuits	0.216 mm ²	0.384 mm ²
Wire diameter, all circuits	0.524 mm	0.699 mm

(45 independent circuits, each with 3.74 turns in its coil)

TABLE VI. MASS SUMMARY FOR BASELINE 1-km-DIAMETER
REFLECTOR SPACECRAFT (FLIGHT CONDITION
2400-km ORBIT)

ITEM	MASS (KG)
<u>REFLECTOR MEMBRANE</u>	
Area = 785,400 m ² at 4 gm/m ²	<u>3142</u>
	3142
<u>STRUCTURAL COMPONENTS</u>	
Edge tendons (90)	12
Film-expansion compensators (90)	330
Rim truss	1760
Storage canisters and mechanisms	552
Rim hinges and motors (6)	30
Stay tapes, front and back (180)	367
Tape reels	42
Central masts and canisters (500 m)	364
Center tube	<u>48</u>
	3505
<u>CONTROL ACTUATOR</u>	
Control-moment gyro twin-rotors	1000
Control-moment gyro suspension	1000
Magnetic loop control (90 circuits)	<u>335</u>
	2335
<u>COMMUNICATIONS, POWER SUPPLY, AND CONTROL ELECTRONICS</u>	
Solar power supply (200 W avg. 100 W-hrs)	60
Hemispherical antennas (2)	20
Rate gyros and sensors	50
Communications and data handling	100
Computer	<u>46</u>
	<u>376</u>
TOTAL	9368

TABLE VII. PROPERTIES OF COMPOSITE MATERIALS

PROPERTY	GRAPHITE-EPOXY		FIBERGLASS EPOXY
	ROD AND STRIP	TUBE	
Young's modulus, N/m ²	124.5 x 10 ⁹	110.6 x 10 ⁹	52 x 10 ⁹
Density, kg/m ³	1520	1520	2000
Maximum strain, %	0.6	0.6	3

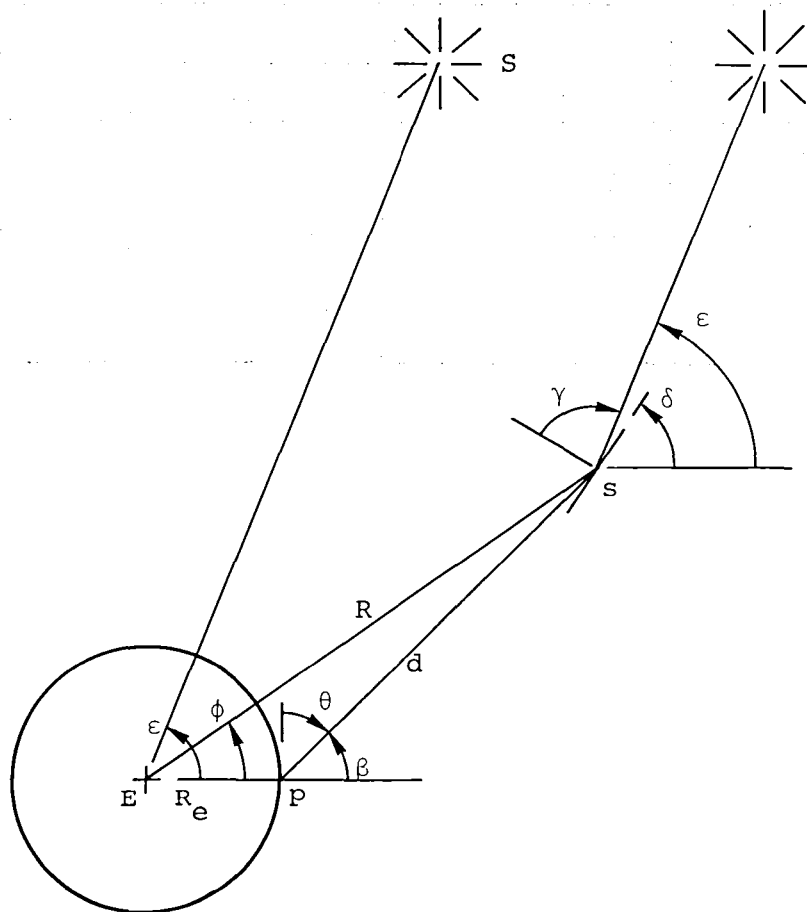


Figure 1. Geometry of geocentric satellite orbit coplanar with Earth and Sun.

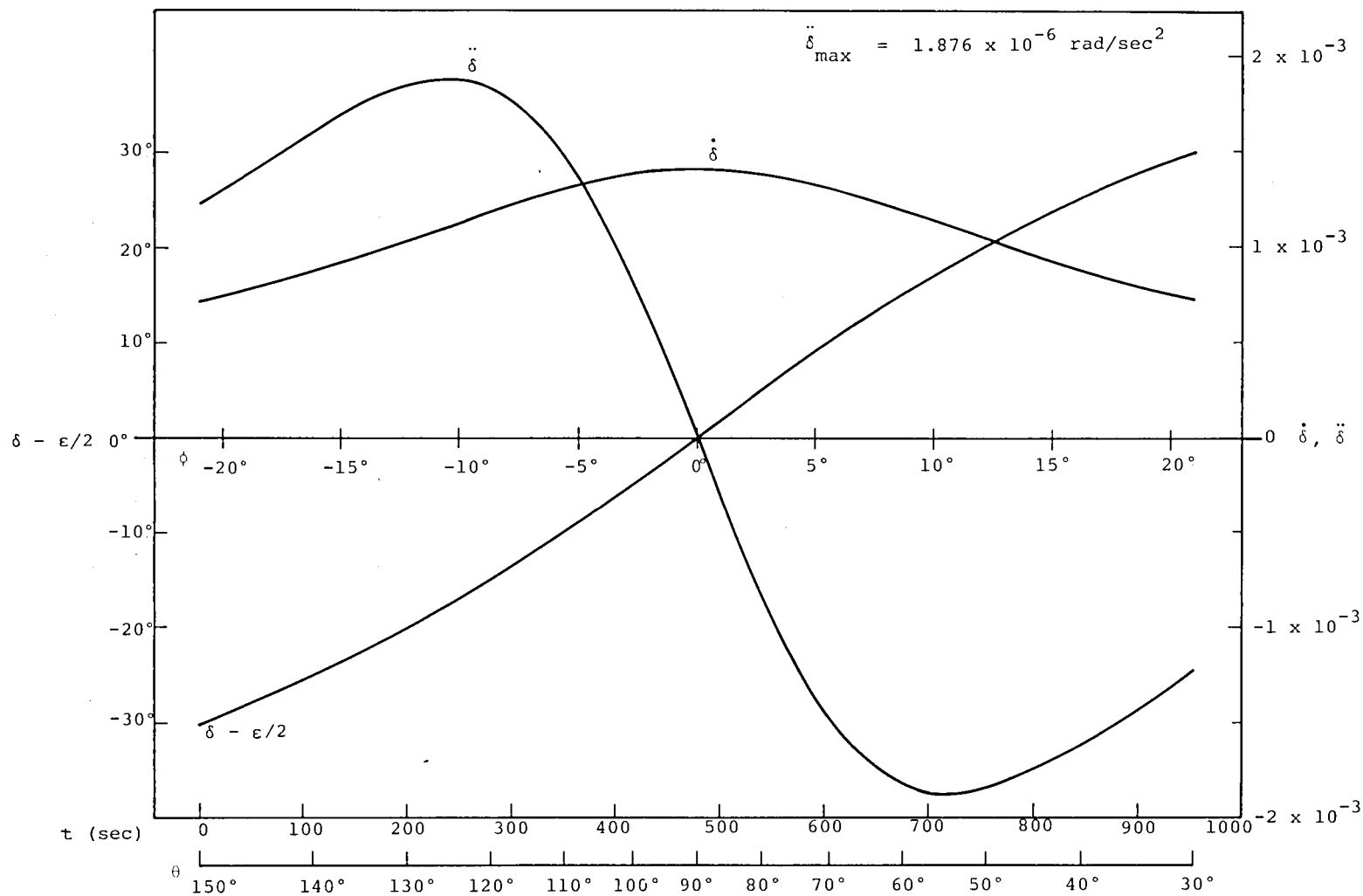


Figure 2. Kinematics of satellite tracking maneuver for an orbital altitude of 2400 km (δ in degrees, $\dot{\delta}$ in rad/s, $\ddot{\delta}$ in mrad/s²).

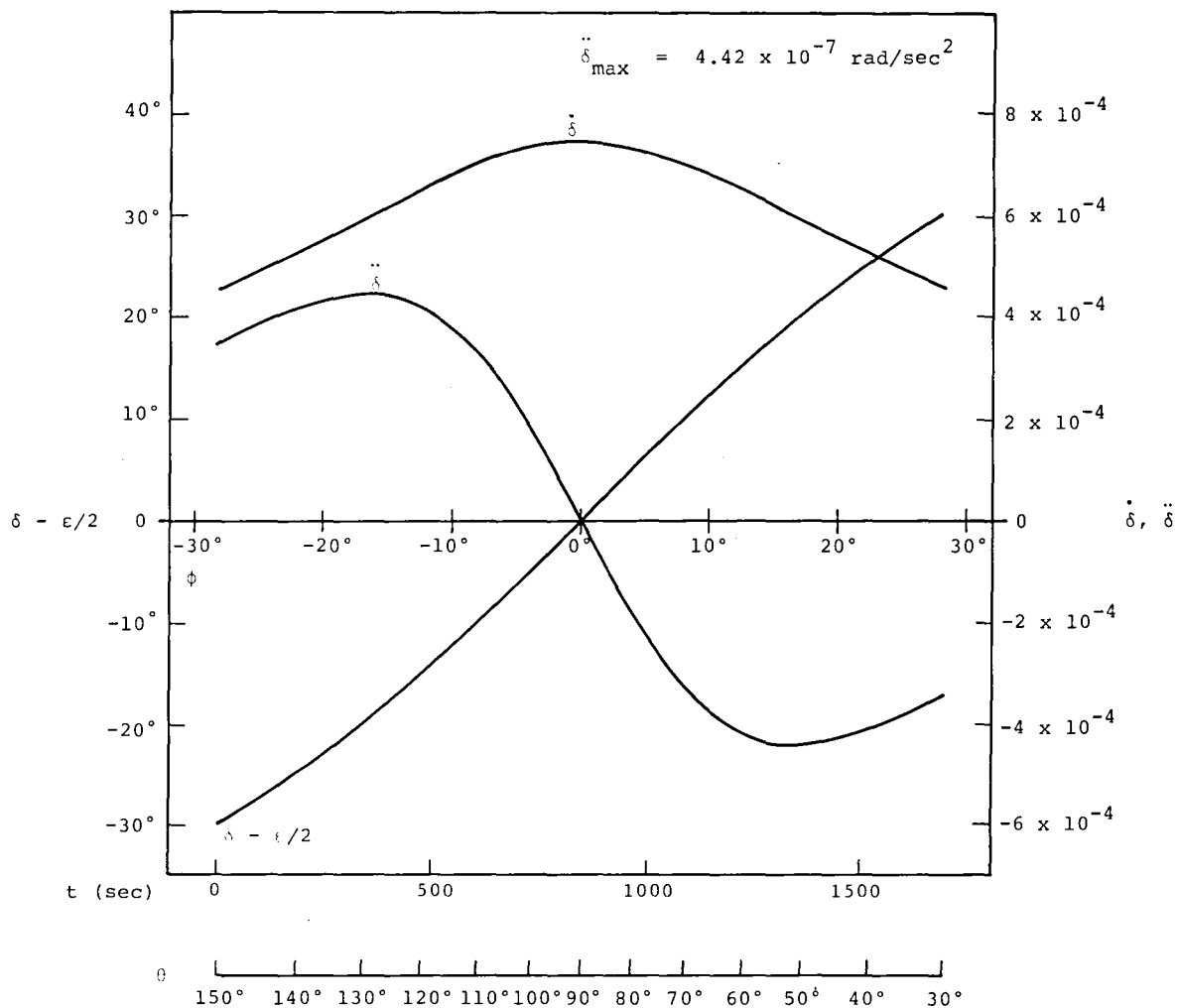


Figure 3. Kinematics of satellite tracking maneuver for an orbital altitude of 4146 km (maximum angular acceleration is $4.42 \times 10^{-7} \text{ rad/s}^2$) (δ in degrees, $\dot{\delta}$ in rad/s , $\ddot{\delta}$ in mrad/s^2).

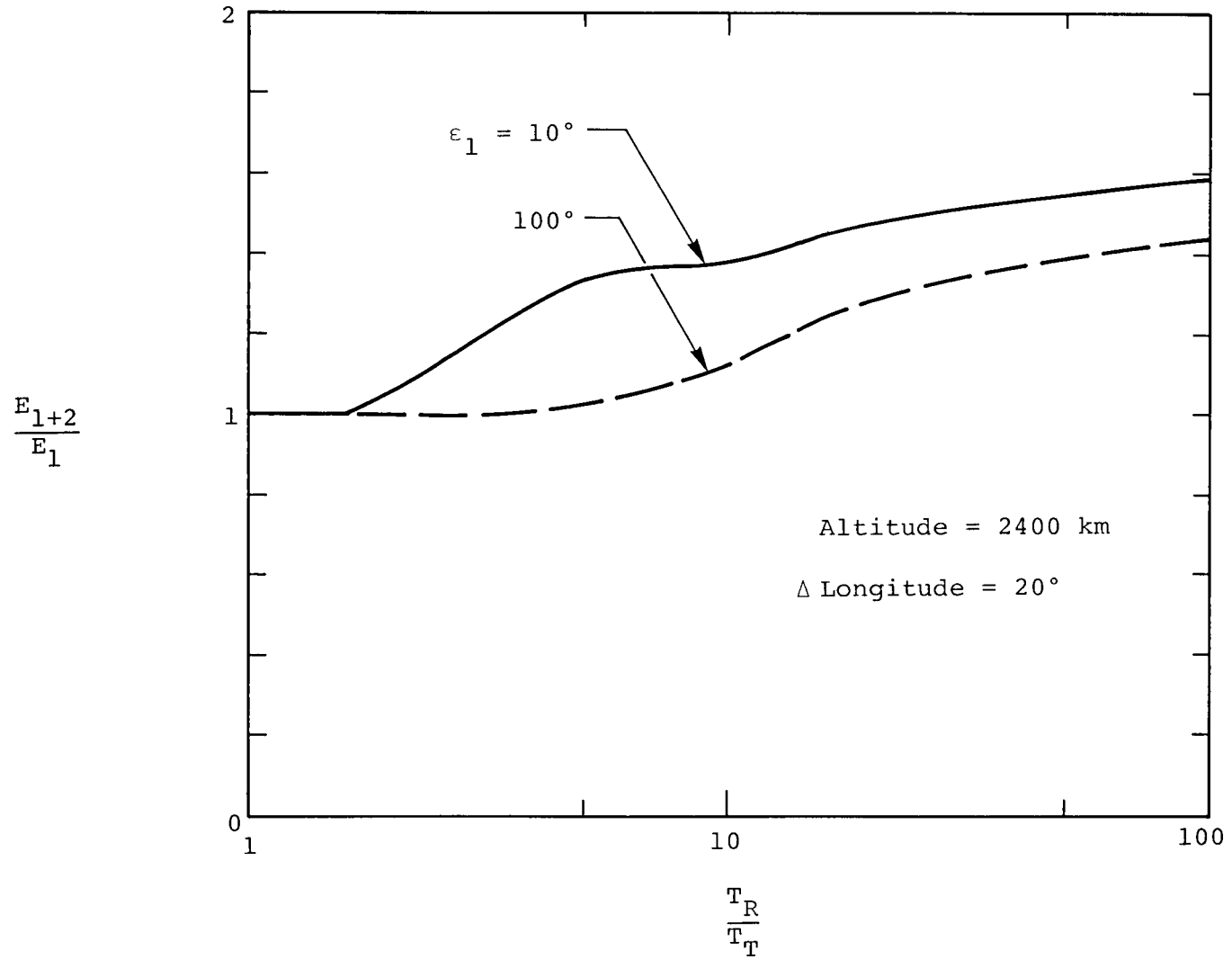


Figure 4. Increase in total reflected energy as a function of control torque ratio for two Sun angles (orbital altitude = 2400 km, 18 equidistant Earth sites).

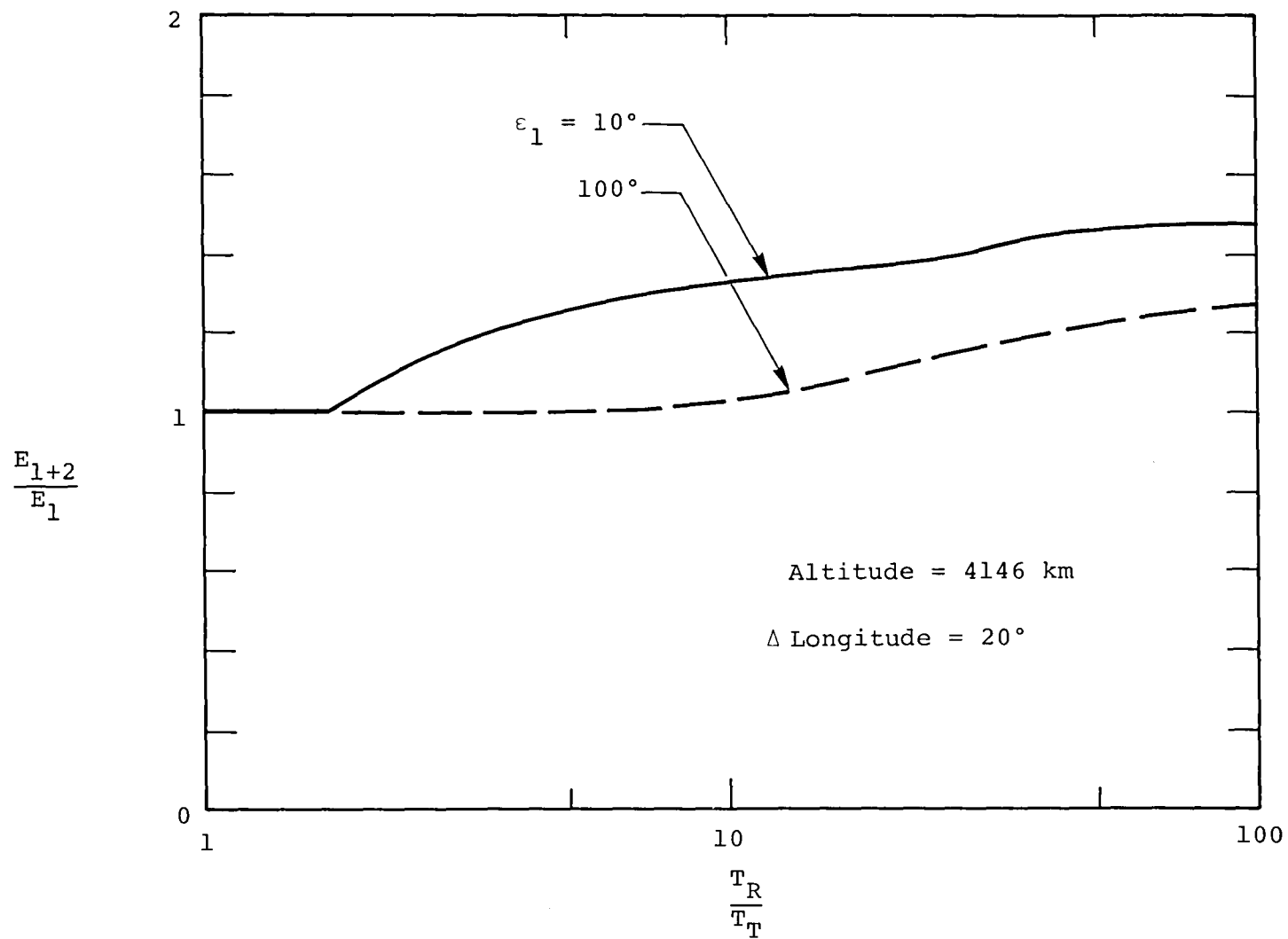


Figure 5. Increase in total reflected energy as a function of control torque ratio for two Sun angles (orbital altitude = 4146 km, 18 equidistant Earth sites).

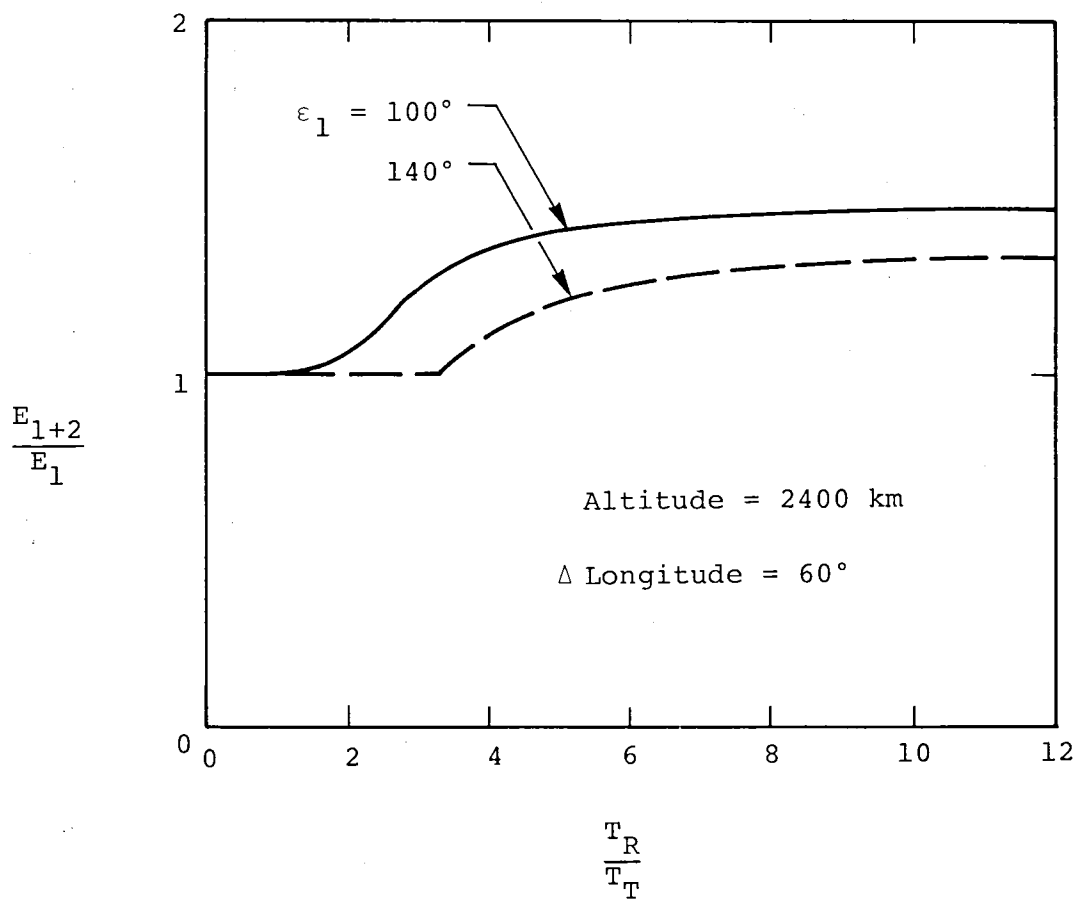


Figure 6. Increase in total reflected energy as a function of control torque ratio for two Sun angles (orbital altitude = 2400 km, six equidistant Earth sites).

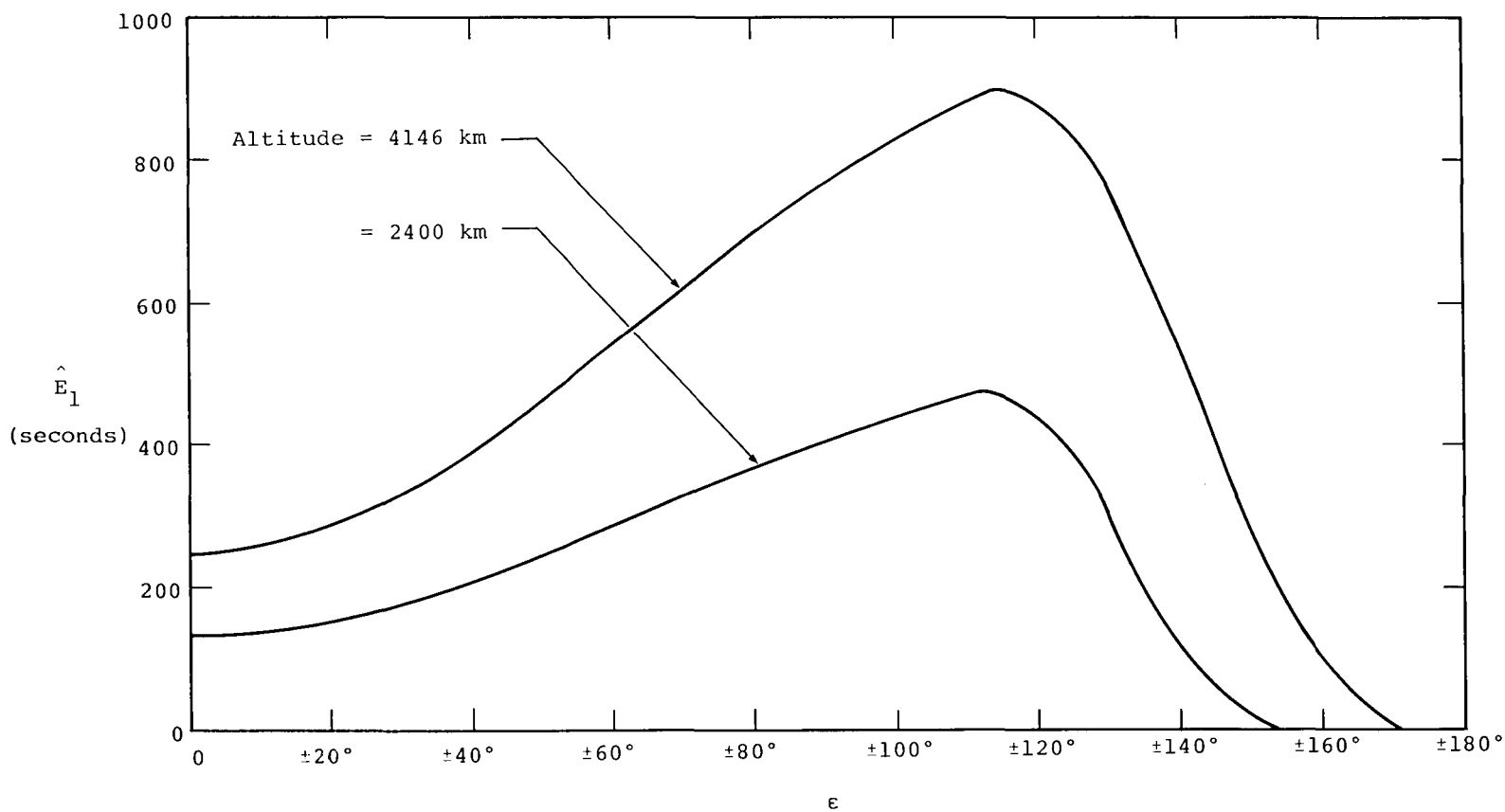


Figure 7. Normalized total reflected energy \hat{E}_1 as a function of local Sun angle ϵ for two orbital altitudes.

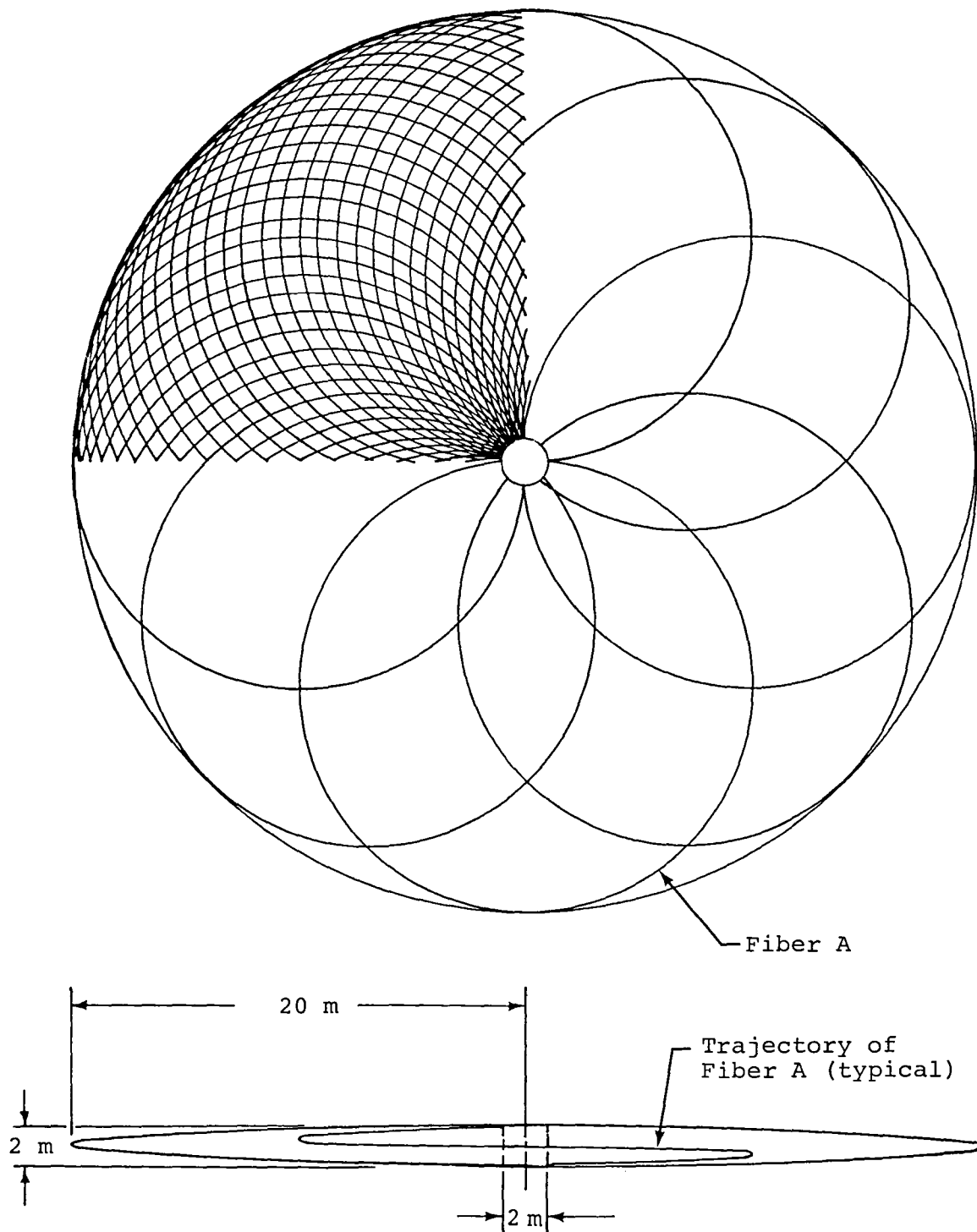


Figure 8. Deployable filamentary flywheel for control-moment gyro.

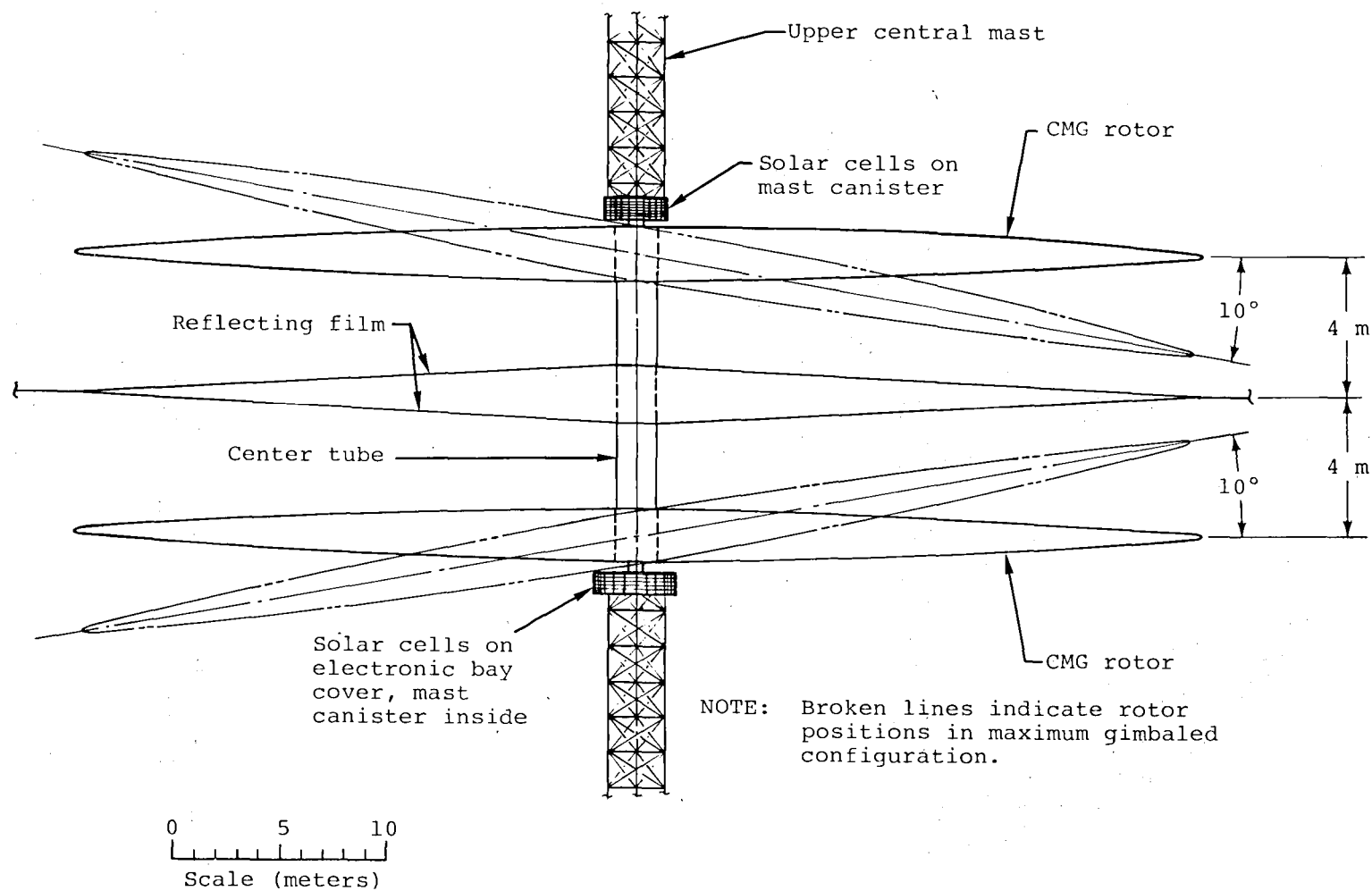


Figure 9. Closeup of center body showing twin-rotor control-moment gyro.

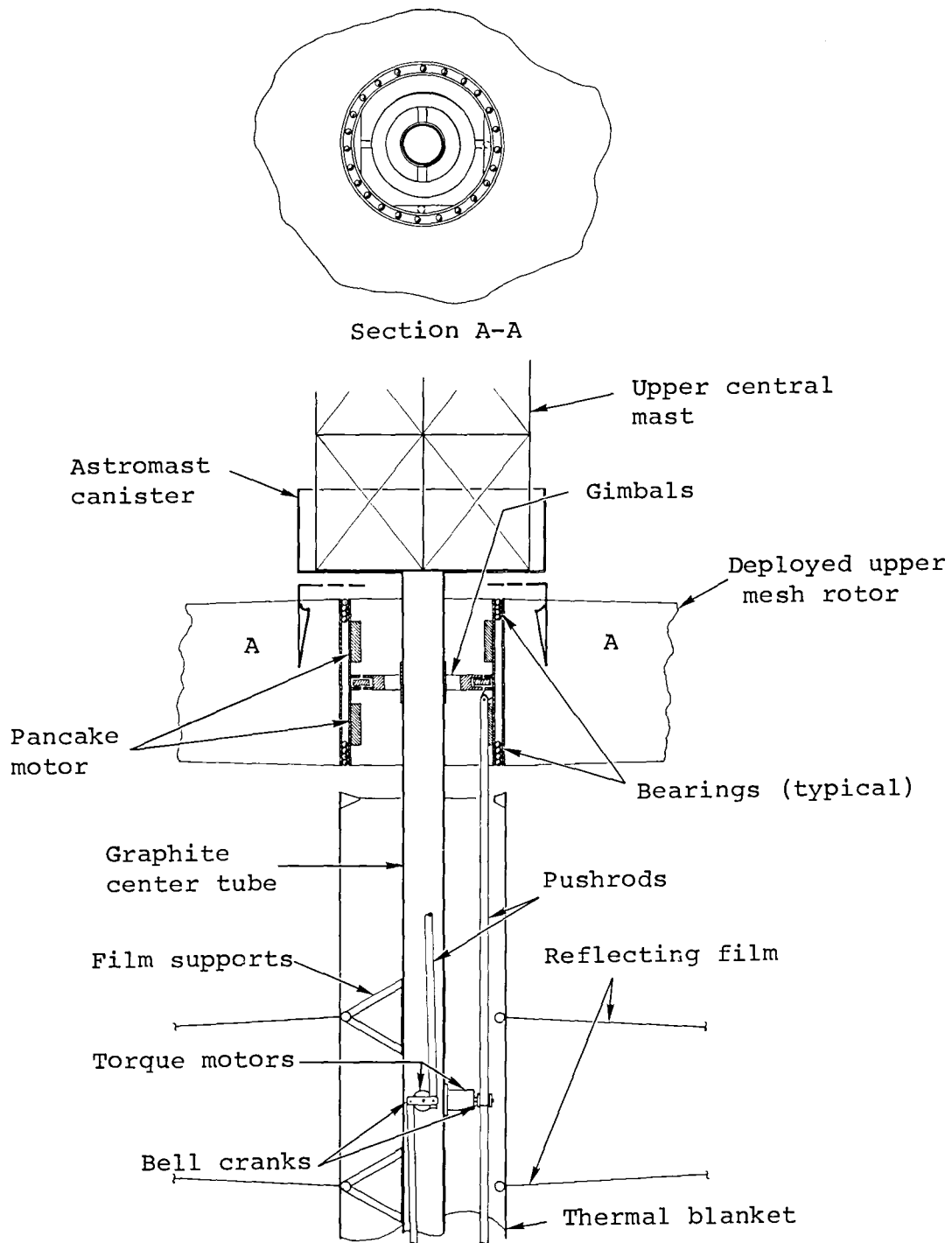


Figure 10. Cutaway view of center body showing details of twin-rotor control-moment gyro.

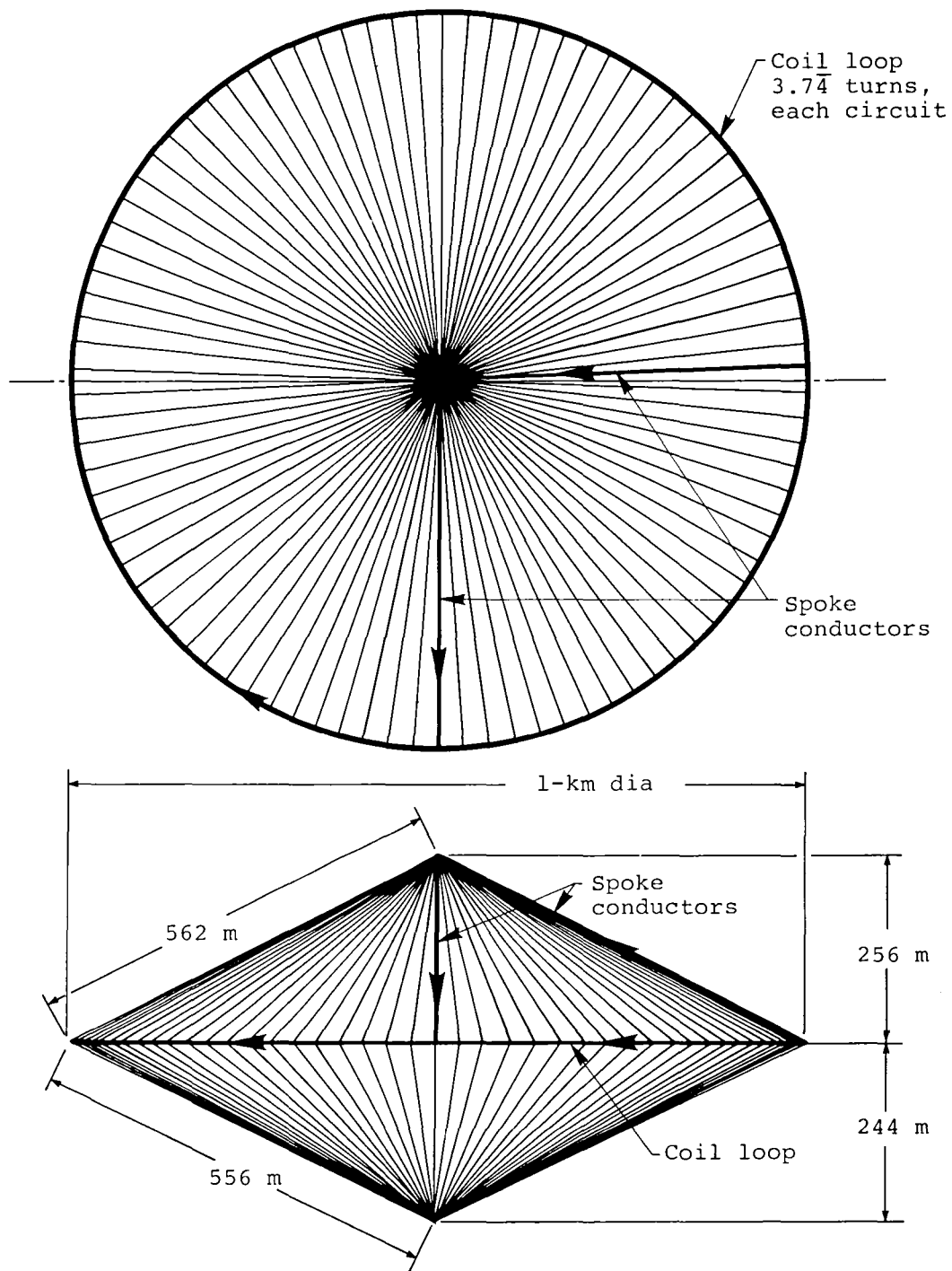


Figure 11. Typical MLC circuit loop (arrows indicate possible current direction).

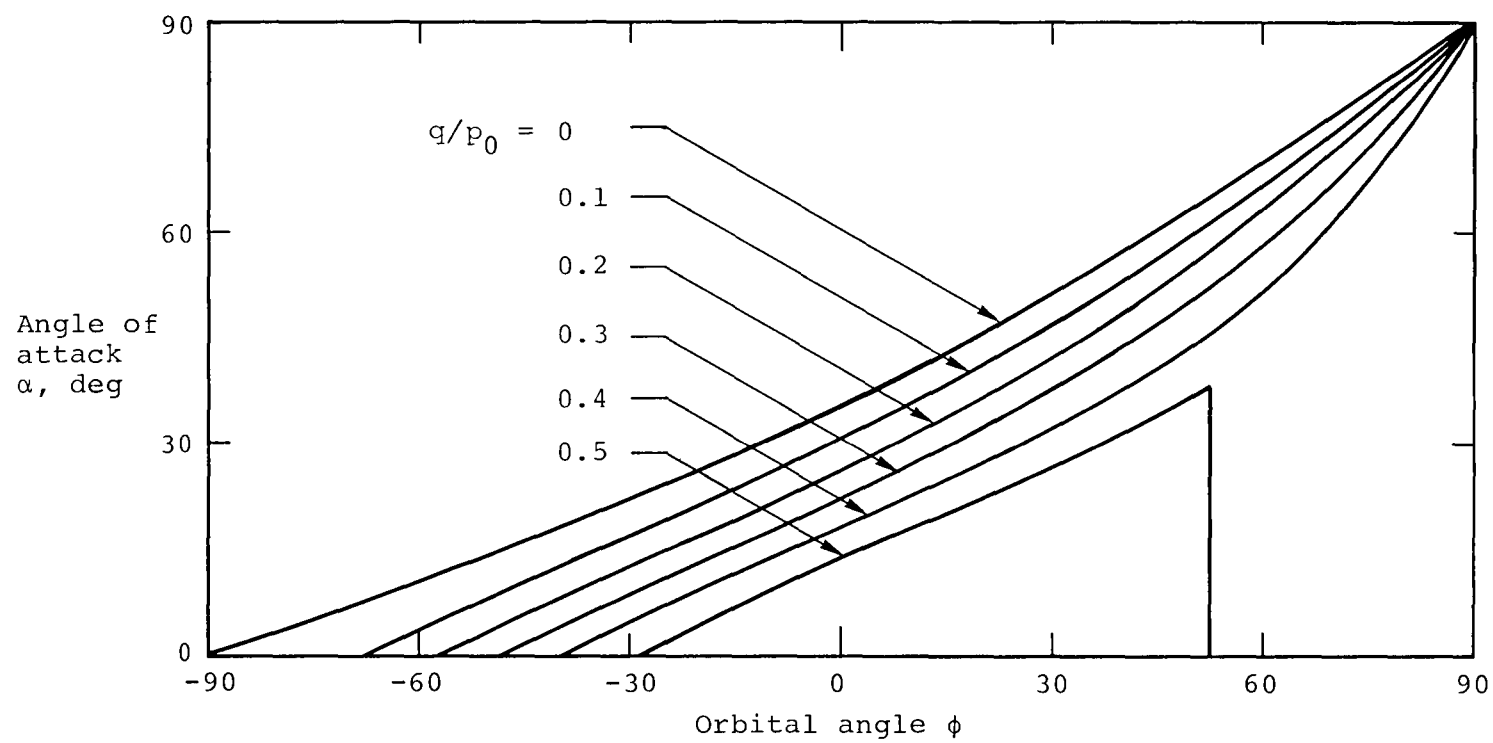


Figure 12. Angle-of-attack program for maximum net thrust ($\lambda = 0.25$).

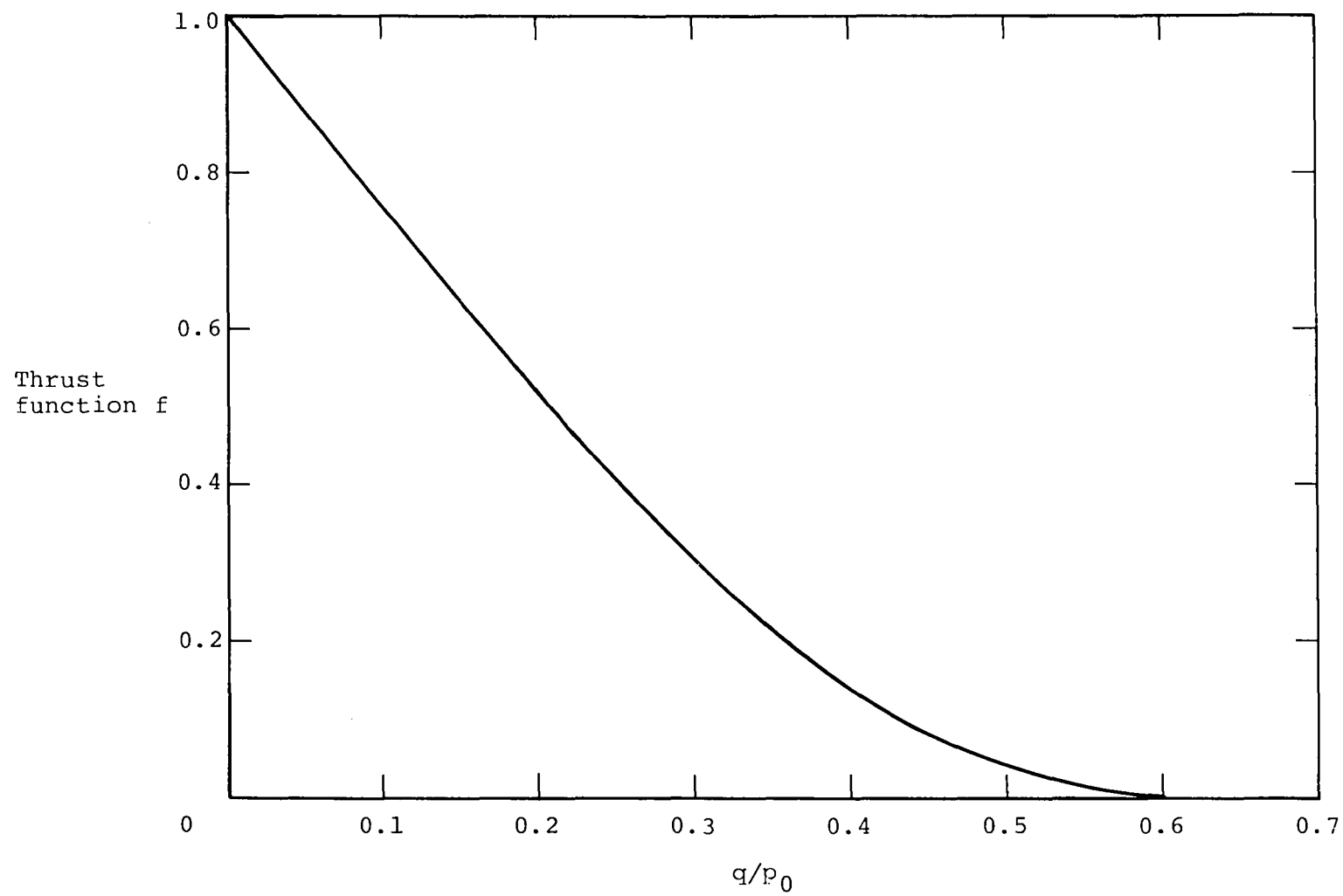


Figure 13. Variation of average net thrust with dynamic pressure ($\lambda = 0.25$).

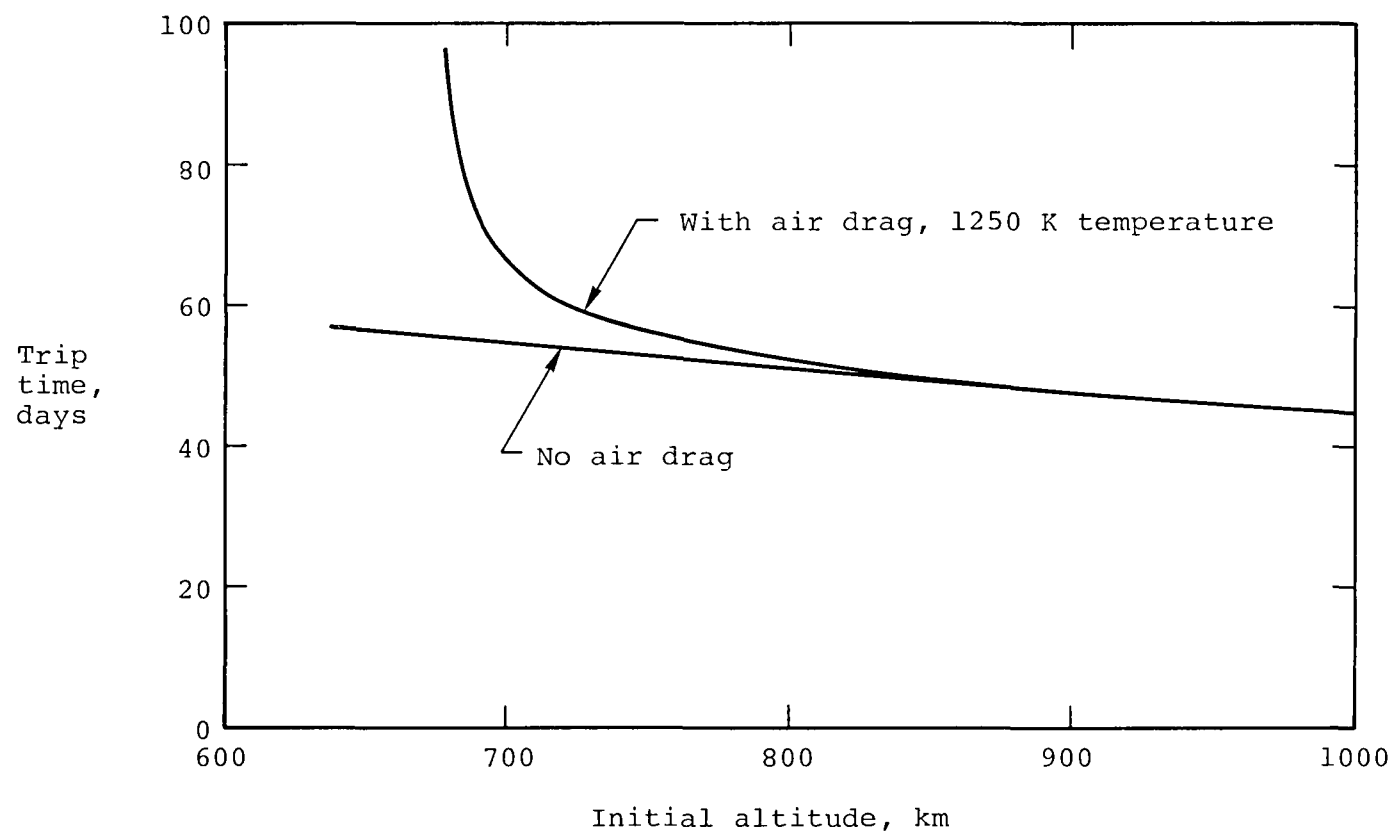


Figure 14. Trip time to 2400 km.

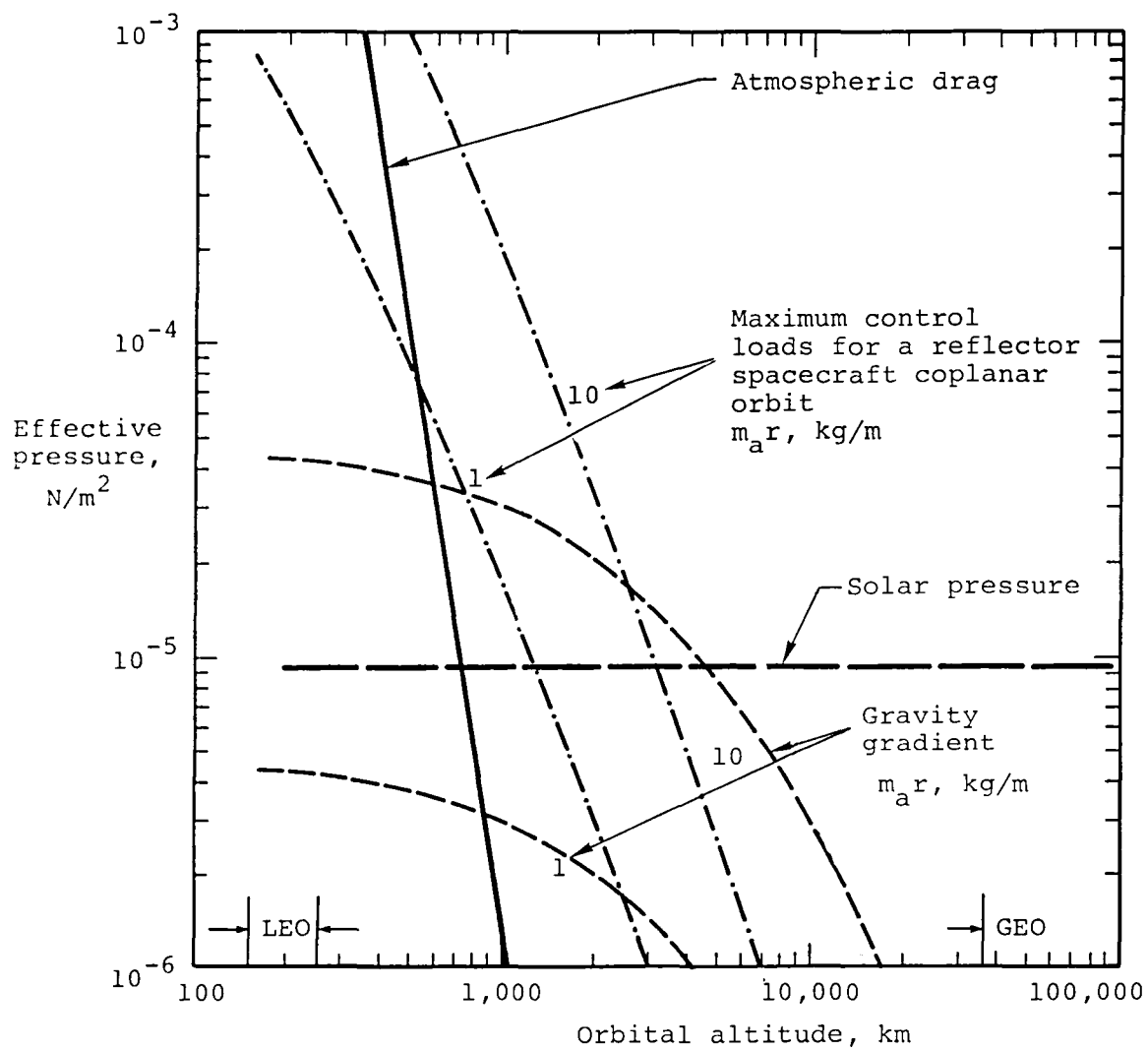


Figure 15. Maximum lateral loads on reflecting films at different orbital altitudes.

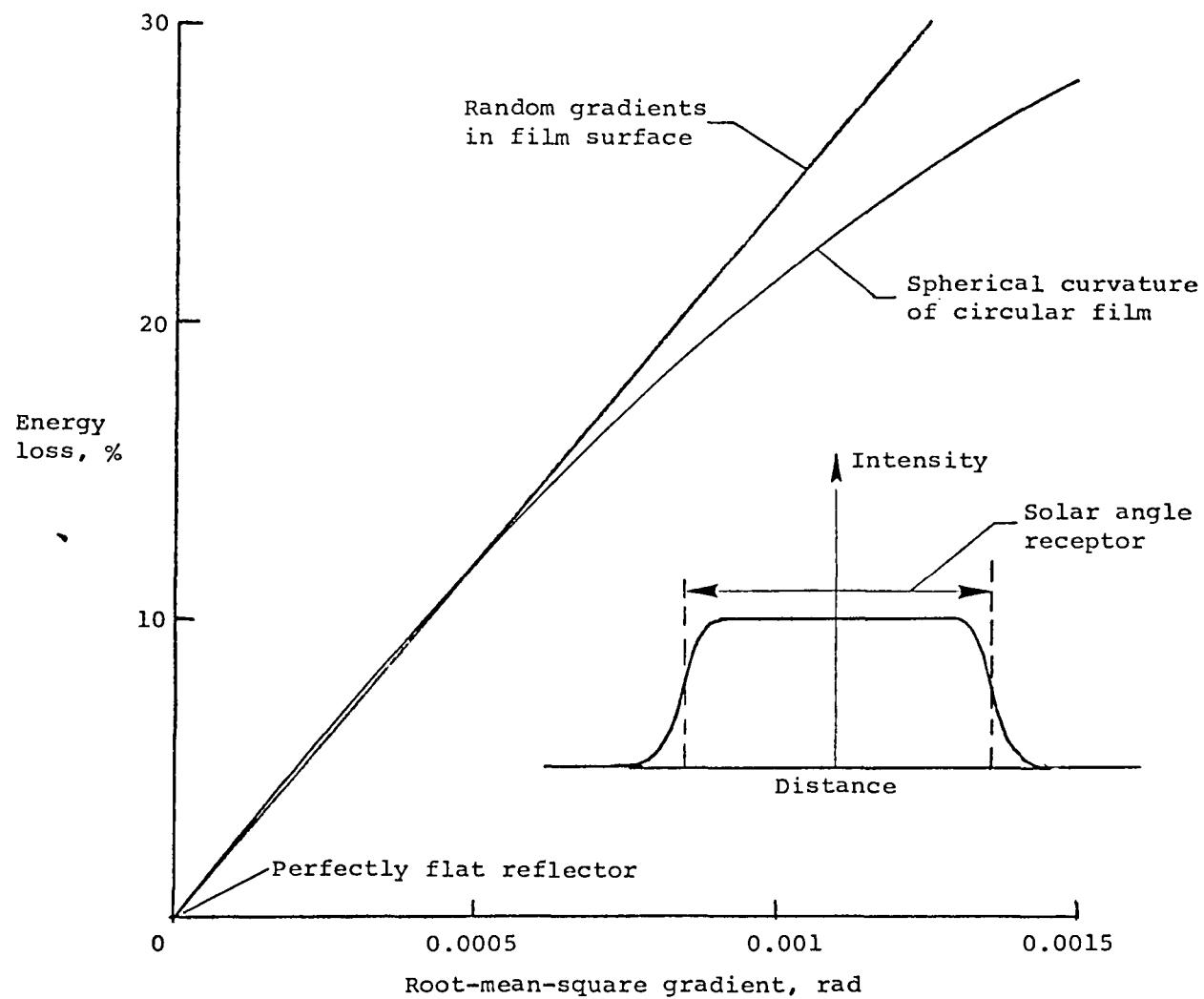


Figure 16. Effect of local gradients on mirror beam spreading.

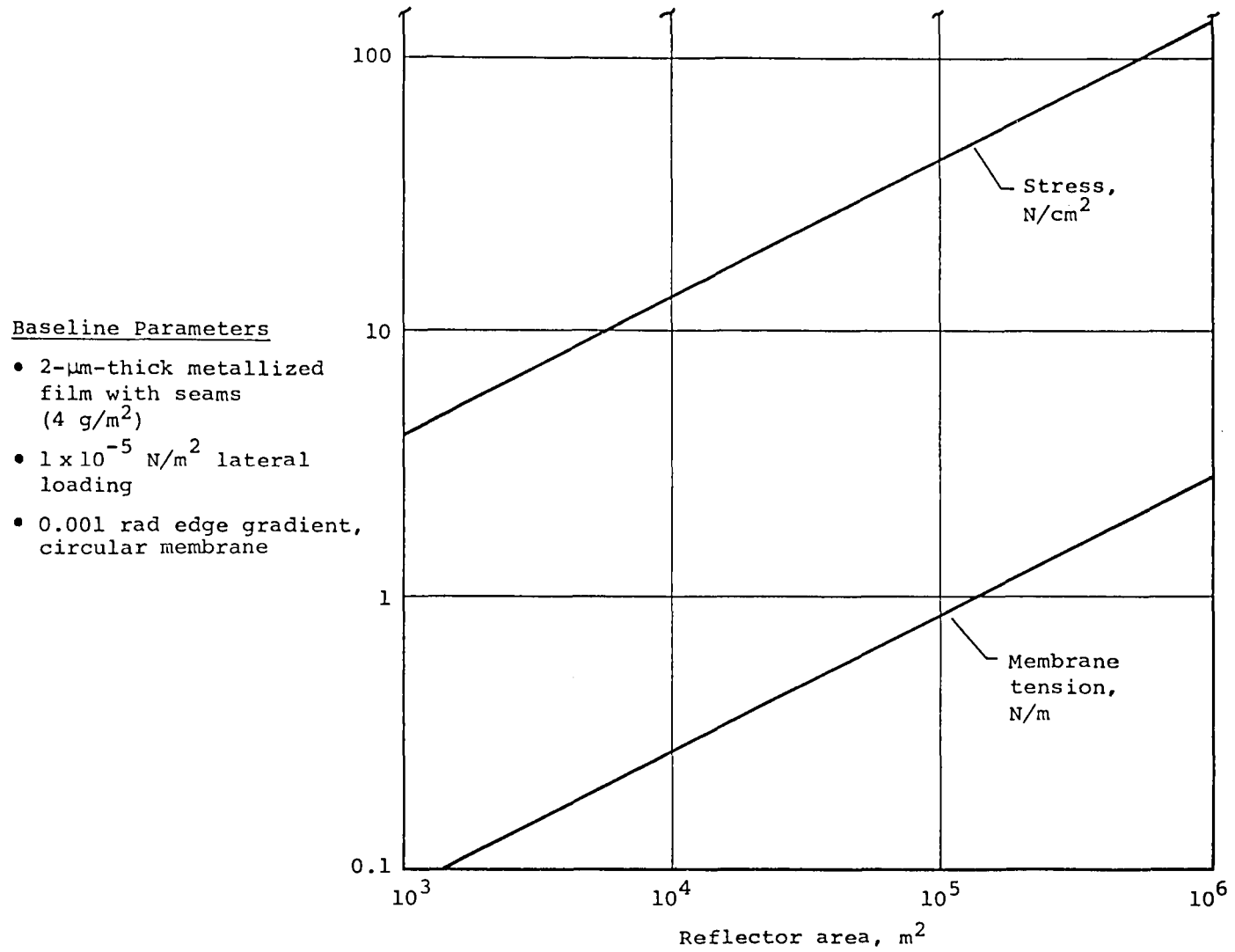


Figure 17. Film tension required to limit membrane reflector curvature.

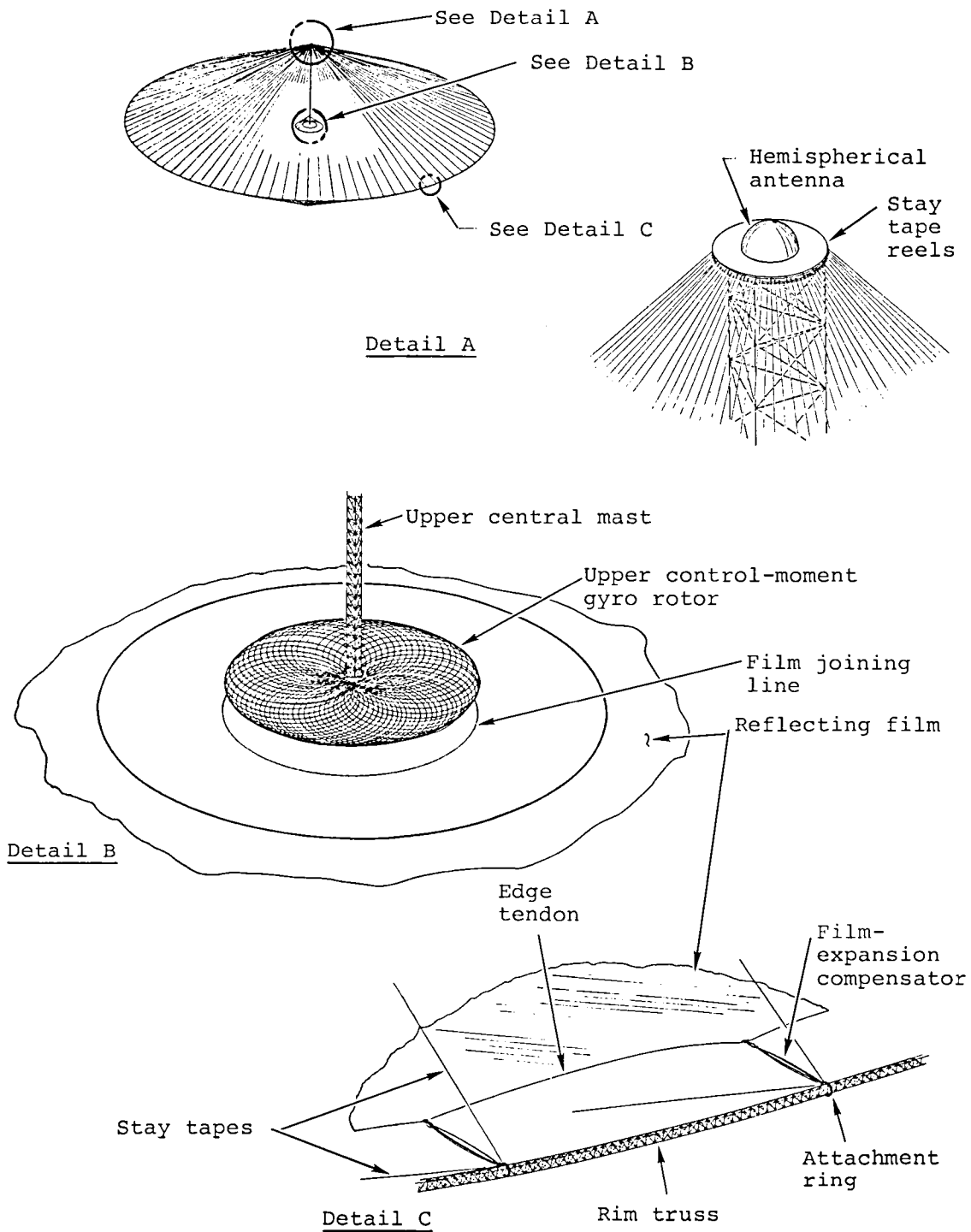


Figure 18. Circular solar-reflector spacecraft design.

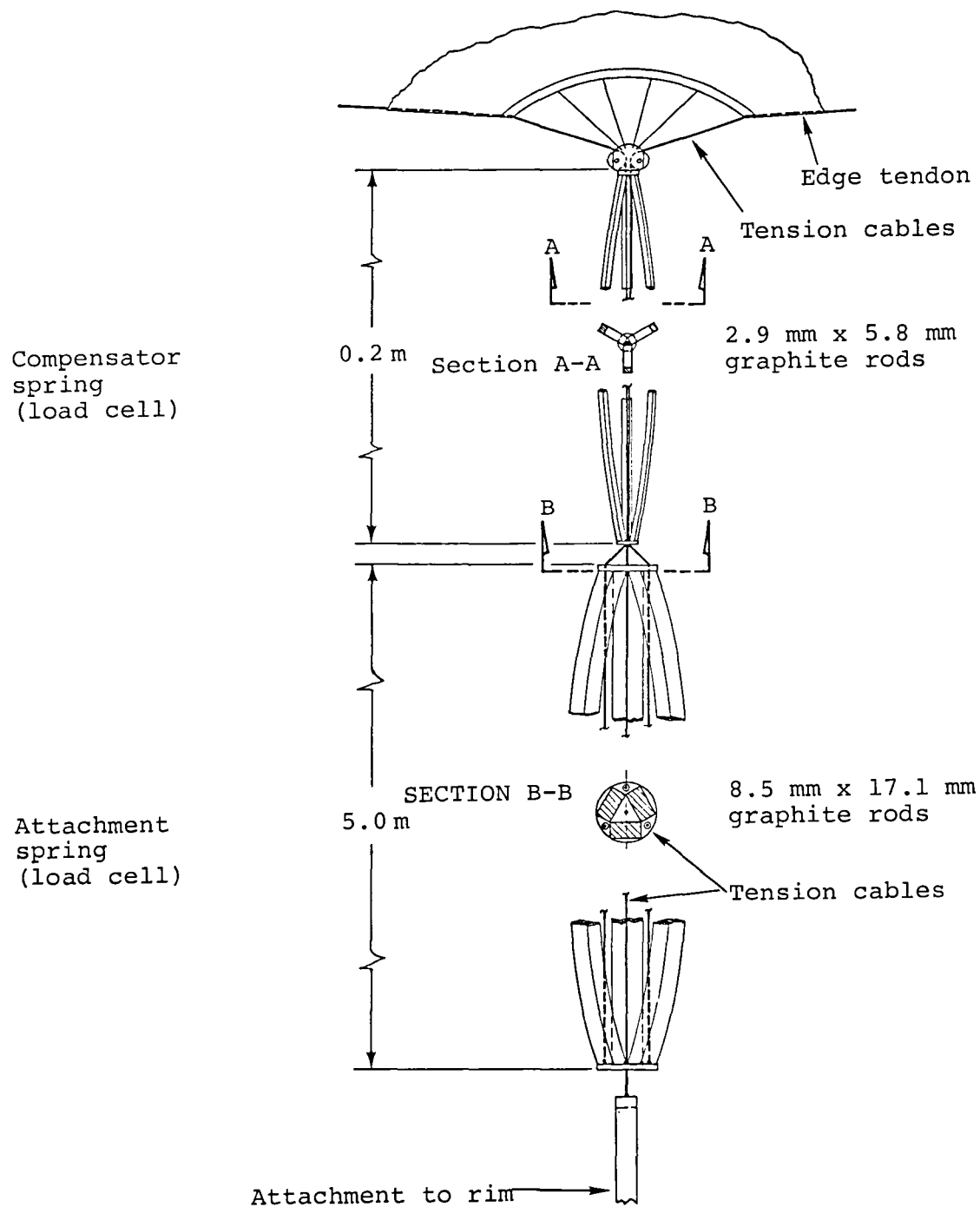


Figure 19. Baseline design of the film-expansion compensator.

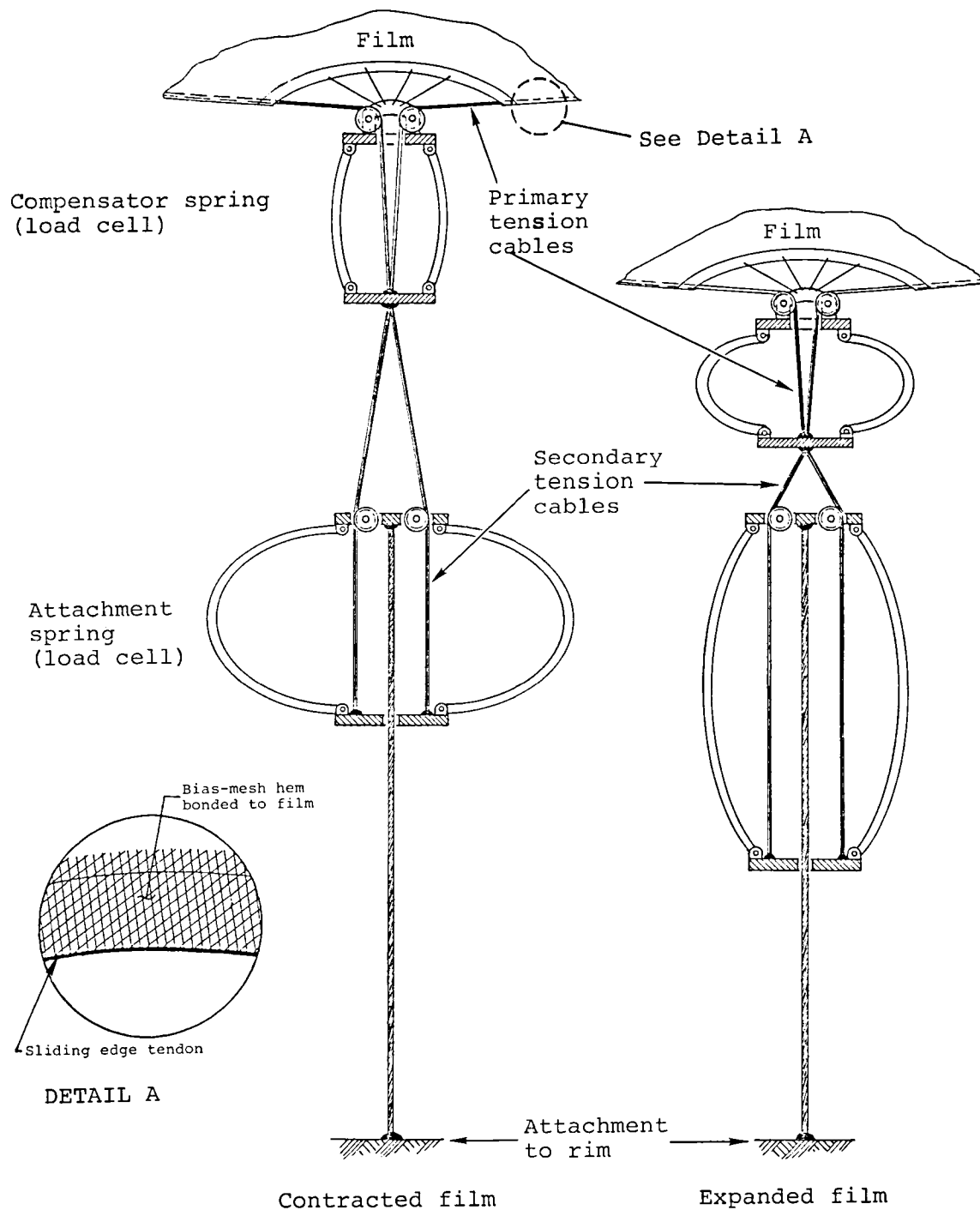


Figure 20. Schematic of film-expansion compensator.

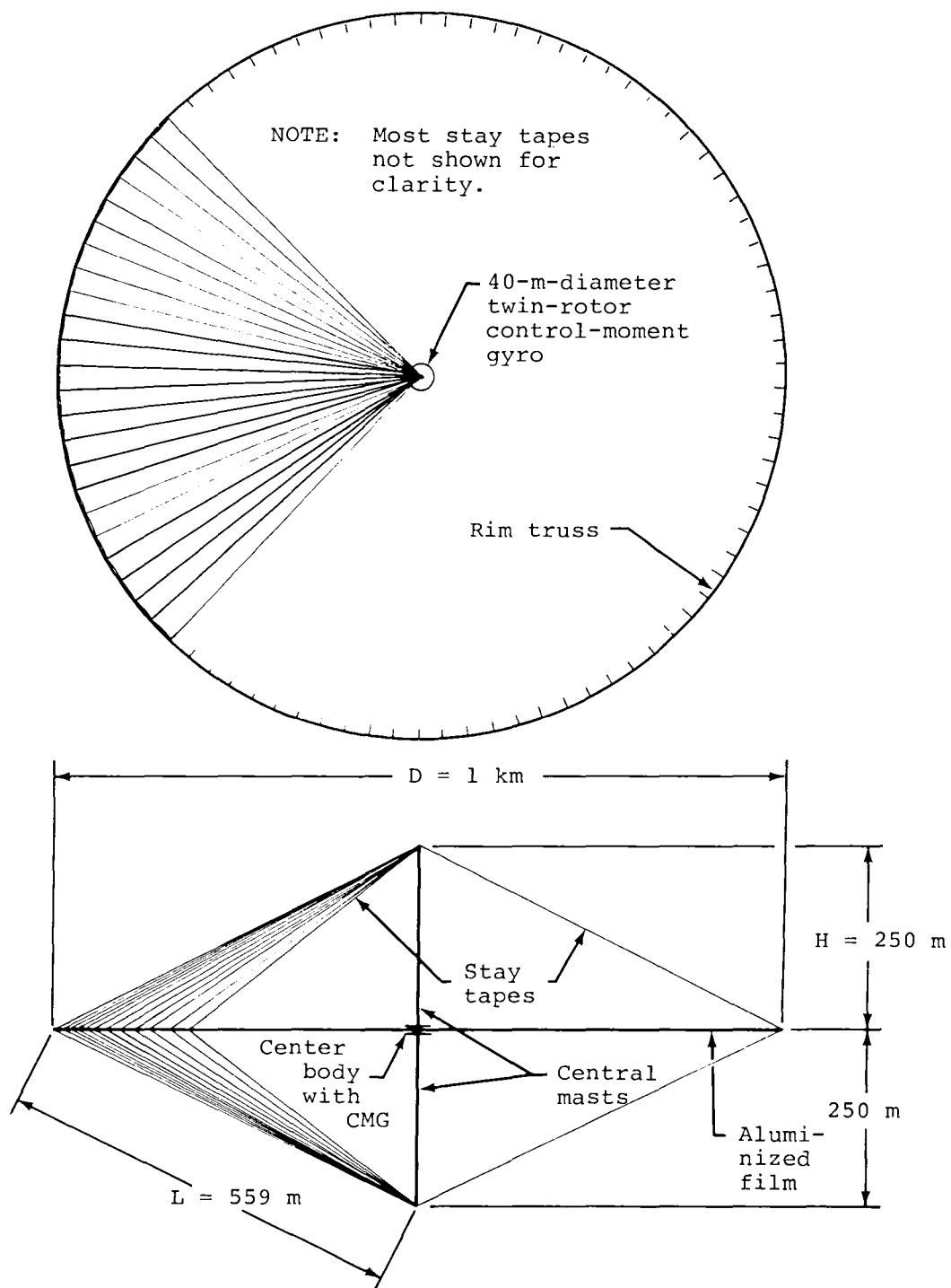


Figure 21. Baseline configuration of a solar-reflector spacecraft.

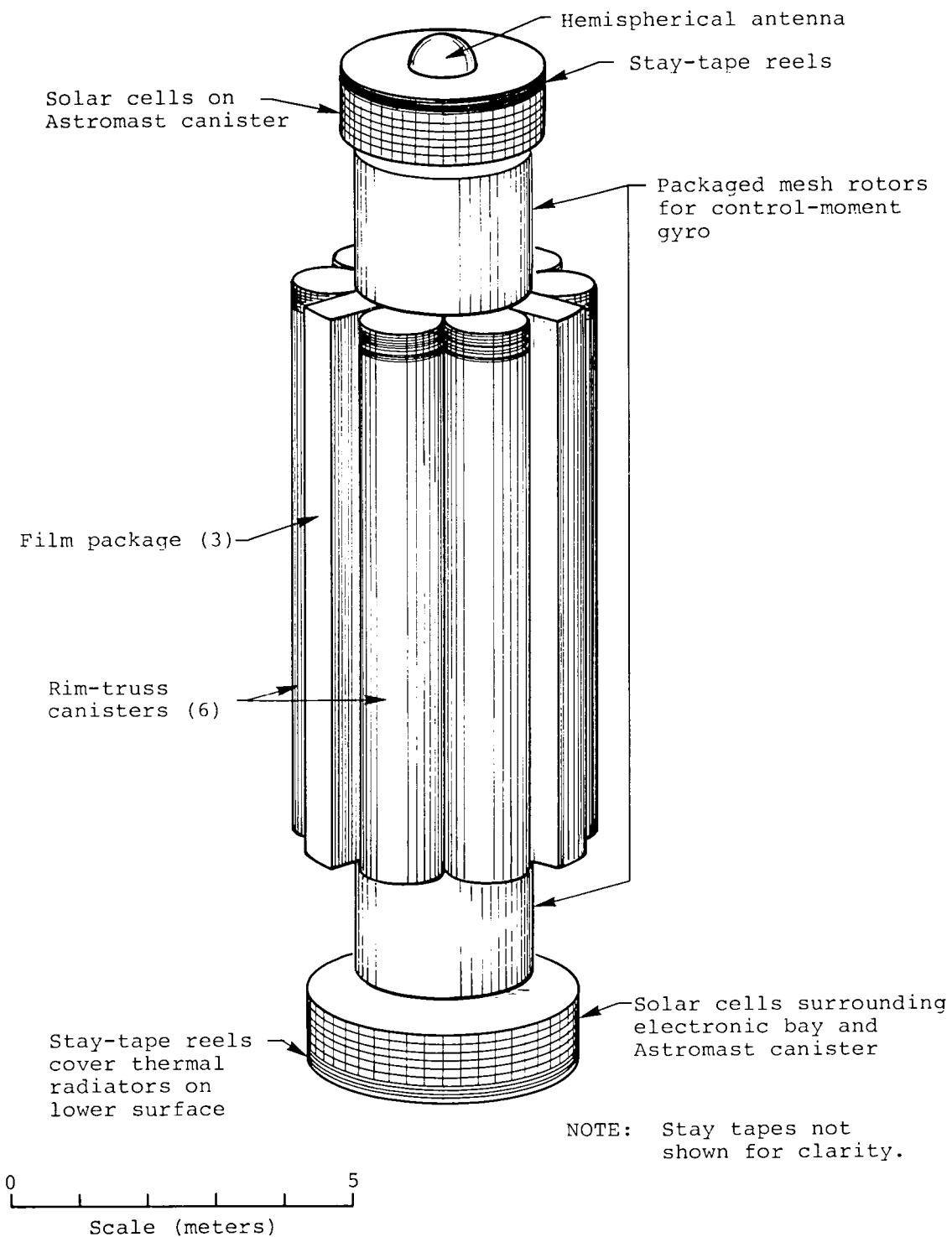


Figure 22. 1-km-diameter reflector spacecraft packaged for Shuttle cargo bay.

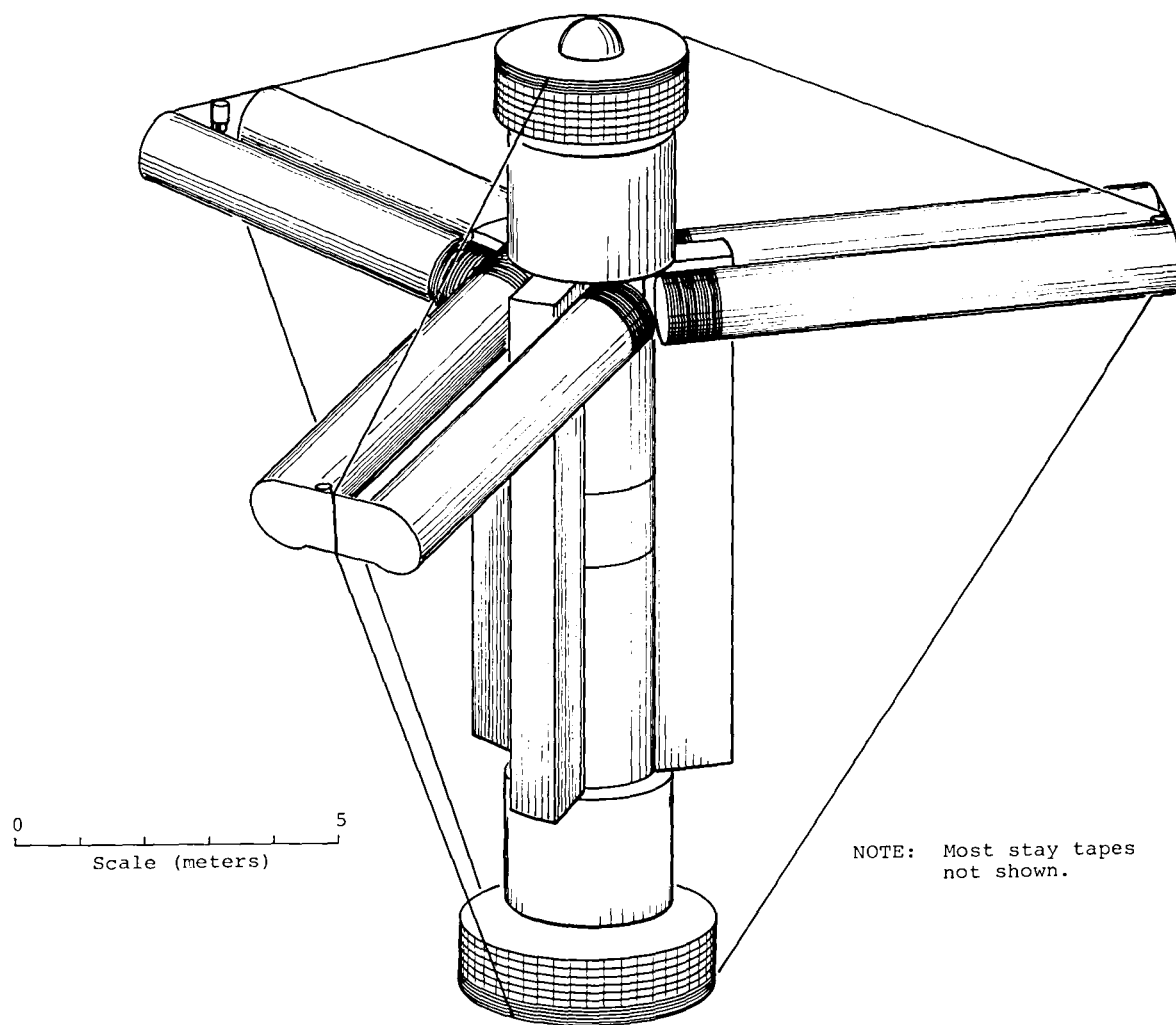


Figure 23. First phase of deployment showing truss-rim canisters after 90-degree rotation.

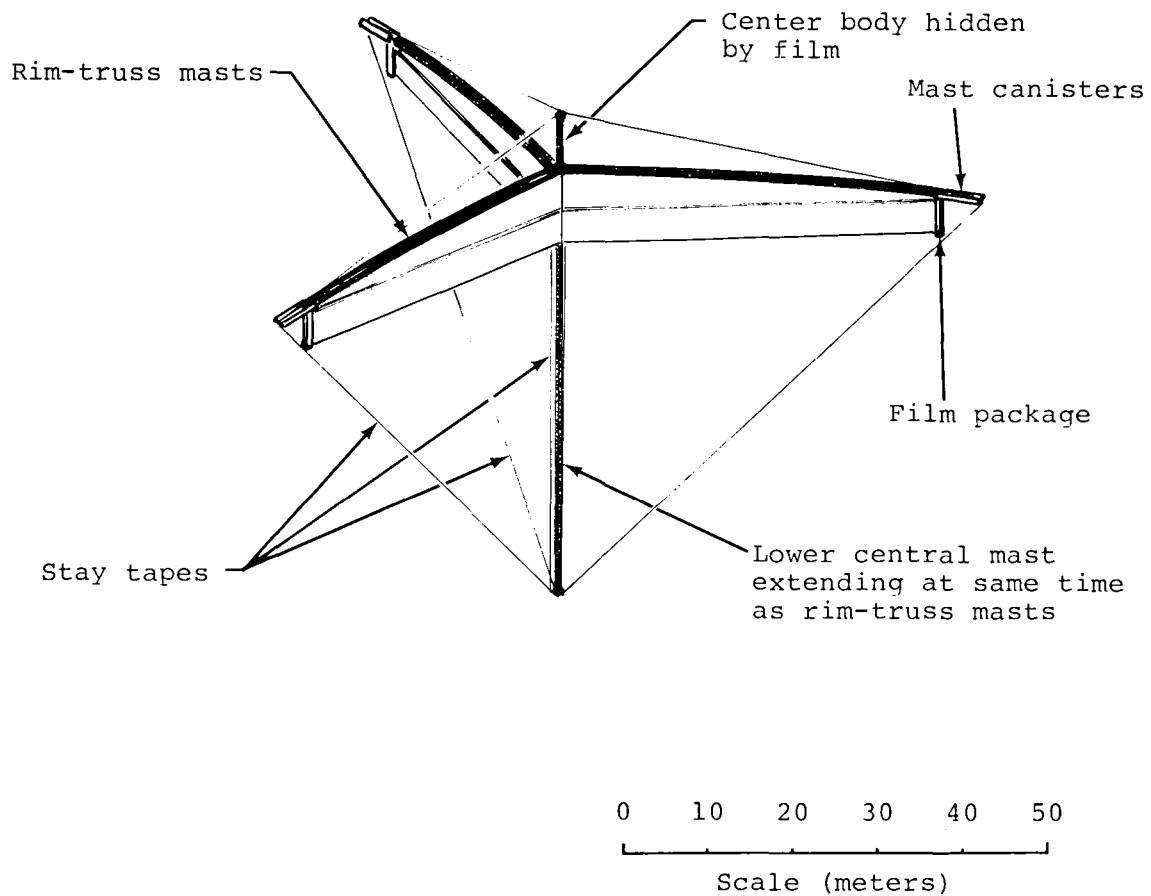


Figure 24. Solar-reflector spacecraft during early part of second deployment phase.

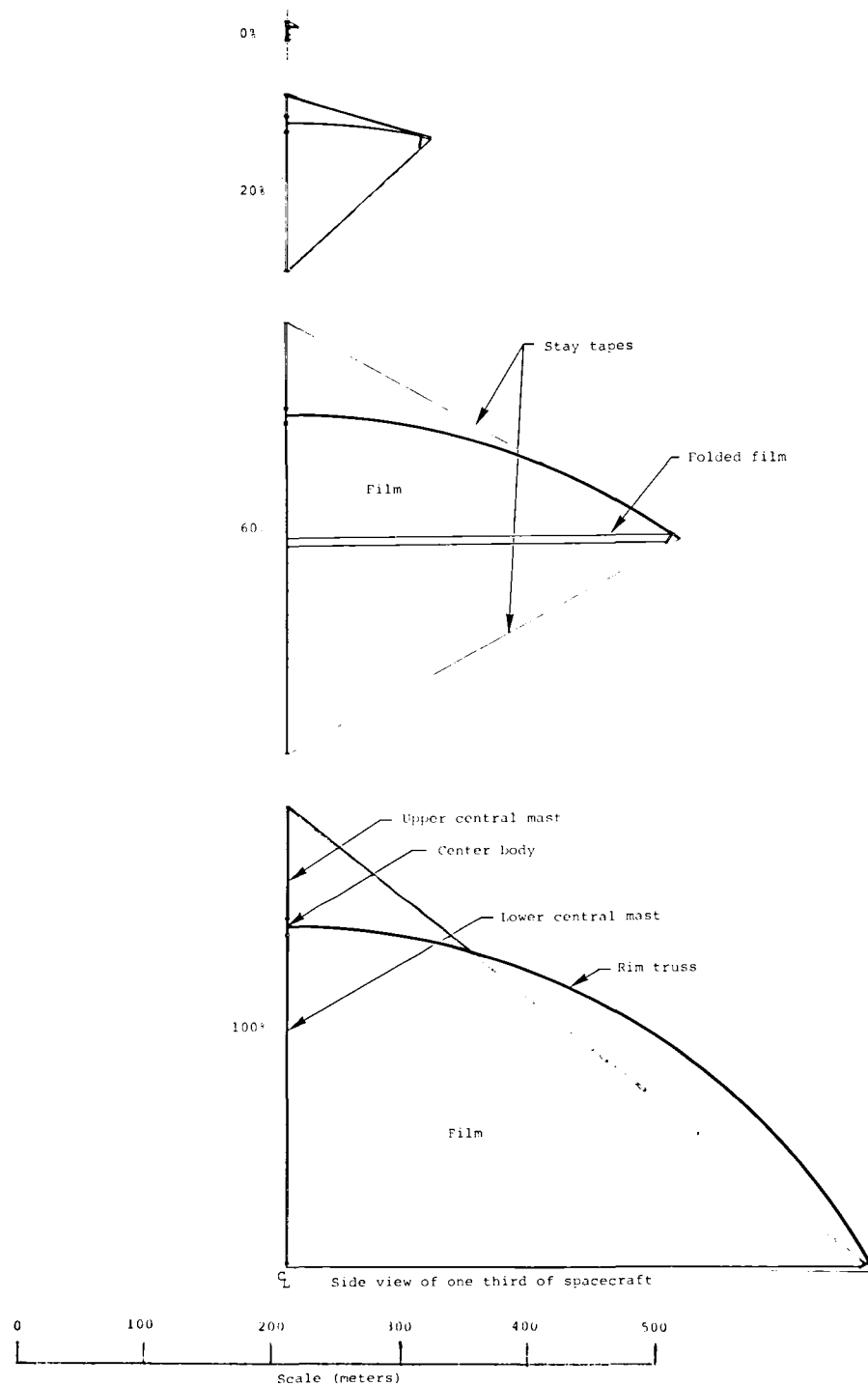
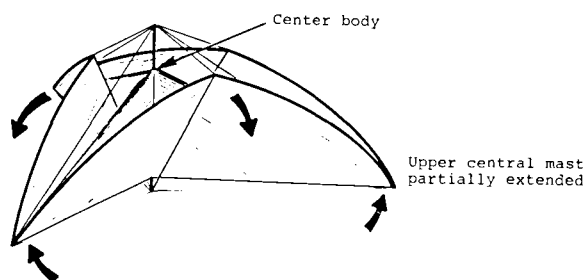
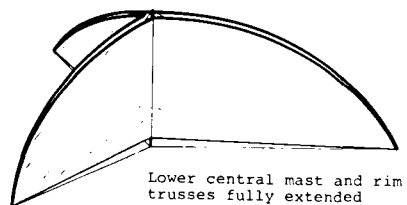
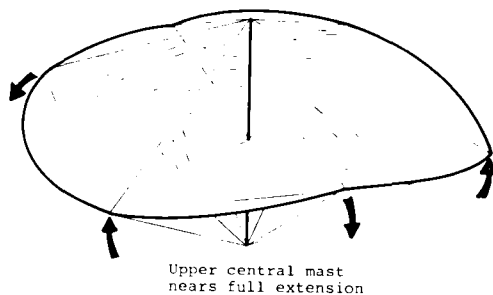


Figure 25. Progressive deployment of masts and film in second deployment phase.



NOTE: Mast stay tapes not shown.



0 500
Scale (meters)

Film and rim fully deployed in final configuration

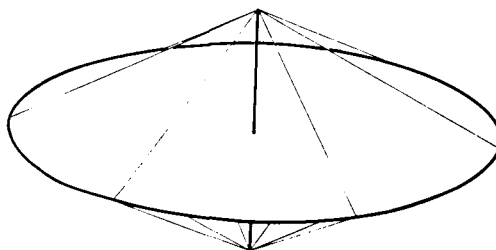


Figure 26. Third phase of the deployment sequence.

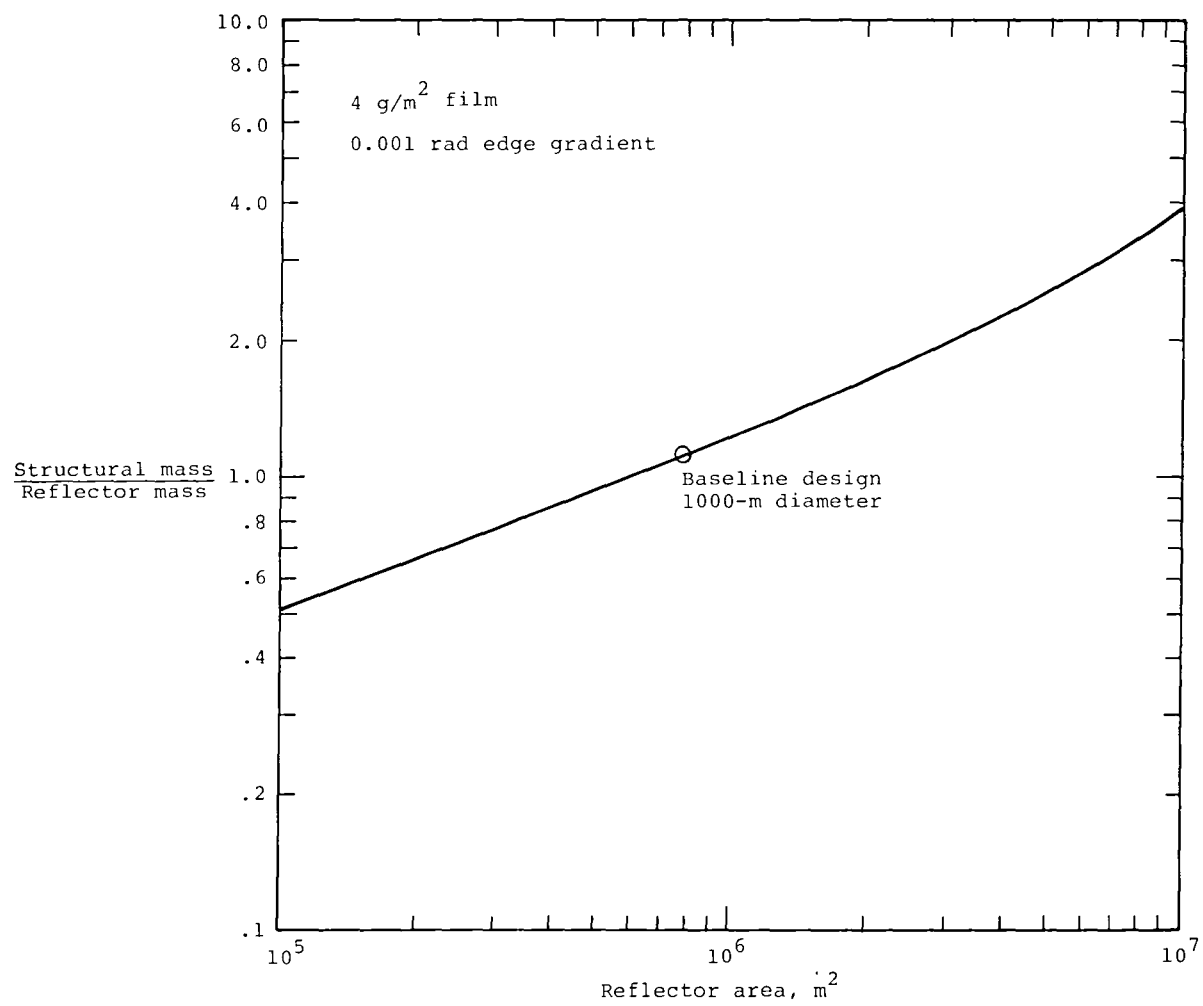


Figure 27. Structural mass fraction
for circular reflector satellite.

REFERENCES

1. Hedgepeth, J.M.; Knapp, K.K.; and Finley, L.A.: Structural Design of Free-Flying Solar-Reflecting Satellites. SAWE Paper No. 1303. Presented at the 38th Annual Conference of the Society of Allied Weight Engineers, Inc. New York, New York, 7-9 May 1979.
2. Mikulas, M.M., Jr.; Bush, H.G.; and Card, M.F.: Structural Stiffness, Strength and Dynamic Characteristic of Large Tetrahedral Space Truss Structures. NASA TM X-74001, March 1977.
3. Jacot, A.D.; and Liska, D.J.: Control Moment Gyros in Attitude Control. J. Spacecraft and Rockets, vol. 3, pp. 1313-1320, 1966.
4. Millner, A.R.: Flywheel Components for Satellite Applications. MIT Lincoln Lab TN-1978-4, May 1978.
5. Robbins, W.M., Jr.: Electromagnetic Forces on Space Structures. NASA CR-476, May 1966.
6. Wheeler, P.C.: Spinning Spacecraft Attitude Control via the Environmental Magnetic Field. J. Spacecraft, vol. 4, pp. 1631-1637, 1967.
7. Study of an Orbiting Low Frequency Radio Telescope. ARC-R-262. Astro Research Corporation, pp. 204-209, 22 November 1967.
8. Robbins, W.M., Jr.: The Feasibility of an Orbiting 1500-Meter Radiotelescope. NASA CR-792, June 1967.
9. Connell, G.M.: Preliminary Control System Studies for Scanning Operation. ARC-LTN-5, Astro Research Corporation, 18 March 1969.
10. Adams, L.R.: Application of Isotensoid Flywheels to Spacecraft Energy and Angular Momentum Storage. NASA CR-1971, February 1972.
11. Fraser, A.F.; Preiswerk, P.R.; Benton, M.D.; and Burggraf, O.R.: Axisymmetric Filamentary Structures. NASA CR-1518, April 1970.
12. Hedgepeth, J.M.; Mikulas, M.M., Jr.; and MacNeal, R.H.: Practical Design of Low-Cost Large Space Structures. Astronautics & Aeronautics, pp. 30-34, October 1978.

13. Hedgepeth, J.M.: Primary Design Requirements for Large Space Structures. Paper No. AIAA-81-0443. Presented at the 2nd AIAA Conference on Large Space Platforms, San Diego, CA, 2-4 February 1981.
14. Robbins, W.M. Jr.: Experiment Definition Study and Model Testing for Orbiting Radio Telescopes, Part I. ARC-R-432, Astro Research Corporation, 15 April 1971.
15. Models of Earth's Atmosphere (90 to 2500 km). NASA SP-8021, Revised March 1973.
16. Hedgepeth, J.M.: Deflection of a Membrane with Tension-Tendon-Supported Edges. ARC-TN-1070, Astro Research Corporation, 17 November 1978.
17. Preiswerk, P.R.; and Stammreich, J.C.: Assessment of Current and Projected Performance Characteristics of Deployable Structural Masts. ARC-TN-1085, Astro Research Corporation, 15 April 1980.
18. Rowe, W.M.; Luedke, E.E.; and Edwards, D.K.: Thermal Radiative Properties of Solar Sail Film Materials. Thermophysics and Thermal Control, Progress in Astronautics and Aeronautics, vol. 65, pp. 3, 1979.
19. Finley, L.A.; and Hedgepeth, J.M.: The Support of Large-Area Thin Films without Wrinkles. ARC-TN-1067, Astro Research Corporation, 21 November 1978.
20. Hedgepeth, J.M.; and Miller, R.R.: Effects of Member Length Imperfections on the Deformations and Loads in an Isogrid-Truss Structure. ARC-R-1012, Astro Research Corporation, 1 April 1980.

1. Report No. NASA CR-3438		2. Government Accession No.		3. Recipient's Catalog No.	
4. Title and Subtitle Conceptual Design Studies for Large Free-Flying Solar-Reflector Spacecraft				5. Report Date June 1981	
				6. Performing Organization Code	
7. Author(s) John M. Hedgepeth, Richard K. Miller, and Karl Knapp				8. Performing Organization Report No. ARC-R-1015	
9. Performing Organization Name and Address Astro Research Corporation 6390 Cindy Lane Carpinteria, California 93013				10. Work Unit No.	
				11. Contract or Grant No. NAS1-15347	
12. Sponsoring Agency Name and Address National Aeronautics and Space Administration Washington, DC 20546				13. Type of Report and Period Covered Contractor Report	
				14. Sponsoring Agency Code	
15. Supplementary Notes Langley Technical Monitors: Melvin Anderson, John E. Canady, Jr., and Claude R. Keckler Topical Report					
16. Abstract This report describes the conceptual mechanical design of an Earth-orbiting solar-reflecting spacecraft. The 1-km-diameter reflecting film surface is supported by a lightweight structure which may be automatically deployed after launch in the Space Shuttle. A twin-rotor, control-moment gyroscope, with deployable rotors, is included as a primary control actuator. The vehicle has a total specific mass of less than 12 g/m ² , including allowances for all required subsystems. The structural elements have been sized to accommodate the loads of a typical SOLARES-type mission where a swarm of these free-flying satellites is employed to concentrate sunlight on a number of energy conversion stations on the ground.					
17. Key Words (Suggested by Author(s)) Solar reflector, Ultralightweight spacecraft, Membrane structures, Deployable space structures				18. Distribution Statement Unclassified - Unlimited Star Category 18	
19. Security Classif. (of this report) Unclassified		20. Security Classif. (of this page) Unclassified		21. No. of Pages 119	
				22. Price A06	

For sale by the National Technical Information Service, Springfield, Virginia 22161

End of Document